UC San Diego

UC San Diego Electronic Theses and Dissertations

Title

Overcoming the Kerr-Induced Capacity Limit in Optical Fiber Communications

Permalink

https://escholarship.org/uc/item/0pd2809b

Author

Temprana Giraldo, Eduardo

Publication Date

2017

Peer reviewed|Thesis/dissertation

eScholarship.org Powered by the California Digital Library
University of California

UNIVERSITY OF CALIFORNIA SAN DIEGO

Overcoming the Kerr-Induced Capacity Limit in Optical Fiber Communications

A dissertation submitted in partial satisfaction of the
requirements for the degree Doctor of Philosophy

in

Electrical Engineering (Photonics)

by

Eduardo Temprana Giraldo

Committee in charge:

Stojan Radic, Chair
Nikola Alic
Leonid Butov
Miroslav Krstic
Shayan Mookherjea
George Papen

2017

Copyright

Eduardo Temprana Giraldo, 2017

All rights reserved.

The Dissertation of Eduardo Temprana Giraldo is approved, and it is acceptable in quality and form for publication on microfilm and electronically:

_____

_____

_____

_____

_____

_____

Chair

University of California, San Diego

2017

DEDICATION

To my wife, my family, and friends

for their love and support.

TABLE OF CONTENTS

LIST OF TABLES AND FIGURES

LIST OF ABBREVIATIONS

dB	Decibels
EDFA	Erbium Doped Fiber Amplifiers
OEO	Optical-to-Electrical-to-Optical
WDM	Wavelength Division Multiplexed
IM-DD	Intensity-Modulated Direct-Detection
DSP	Digital Signal Processing
CD	Chromatic Dispersion
GVD	Group-Velocity Dispersion
PMD	Polarization-Mode Dispersion
NLC	Nonlinearity Cancellation
NLSE	Nonlinear Schrodinger Equation
SMF	Single-Mode Fibers
PSCF	Pure Silica Core Fibers
ISI	Inter-Symbol Interference
SPM	Self-Phase Modulation
XPM	Cross-Phase Modulation
FWM	Four-Wave Mixing
SSFM	Split-Step Fourier Method
I	In-Phase
Q	Quadrature
IQ	In-Phase and Quadrature

IQM	In-Phase and Quadrature Modulator
QAM	Quadrature Amplitude Modulation
MZM	Mach-Zehnder Modulator
NMZM	Nested Mach-Zehnder Modulator
Q-Factor	Quality Factor
AWGN	Additive White Gaussian Noise
BER	Bit-Error Rate
ADC	Analog-to-Digital Converter
DAC	Digital-to-Analog Converters
FIR	Finite Impulse Response
DGD	Differential Group Delay
PSP	Principal States of Polarization
PDL	Polarization Dependent Loss
CMA	Constant Modulus Algorithm
RD-CMA	Radius Direct CMA
LMS	Least-Mean Squares
OSNR	Optical Signal-to-Noise Ratio
SNR	Signal-to-Noise Ratio
G	Gain
NF	Noise Figure
ASE	Amplified Spontaneous Emission
GN	Gaussian Noise

NLI	Nonlinear Interference
SDM	Space-Division Multiplexing
NLC	Nonlinearity Cancellation
DBP	Digital Back Propagation
TS-NLC	Transmitter-Side Nonlinearity Compensation
RS-NLC	Receiver-Side Nonlinearity Compensation
EDC	Electronic Dispersion Compensation
DCF	Dispersion Compensating Fiber
DCM	Dispersion Compensating Modules
OFC	Optical Frequency Comb
CW	Continuous-Wave
FRC	Frequency-Referenced Carriers
ITU	International Telecommunication Union
ECL	External Cavity Lasers
iTLA	Integrated Tunable Laser Assembly
RF	Radio-Frequency
HNLF	Highly Nonlinear Fiber
DFB	Distributed Feedback
FPL	Fabry-Perot Laser
HNLF	Highly Nonlinear Fiber
SBS	Stimulated Brillouin Scattering
OP	Optical Processor

PRBS	Pseudo-Random Bit Sequences
PBS	Polarization Beam Splitter
VOA	Variable Optical Attenuation
PBS	Polarization Beam Splitter
TX	Transmitter
RX	Receiver
SSMF	Standard Single-Mode Fiber
FEC	Forward Error Correction
SD-FEC	Soft-Decision Forward Error Correction
SSMF	Standard Single-Mode Fiber
ASIC	Application Specific Integrated Circuits
MIMO	Multiple Input–Multiple Output
IL	Injection Locking
ENOB	Effective Number of Bits
RS	Reed-Salomon
OSA	Optical Spectrum Analyzer
SE	Spectral Efficiency
PM	Polarization Multiplexed
CMOS	Complementary Metal-Oxide Semiconductor
DA	Driver Amplifier
DP-NMZM	Dual-Polarization Nested Mach-Zehnder

ACKNOWLEDGEMENTS

Chapter 3, in part is a reprint of the material as it appears in Optics and Photonics News, vol. 27, no. 3, pp. 30-37, (2016), titled "Beating the nonlinear capacity limit," by Eduardo Temprana, Nikola Alic, Bill P.-P. Kuo, and Stojan Radic. In addition, Chapter 3 in part is a reprint of the material as it appears in Science, vol. 348, no. 6242, pp. 1445-1448, (2015), titled "Overcoming Kerr-induced capacity limit in optical fiber transmission," by Eduardo Temprana, Evgeny Myslivets, Bill P.-P. Kuo, Lan Liu, Vahid Ataie, Nikola Alic, and Stojan Radic. Lastly, Chapter 3 in part is a reprint of the material as it appears in Optics Express, vol. 23, no. 16, pp. 20774-20783, (2015), titled “Two-fold transmission reach enhancement enabled by transmitter-side digital backpropagation and optical frequency comb-derived information carriers,” by Eduardo Temprana, Evgeny Myslivets, Lan Liu, Vahid Ataie, Andreas O.J. Wiberg, Bill P.-P. Kuo, Nikola Alic, and Stojan Radic. The dissertation author was the primary investigator, and the primary author of these articles.

Chapter 4, in part is a reprint of the material as it appears in Journal of Lightwave Technology, vol. 34, no. 15, pp. 3544-3549, (2016), titled "Transmitter-Side Digital Back Propagation with Optical Injection-Locked Frequency Referenced Carriers," by Eduardo Temprana, Evgeny Myslivets, Bill P.-P. Kuo, Nikola Alic, and Stojan Radic. In addition, Chapter 4 contains material presented in the Frontiers in Optics Conference, San Jose, (2015), titled "50 GBaud 16-QAM Transmission Over 2125 km Based on an Injection-Locked Fabry-Perot Laser Carrier," by Eduardo Temprana, Bill P.-P. Kuo, Nikola Alic

and Stojan Radic. The dissertation author was the primary investigator, and the primary author of these articles.

Chapter 5, in part contains material presented in the European Conference on Optical Communication, (2016), Dusseldorf, titled "Demonstration of Coherent Transmission Reach Tripling by Frequency-Referenced Nonlinearity Pre-compensation in EDFA-only SMF Link," by Eduardo Temprana, Evgeny Myslivets, Vahid Ataie, Bill P.-P. Kuo, Nikola Alic, Vijay Vusirikala, Vinayak Dangui and Stojan Radic. In addition, Chapter 5 in part contains material currently prepared for submission to Photonics Technology Letters, titled “Penalties Associated with Polarization-Power Imbalance and Polarization-Timing Skew in Multichannel Transmitter-Side Digital Back Propagation”, by Eduardo Temprana, Evgeny Myslivets, Bill P.-P. Kuo, Nikola Alic and Stojan Radic. Lastly Chapter 5 in part or in full contains material currently being prepared for submission to Journal of Lightwave Technology, titled “Demonstration of Coherent Transmission Reach Tripling by Frequency-Referenced Nonlinearity Pre-compensation in EDFA-only SMF Link,” by Eduardo Temprana, Evgeny Myslivets, Vahid Ataie, Bill P.-P. Kuo, Nikola Alic, and Stojan Radic. The dissertation author was the primary investigator, and the primary author of these articles.

VITA

2013 Bachelor of Science, Electrical Engineering, University of California, San Diego, USA.

2015 Master of Science, Electrical Engineering (Photonics), University of California, San Diego, USA.

2017 Doctor of Philosophy, Electrical Engineering (Photonics), University of California, San Diego, USA.

PUBLICATIONS

Journal Articles:

[1] B. P.-P. Kuo, E. Myslivets, V. Ataie, **E. Temprana**, N. Alic and S. Radic, "Wideband parametric frequency comb as coherent optical carrier," Journal of Lightwave Technology, pp. 3414-3419, 2013.

[2] A. Wiberg, D. Esman, **E. Temprana**, E. Myslivets, B. P.-P. Kuo, N. Alic and S. Radic, "High-speed, rate-scalable photonic-assisted digitizer equalization by frequency comb referencing," Optics Express, vol. 22, no. 18, pp. 21227-21235, 2014.

[3] **E. Temprana**, V. Ataie, B. P.-P. Kuo, E. Myslivets, N. Alic and S. Radic, "Low-noise parametric frequency comb for continuous C-plus-L-band 16-QAM channels generation," Optics Express, vol. 22, no. 6, pp. 6822-6828, 2014.

[4] N. Alic, E. Myslivets, **E. Temprana**, B. P.-P. Kuo and S. Radic, "Nonlinearity cancellation in fiber optic links based on frequency referenced carriers," Journal of Lightwave Technology, vol. 32, no. 15, pp. 2690-2698, 2014.

[5] V. Ataie, **E. Temprana**, L. Liu, E. Myslivets, B. P.-P. Kuo, N. Alic and S. Radic, "Ultrahigh count coherent WDM channels transmission using optical parametric comb-based frequency synthesizer," Journal of Lightwave Technology, vol. 33, no. 3, pp. 694-699, 2015.

[6] **E. Temprana**, E. Myslivets, B. P.-P. Kuo, L. Liu, V. Ataie, N. Alic and S. Radic, "Overcoming Kerr-induced capacity limit in optical fiber transmission," Science, vol. 348, no. 6242, pp. 1445-1448, 2015.

[7] **E. Temprana**, E. Myslivets, L. Liu, V. Ataie, A. Wiberg, B. P.-P. Kuo, N. Alic and S. Radic, "Two-fold transmission reach enhancement enabled by transmitter-side digital backpropagation and optical frequency comb-derived information carriers," Optics Express, vol. 23, no. 16, pp. 20774-20783, 2015.

[8] L. Liu, **E. Temprana**, V. Ataie, A. O. Wiberg, B. P.-P. Kuo, E. Myslivets, N. Alic and S. Radic, "All optical wavelength multicaster and regenerator based on four-mode phase-sensitive parametric mixer," Optics Express, vol. 23, no. 24, pp. 30956-30969, 2015.

[9] **E. Temprana**, N. Alic, B. P.-P. Kuo and S. Radic, "Beating the nonlinear capacity limit," Optics and Photonics News, vol. 27, no. 3, pp. 30-37, 2016.

[10] **E. Temprana**, E. Myslivets, B. P.-P. Kuo, N. Alic and S. Radic, "Transmitter-Side Digital Back Propagation with Optical Injection-Locked Frequency Referenced Carriers," Journal of Lightwave Technology, vol. 34, no. 15, pp. 3544-3549, 2016.

[11] D. J. Esman, V. Ataie, B. P.-P. Kuo, **E. Temprana**, N. Alic and S. Radic, "Detection of Fast Transient Events in a Noisy Background," Journal of Lightwave Technology, vol. 34, no. 24, pp. 5669-5674, 2016.

[12] **E. Temprana**, E. Myslivets, B. P.-P. Kuo, N. Alic and S. Radic, “Penalties Associated with Polarization-Power Imbalance and Polarization-Timing Skew in Multichannel Transmitter-Side Digital Back Propagation,” prepared for submission to Photonics Technology Letters.

[13] **E. Temprana**, E. Myslivets, B. P.-P. Kuo, N. Alic and S. Radic, “Demonstration of Coherent Transmission Reach Tripling by Frequency-Referenced Nonlinearity Pre-compensation in EDFA-only SMF Link,” being prepared for submission to Journal of Lightwave Technology.

Conference Proceedings:

[14] D. J. Esman, A. O. Wiberg, **E. Temprana**, Y. Myslivets, B. P.-P. Kuo, N. Alic and S. Radic, "A fully frequency referenced parametric polychromatically sampled analog-to-digital conversion," in Optical Fiber Communication Conference, San Francisco, 2014.

[15] **E. Temprana**, V. Ataie, A. Peric, N. Alic and S. Radic, "Wavelength Conversion of QPSK Signals in Single-Pump FOPA with 20 dB Conversion Efficiency," in Optical Fiber Communication Conference, OSA Technical Digest, San Francisco, 2014.

[16] L. Liu, **E. Temprana**, V. Ataie, E. Myslivets, B. P.-P. Kuo, A. O. Wiberg, N. Alic and S. Radic, "Demonstration of enhanced amplitude regeneration in four-mode

phase-sensitive parametric multicasting mixer," in Optical Communication (ECOC), 2014 European Conference on, Cannes, 2014.

[17] **E. Temprana**, V. Ataie, B. P.-P. Kuo, E. Myslivets, N. Alic and S. Radic, "Dynamic reconfiguration of parametric frequency comb for superchannel and flex-grid transmitters," in Optical Communication (ECOC), 2014 European Conference on, Cannes, 2014.

[18] V. Ataie, **E. Temprana**, N. Alic and S. Radic, "Demonstration of local-oscillator phase-noise tolerant 40 GBaud/s coherent transmitter," in Optical Communication (ECOC), 2014 European Conference on, Cannes, 2014.

[19] V. Ataie, **E. Temprana**, L. Liu, Y. Myslivets, B. P.-P. Kuo, N. Alic and S. Radic, "Flex-grid compatible ultra wide frequency comb source for 31.8 Tb/s coherent transmission of 1520 UDWDM channels," in Optical Fiber Communication Conference, San Francisco, 2014.

[20] L. Liu, **E. Temprana**, V. Ataie, B. P.-P. Kuo, E. Myslivets, A. O. Wiberg, N. Alic and S. Radic, "The first demonstration of phase and amplitude regenerative multicasting by a four-mode phase-sensitive process," in Photonics Conference (IPC), 2014 IEEE, San Diego, 2014.

[21] **E. Temprana**, B. P.-P. Kuo, N. Alic and S. Radic, "50 GBaud 16-QAM Transmission Over 2125 km Based on an Injection-Locked Fabry-Perot Laser Carrier," in Frontiers in Optics, San Jose, 2015.

[22] N. Alic, **E. Temprana**, E. Myslivets and S. Radic, "Nonlinearity compensation: Is the knowledge of absolute amplitude and phase really necessary?," in Digital Communications (TIWDC), 2015 Tyrrhenian International Workshop on, Florence, 2015.

[23] **E. Temprana**, E. Myslivets, B. P.-P. Kuo, N. Alic and S. Radic, "Penalties associated with dispersion parameter mismatch and limited steps-per-span in Transmission-Side Digital Back Propagation," in Photonics Conference (IPC), 2015, Reston, 2015.

[24] **E. Temprana**, E. Myslivets, L. Liu, A. Pejkic, V. Ataie, B. P.-P. Kuo, D. Esman, A. Wiberg, N. Alic and S. Radic, "Transmission reach doubling enabled by transmitter-side digital back propagation and frequency referenced carriers," in Optical Communication (ECOC), 2015 European Conference on, Valencia, 2015.

[25] **E. Temprana**, E. Myslivets, V. Ataie, B. P.-P. Kuo, N. Alic, V. Vusirikala, V. Dangui and S. Radic, "Demonstration of Coherent Transmission Reach Tripling by Frequency-Referenced Nonlinearity Pre-compensation in EDFA-only SMF Link," in ECOC 2016; 42nd European Conference on Optical Communication; Proceedings of, Dusseldorf, 2016.

[26] J. Zhang, **E. Temprana**, B. P.-P. Kuo, N. Alic, S. Radic, "Wavelength Multicasting of 4/16QAM Channel in a Dual-pump Two-stage Silicon Mixer," in Asia Communications and Photonics Conference, Wuhan, 2016.

[27] **E. Temprana**, B. P.-P. Kuo, N. Alic, S. Radic and S. Grubb, "400 Gb/s WDM DP-256-QAM transmission with 50 GHz channel separation," Postdeadline Paper in IEEE Photonics Conference (IPC), 2016 IEEE, Kona, 2016.

[28] H. Hu, D. J. Esman, V. Ataie, **E. Temprana**, B. P.-P. Kuo, N. Alic, S. Radic, "Comb-Assisted Real-Time Discrete Fourier Transform Processor," in Optical Fiber Communication Conference, Los Angeles, 2017

ABSTRACT OF THE DISSERTATION

Overcoming the Kerr-Induced Capacity Limit in Optical Fiber Communications

by

Eduardo Temprana

Doctor of Philosophy in Electrical Engineering (Photonics)

University of California, San Diego, 2017

Professor Stojan Radic, Chair

Wavelength Division Multiplexed optical networks serve as the backbone of the telecommunications infrastructure around the world. Presently, the dominant impairment in such systems is the Kerr-induced nonlinear crosstalk, which imposes a fundamental limit to their information-carrying capacity. Until recently, digital signal processing-

based approaches used for the compensation of nonlinear crosstalk have had limited success for reasons that have remained unclear. In this dissertation, the frequency stability and mutual coherence of the optical carriers is for the first time proven to play a critical role in Kerr-mediated interactions.

As a solution, optical frequency combs are leveraged to provide a stable frequency reference, enabling the precompensation of nonlinear crosstalk in multichannel systems. Supporting experimental demonstrations indicate that the fiber capacity and system reach can be significantly increased over previously established limits. This dissertation accordingly proposes and validates three different comb-based frequency-referenced transmitter architectures, and finally, an experiment encompassing the developed groundwork is demonstrated to achieve record nonlinearity cancellation in a state-of-the-art high-capacity system.

Chapter 1. Introduction

1.1 Motivation

With the widespread adoption of bandwidth-intensive applications like cloud computing, high-definition video streaming and online gaming, capacity demands are growing at an unprecedented rate. Internet traffic is soon expected to surpass the Zettabyte (10^{21} bytes) threshold [1], and will continue marching steadily towards the certain exhaustion of the available bandwidth of deployed optical networks.

In the past, traffic demands have been met by improvements in technology [2]. The optical fiber waveguide, originally envisioned in 1960 by Charles Kao and George Hockham [3], was first realized with a telecommunications-suitable, at the time record-low attenuation of 20 dB/km by Corning Glass Works in 1970. Shortly thereafter, research efforts lead by Corning progressed to reduce fiber attenuation by two orders of magnitude, bringing the loss down to 0.2 dB/km, a figure that is staggeringly close to the theoretical minimum of 0.15 dB/km. Meanwhile, improvements in semiconductor lasers and photodiodes were accompanied by the explosion of the electronics industry, which provided a cost-efficient fabrication infrastructure to supply the growing demand.

Later, the development of the Erbium Doped Fiber Amplifiers (EDFA) in 1987 [4] resulted in a significant enhancement of the capacity of optical links. The EDFA, which would become the workhorse [5] of optical communications, provided two significant improvements; first, it eliminated the need of costly Optical-to-Electrical-to-Optical (OEO) regenerators, and second, it enabled the transition from single- to multi-channel Wavelength Division Multiplexed (WDM) systems. The adoption of WDM revolutionized

optical communications, boosting system bandwidth right at a time when the capacity of optical networks was starting to become exhausted [6].

More recently, with the growth of the internet, the optical communications industry reignited its interest in coherent optical technology. Initially investigated due to its superior sensitivity over Intensity-Modulated Direct-Detection (IM-DD) systems, coherent transmission lost traction after the development of EDFAs due to the poor frequency-stability and broad linewidth of lasers [7]. Coherent modulation, which had been long utilized in cable, satellite, wireless and broadband internet links, offered two important improvements over IM-DD systems; first, it enabled significantly higher spectral efficiency by relying upon higher-order modulation formats. Second, it was conductive to simpler digital signal processing (DSP) applications, enabling the compensation of linear transmission impairments such as Chromatic Dispersion (CD) or Polarization-Mode Dispersion (PMD) [8], which at the time were the limiting factors for transmission capacity and reach.

Presently, linear transmission impairments no longer impose a limit in the capacity of optical links and it is actually a nonlinear effect, namely the optical Kerr-effect that limits fiber capacity. The optical fiber material -silica- has a small nonlinear response, whose effect onto the information-bearing signal accumulates to significant amounts in optical fiber transmission due to the high confinement of light in the core, low loss, and the long interaction lengths [9]. This capacity limit, coined in the literature as the “nonlinear capacity limit” [10], is the only remaining transmission impairment that constrains the capacity of optical links. At this point, to accommodate the growing traffic demand, we

must either deploy more fibers, which is costly, inefficient and polluting, or we must devise a technique that will allow us to overcome the Kerr-induced capacity limit.

Nonlinearity Cancellation (NLC) is currently an extremely popular topic for this very reason. Naturally, the DSP-architecture available in modern transceivers is shaping to be the ideal medium to implement NLC applications. However, very few experimental demonstrations have been able to achieve noteworthy improvements with DSP-based NLC in multichannel systems. One important challenge that has been theoretically unveiled recently is the requirement of a stable frequency reference in systems that implement NLC by inverting the Nonlinear Schrodinger Equation (NLSE) in the digital domain [11]. The use of uncorrelated laser sources results in stochastic variations in the relative frequency between the channels, which, through the fiber dispersion, becomes transformed in a stochastic rate of walk-off between the channels, essentially randomizing the nonlinear interactions. As such, the nonlinear crosstalk becomes an equally stochastic process that, needless to say, cannot be compensated.

1.2 Dissertation Overview

This dissertation aims to assert and demonstrate that the frequency stability and mutual coherence of the optical carriers represent a critical and necessary condition in DSP-based nonlinearity compensation applications.

Chapter 2 serves as a review of the relevant background regarding optical fiber transmission systems. It starts with the theory that governs wave propagation, continuing with a survey of coherent transmission technology, as well as optical communication link

architectures. The chapter concludes by exposing the considerations of the optical fiber capacity and its limitations as a communications channel.

Chapter 3 introduces the concepts of nonlinearity cancellation in coherent transmission systems, and points out the challenges in implementing such a technique in practical applications. Results generated with system simulations are used to aid the discussion and three experimental demonstrations investigating the role of frequency reference in practical systems.

Chapter 4 proposes and demonstrates two alternative architectures to generate frequency referenced carriers by means of optical injection locking lasers to optical frequency combs, whereas two experimental demonstrations feature the proposed architectures.

Lastly, Chapter 5 contains an extensive experimental demonstration encompassing all the groundwork developed in the preceding chapters. In this last chapter, NLC is applied to a system that employs Dense Wavelength Division Multiplexing, high cardinality modulation, and polarization multiplexing, wherein the results show an unprecedented tripling of the system reach with respect to the uncompensated system.

Chapter 2. Optical Fiber Transmission

2.1 Introduction

As a communications system, the goal of optical links is to transport information from a transmitter in one location to a receiver in another. This chapter serves as a review of the relevant background of optical fiber transmission, starting with the theory that governs wave propagation in optical fibers, continuing with coherent transmission concepts, explaining how optical links are architected in practice and lastly considering the capacity of the optical fiber and its limitations as a communications channel.

2.2 Propagation in Optical Fiber

Propagation effects can be easily understood by analyzing the evolution of a monochromatic plane wave, typically denoted by

$$E(z,t) = \Re\{E(z,t)e^{-i(\beta_0 z-\omega_0 t)}\} \tag{2.2.1}$$

where $\Re$ denotes the real part, $E(z,t)$ is the complex envelope of the field at location z and time t, β_0 is the propagation constant of the wave in the medium and ω_0 is the center frequency of the optical carrier.

Wave propagation in optical fibers is governed by the Nonlinear Schrödinger Equation [9], which in scalar representation has the form

$$\frac{\partial E}{\partial z} = -\frac{\alpha}{2}E + i\sum_n (-i)^n \frac{\beta_\mathrm{n}}{n!}\frac{\partial^\mathrm{n} E}{\partial t^\mathrm{n}} + i\gamma|E|^2 E \tag{2.2.2}$$

where E is the slowly-varying envelope of the electric field, α is the attenuation coefficient, β_n are the propagation constants, and γ is the nonlinear coefficient.

A brief discussion on the physical origin and the corresponding implications of each of the right-hand terms provides interesting insight that will become relevant throughout this dissertation.

2.2.1 Attenuation

The loss of power of an optical wave as it propagates through a medium often referred to as attenuation. In fibers, there are multiple factors that contribute to the total attenuation, such as absorption, scattering, bending losses, and losses in the interface between the core and cladding. Typically, all the propagation losses are bundled together into a single coefficient α, which has linear units of [1/m] but is usually expressed in [dB/km]. The power evolution along the fiber can be derived by solving the NLSE while including the attenuation term only, i.e.

$$\frac{\partial E}{\partial z} = -\frac{\alpha}{2}E \tag{2.2.3}$$

The solution for this simple differential equation gives rise to Beer's law of attenuation

$$E(z) = E(0)e^{-\frac{\alpha}{2}z} \tag{2.2.4}$$

$$P(z) = P(0)e^{-\alpha z} \tag{2.2.5}$$

where $P = |E|^2$ refers to the optical power, $P(0)$ is the power (or intensity) at the input of the fiber, α is the total attenuation coefficient, and z is the longitudinal direction of propagation. As shown in (2.2.5), the power of an optical wave propagating through a fiber decreases exponentially with the propagated distance. Typically, Single-Mode Fibers (SMF) exhibit a loss of about 0.2 dB/km (0.17 dB/km for most recently designed fibers),

whereas more modern fibers like Pure Silica Core Fibers (PSCF) can exhibit losses as low as 0.155 dB/km [12].

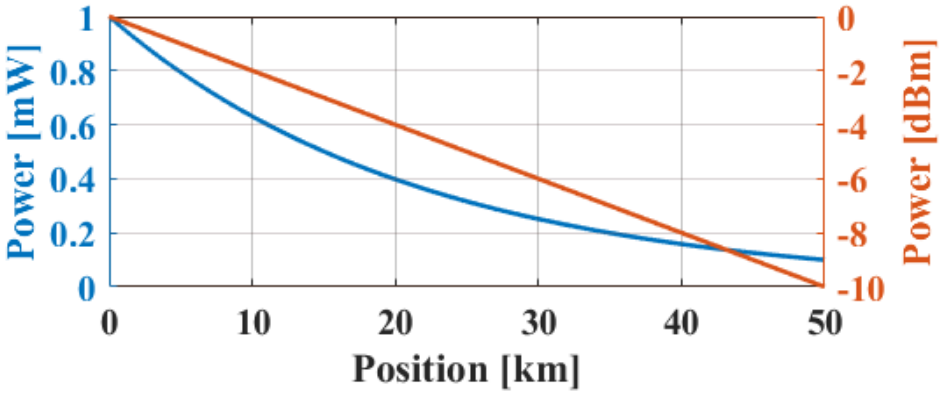

Figure 1. Power evolution in a fiber with α = 0.2 dB/km

2.2.2 Chromatic Dispersion

It is a well-known fact that the index of refraction of any medium is frequency-dependent. As a direct consequence, the frequencies associated with the pulses of light (representing wave-packets with finite bandwidth) will propagate through optical fiber with different group velocity, thereby accruing unequal delays. This phenomenon, known as chromatic dispersion, is the dominant dispersion mechanism in SMF and must be considered in the design of optical links [13].

The propagation constant β of an optical wave travelling through a dielectric is related to the index of refraction of the medium $n_0(\omega)$ and the propagation constant in the vacuum k_0 by

$$\beta(\omega) = n_0(\omega)k_0 = n_0(\omega)\frac{\omega}{c} \tag{2.2.6}$$

where c is the speed of light in vacuum, i.e. 299,792,458 m/s.

It is convenient to decompose $\beta(\omega)$ by applying a Taylor series expansion about a reference frequency ω_0

$$\beta(\omega) = \beta_0 + \beta_1(\omega - \omega_0) + \frac{1}{2}\beta_2(\omega - \omega_0)^2 + \frac{1}{6}\beta_3(\omega - \omega_0)^3 + \cdots \quad (2.2.7)$$

where $\beta_n = \frac{d^n\beta}{d\omega^n}$ is the n-th dispersion coefficient. Practically, however, only the first three orders are of interest in the applications considered in this thesis.

Correspondingly, β_1 is the inverse of the group velocity

$$\beta_1 = \frac{1}{v_g} = \frac{d\beta}{d\omega} \quad (2.2.8)$$

with units of [s/m] and β_2 is the group-velocity dispersion (GVD)

$$\beta_2 = \frac{d^2\beta}{d\omega^2} \quad (2.2.9)$$

which has units of [s^2/m].

In engineering practice, it becomes convenient to consider dispersion as a function of wavelength. Utilizing the relation

$$\beta_2(\omega)d\omega = D(\lambda)d\lambda \quad (2.2.10)$$

we can define the dispersion parameter D, which is usually expressed in units of [ps/(nm · km)] and dispersion slope S, with units of [ps^2/(nm · km)]

$$D(\lambda) = -\frac{2\pi c}{\lambda^2}\beta_2(\omega_0) \quad (2.2.11)$$

$$S(\lambda) = \frac{(2\pi c)^2}{\lambda^3}\beta_3(\omega_0) - 2D(\lambda) \quad (2.2.12)$$

where $\omega_0 = \frac{2\pi c}{\lambda_0}$.

Significant insight on the effect of chromatic dispersion can be gained by solving the NLSE in the absence of attenuation and nonlinearity

$$\frac{\partial E}{\partial z} = -i\frac{\beta_2}{2}\frac{\partial^2 E}{\partial t^2} \tag{2.2.13}.$$

The solution to this equation is most elegantly found by transforming into the frequency domain using the Fourier transform

$$\mathcal{F}\left\{\frac{\partial \mathrm{E}}{\partial z}\right\} = \mathcal{F}\left\{i\frac{\beta_2}{2}\frac{\partial^2 \mathrm{E}}{\partial t^2}\right\} \tag{2.2.14}$$

$$\frac{\partial \tilde{E}}{\partial z} = i\frac{\beta_2}{2}\omega^2\tilde{E} \tag{2.2.15}$$

$$\tilde{E}(z) = \tilde{E}(0)e^{i\frac{\beta_2 z}{2}\omega^2} \tag{2.2.16}$$

where $\mathcal{F}$ refers to the Fourier Transform operation and $\tilde{E}$ is the frequency domain representation of E, i.e. $\tilde{E}(z) = E(\omega, z) = \mathcal{F}\{E(t, z)\}$.

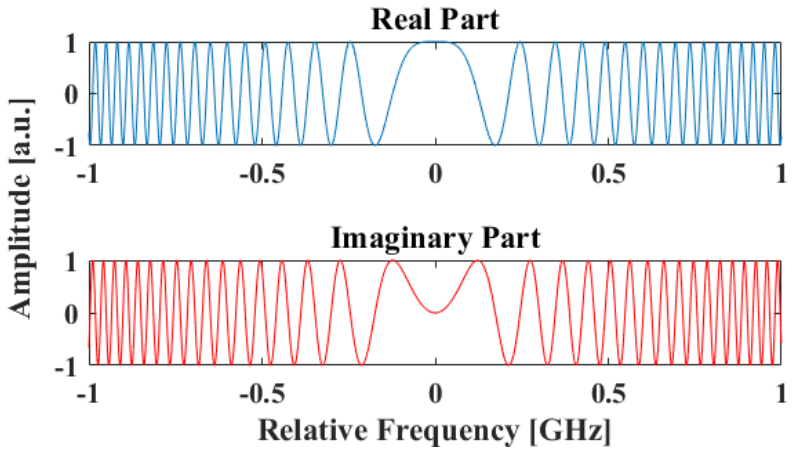

Figure 2. Real and Imaginary parts of quadratic spectral phase shift due to Chromatic Dispersion

As can be seen in Figure 2, essentially, the effect of chromatic dispersion is a quadratic spectral phase shift, which in the time domain represents a series of frequency-dependent temporal delays. Thus, when a train of pulses propagates through fiber, the different frequency components of each pulse will acquire different phase shifts, resulting

in a broadening effect, as can be seen in Figure 3. Pulse broadening due to CD can affect the system performance, as it causes Inter-Symbol Interference (ISI).

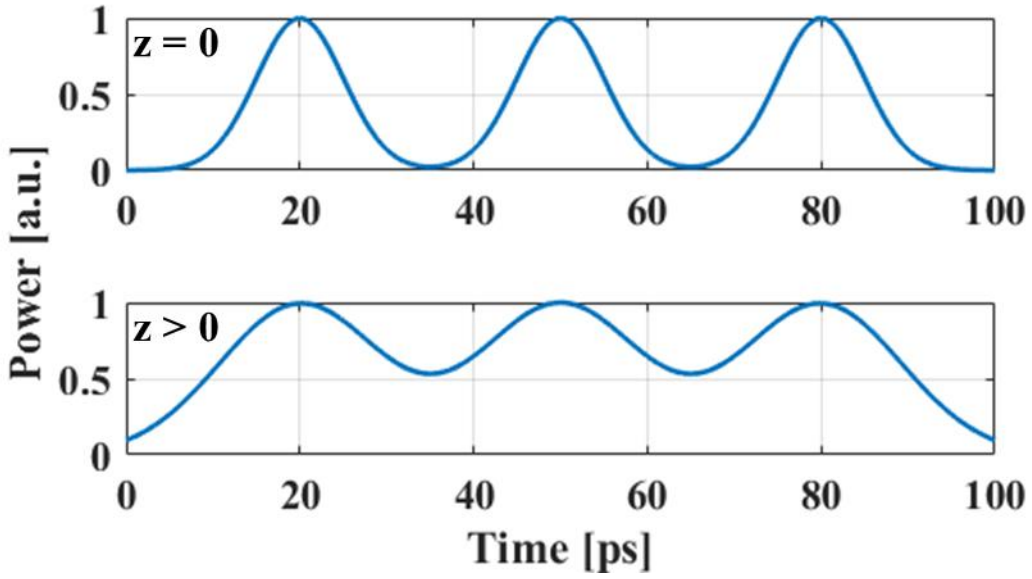

Figure 3. Pulse broadening due to Chromatic Dispersion

2.2.3 Nonlinearity

Silica exhibits a miniscule nonlinear response that is, in most cases, negligible. However, in optical fiber transmission, due to the high confinement of the optical mode in the core, the low propagation loss and the long interaction length, the nonlinearity gives rise to multiple interesting phenomena that are of great importance in the design of optical communications systems [9].

The most relevant nonlinear effect in optical fiber communications is the Kerr-effect, coined in 1875 after Scottish Physicist John Kerr [14]. The Kerr nonlinearity manifests itself as an instantaneous (femtosecond scale) intensity-dependent change in the index of refraction, which modifies the previously introduced expression for $n(\omega)$ with a new term that is dependent on the intensity of the applied electric field. Thus, the index of

refraction becomes dependent on both the frequency of the optical field and its intensity, and is modified to appear as

$$n(\omega, E) = n_0(\omega) + n_2|E|^2 \tag{2.2.17}$$

where $n_0(\omega)$ is the linear frequency-dependent index of refraction, n_2 is the nonlinear index of refraction, which has units of [m^2/W] and $|E|^2$ is the intensity of the applied electric field E. The nonlinear index n_2, which for all intents and purposes is assumed to be instantaneous, is related to the nonlinear coefficient γ by

$$\gamma = \frac{2\pi n_2}{\lambda A_{eff}} \tag{2.2.18}$$

where λ is the wavelength, A_{eff} is the effective area of the fiber, and thus γ has units of [1/(W $\cdot$ m)].

To gain insight on the effect of the Kerr-nonlinearity, we again invoke the NLSE for the sake of easier comprehension we now neglect the linear propagation terms, i.e.

$$\frac{\partial E}{\partial z} = \mathrm{i}\gamma|E|^2 E \tag{2.2.19}$$

which can be solved with the ansatz

$$E(z,t) = E(0,t)e^{i\gamma|E(z,t)|^2 z} \tag{2.2.20}.$$

This result shows that a travelling optical wave will acquire a self-induced phase shift. Not surprisingly, this phenomenon is commonly referred to as Self-Phase Modulation (SPM).

Similarly, if we consider two co-polarized monochromatic waves such that

$$E = E_1 + E_2 \tag{2.2.21}$$

then, the solution to the coupled system of equations becomes

$$E_1 = E_1 e^{i\gamma\left[|E_1|^2+2|E_2|^2\right]z} \tag{2.2.22}$$

$$E_2 = E_2 e^{i\gamma\left[|E_1|^2+2|E_2|^2\right]z} \tag{2.2.23}$$

which shows that each wave will accrue a self-induced phase shift, but it will also acquire a phase shift induced by the other copropagating wave, which is larger by a factor of two than its self-induced counterpart. The cross-coupling is accordingly referred to as Cross-Phase Modulation (XPM). The sum of the self and cross phase shifts accrued due to the Kerr-effect is known as the nonlinear phase shift, defined as $\Delta\varphi_{NL} = \Delta\varphi_{SPM} + \Delta\varphi_{XPM}$.

In addition to SPM and XPM, the optical Kerr-effect gives rise to the phenomenon of Four-Wave Mixing (FWM). However, because FWM requires precise phase-matching conditions, it only contributes significantly in links that employ fibers with low dispersion and closely spaced carriers, which is virtually never realized in commonly deployed systems [9].

2.2.4 Split-Step Fourier Method

Unfortunately, when the effects of attenuation, dispersion and nonlinearity are all considered, which corresponds to the practical case in which these effects act jointly on the propagating field, the NLSE does not have an analytical solution. Nevertheless, it is a well-behaved nonlinear equation that has stable solutions [15, 16], and can be integrated numerically. To approach the most widely used numerical solution, the right-hand side of the NLSE can be rewritten in terms of two operators

$$\frac{\partial E}{\partial z} = \left(\hat{L} + \widehat{NL}\right)E \tag{2.2.24}$$

where $\hat{L}$ is called the linear operator, which accounts for the attenuation and dispersion

$$\hat{L} = -\frac{\alpha}{2} - i\frac{\beta_2}{2}\frac{\partial^2}{\partial t^2} + \frac{\beta_3}{6}\frac{\partial^3}{\partial t^3} \tag{2.2.25}$$

and $\widehat{NL}$ is called the nonlinear operator, which accounts for the Kerr-nonlinearity

$$\widehat{NL} = i\gamma|E|^2 \tag{2.2.26}.$$

Note that, as implied by the NLSE, dispersion and nonlinearity act simultaneously along the fiber, and thus, the two operators cannot be applied separately. However, as is commonly done in similar cases, it is reasonable to approximate that in a short integration step, the linear and nonlinear operators can be factored independently (supported by the physical interpretation that dispersion and nonlinearity act separately), and thus, the operators can be taken sequentially. Obviously, the validity of this approximation increases when the step size decreases, since in shorter distances the changes to the electric field envelope due to the linear and nonlinear effects can be made negligible to the desired accuracy. The described reasoning is precisely the basis for the Split-Step Fourier Method (SSFM) [9, 17].

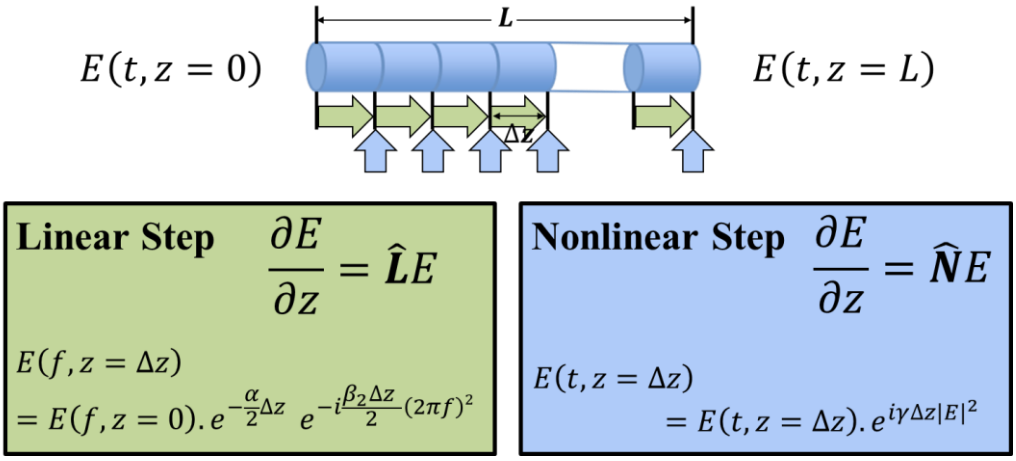

Figure 4. Symmetric Spit-Step Fourier Method

As seen in Figure 4, in the symmetric SSFM, the fiber is divided into small pieces of length Δz, which are chosen such that the sequential action of the operators satisfies the

desired accuracy. Starting with the field at the input of the fiber $E(t, z = 0)$, the algorithm consists of firstly transforming the electric field into the frequency domain by means of a Fourier Transform $E(\omega, z = 0) = \mathcal{F}\{E(t, z = 0)\}$ and applying a linear step of distance $\frac{\Delta z}{2}$ in the frequency domain, i.e.

$$E\left(\omega, z = \frac{\Delta z}{2}\right) = E(\omega, z = 0) e^{i\frac{\beta_2 \frac{\Delta z}{2}}{2}\omega^2} \tag{2.2.27}.$$

Subsequently, the field at $z = \frac{\Delta z}{2}$ is transformed back into the time domain by means of an Inverse Fourier Transform $E\left(t, z = \frac{\Delta z}{2}\right) = \mathcal{F}^{-1}\left\{E\left(\omega, z = \frac{\Delta z}{2}\right)\right\}$, and a nonlinear step of distance $\frac{\Delta z}{2}$ is applied in the time domain,

$$E(t, z = \Delta z) = E\left(t, z = \frac{\Delta z}{2}\right) e^{i\gamma \left|E\left(t, z = \frac{\Delta z}{2}\right)\right|^2 z} \tag{2.2.28}.$$

These two steps are then repeated iteratively until the field at the output of the fiber $E(t, z = L)$ is found.

2.3 Coherent Transmission

Historically, optical links have employed incoherent modulation formats, more commonly referred to as Intensity-Modulation and Direct Detection (IM-DD), where the information is encoded and retrieved from the intensity of the optical field. While IM-DD systems offer low implementation complexity, they suffer from limitations due to the high sensitivity to CD and Polarization-Mode Dispersion (PMD), making them undesirable for high-capacity long-haul transmission.

2.3.1 Modulation and Detection

Coherent transmission systems utilize the amplitude and phase of the optical carrier to encode information. Typically, this scheme is called complex modulation because both the real and imaginary parts of the electric field (also called In-phase and Quadrature components) are utilized to convey information, as in

$$E = I + i \cdot Q = A \cdot e^{\varphi} \tag{2.3.1}$$

where E refers to the complex electric field, I denotes the in-phase component, Q denotes the quadrature component, A is the amplitude, and φ is the phase.

The simplest example of complex modulation occurs when the I- and Q-components of the field are modulated with independent binary signals. Such modulation format is called 4-Quadrature Amplitude Modulation (QAM), because two bits are encoded into one symbol, and thus the total number of possible symbols in the dictionary is $2^2 = 4$. Figure 5 shows how the four symbols are distributed in the complex plane. This type of graphical representation is called a 'constellation diagram', which can be used a visual instrument to evaluate the performance of complex signals.

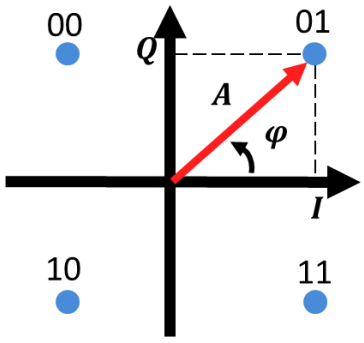

Figure 5. 4-Quadrature Amplitude Modulation

Physically, In-Phase and Quadrature modulation is implemented directly in the optical domain with a Nested Mach-Zehnder Modulator (NMZM), shown in Figure 6. Each arm of the main structure carries itself a Mach-Zehnder Modulator (MZM), wherein the two arms are offset in phase by 90°, setting them in quadrature with respect to each other.

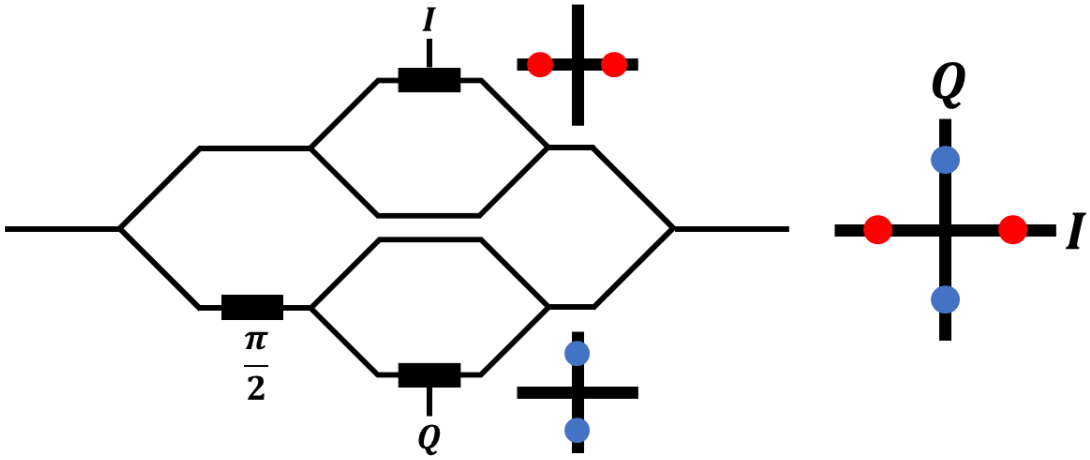

Figure 6. Nested Mach-Zehnder Modulator

At the receiver, the information of the amplitude and phase of the field is recovered by means of coherent detection, which is performed with the aid of a second laser that serves as the Local Oscillator (LO). In the coherent receiver, the signal and LO fields are combined and mixed in a 90° Hybrid, which separates the four tributaries of the optical field, as shown in Figure 7. Subsequently, two pairs of balanced detectors are utilized to convert the heterodyned quadrature components of the of the optical field into the electrical domain, or equivalently, radio-frequency (RF) signals.

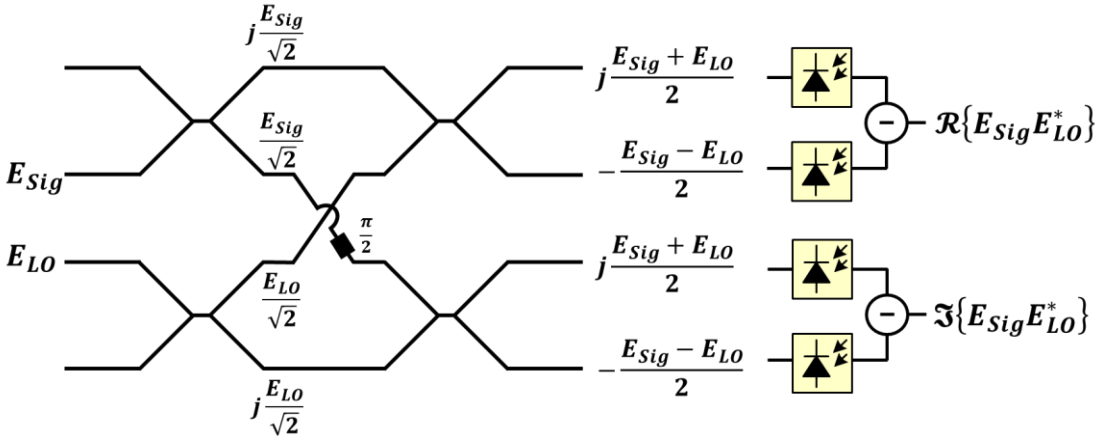

Figure 7. Optical Coherent Receivers

While the constellation points should ideally occur in unique locations, in a practical system implementation, there is noise and other impairments that will cause these points to deviate from their ideal position. Figure 8 shows an example of the in-phase and quadrature waveforms and the corresponding constellation in a realistic system implementation. The deviation of the constellation points will be proportional to the amount of noise in the system; when the noise becomes very strong, the samples may deviate enough to fall within the vicinity of a different constellation point, thereby resulting in a transmission error.

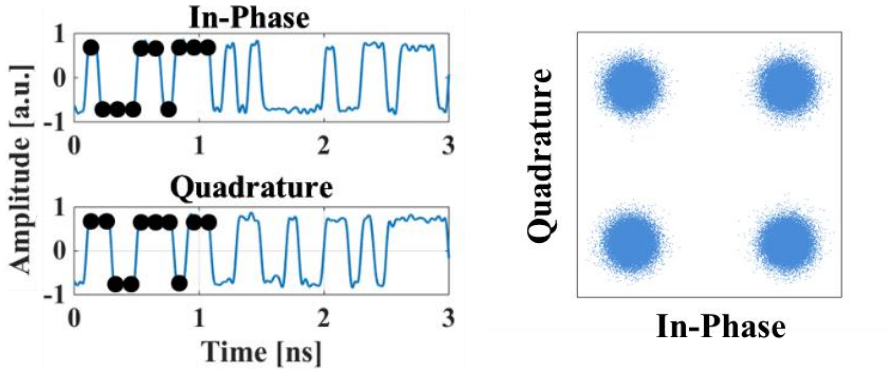

Figure 8. Quadrature waveforms and constellation for a 4-QAM signal in realistic conditions

Ultimately, the performance of any transmission system is defined by its Bit-Error Rate (BER), which is a measure of the quality and reliability of the transmission system, and correspond to the rate of bit-errors occurring in transmission. In optical systems literature, however, the Quality Factor (Q-Factor), which is inversely proportional to the BER, has become a popular metric to quantify system performance [13]. When the signal is corrupted by Additive White Gaussian Noise (AWGN), the Quality Factor (typically expressed in dB), is theoretically related to the BER performance through the relation

$$Q = 20 \cdot \log_{10}\left(\sqrt{2} \cdot erfc^{-1}(2 \cdot BER)\right) \tag{2.3.2}$$

where $erfc^{-1}$ is the inverse complimentary Gauss function [18].

In addition, the Q-Factor is also a measure of how noisy the constellation points are; a higher Q means that the constellation points are smaller and very far away. Mathematically this ratio is defined as

$$Q = \frac{r_1 - r_2}{\sigma_1 + \sigma_2} \tag{2.3.3}$$

where r_i is the mean value of the cloud, and σ_i is the standard deviation.

2.3.2 Modern Transceivers

Coherent transceivers have evolved significantly in the past few years, and currently feature high-speed high-resolution Analog-to-Digital and Digital-to-Analog Converters (ADCs and DACs) [19] that have enabled a wide range of DSP applications [7].

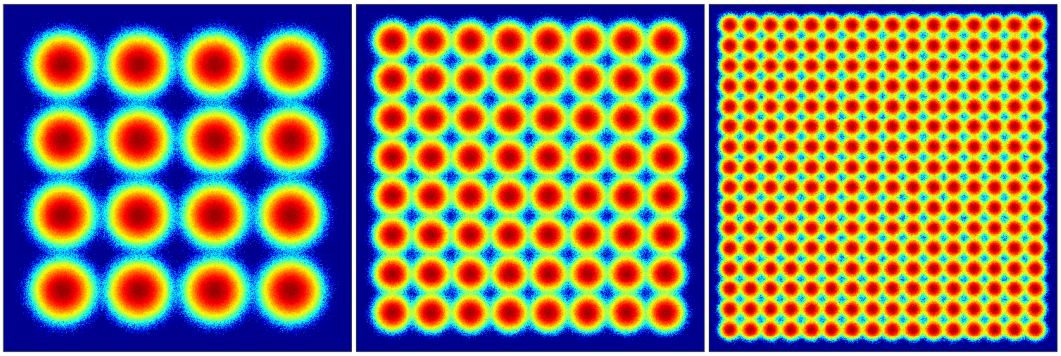

Figure 9. Constellations of 16, 64 and 256-QAM signals

Higher order (multilevel) modulation formats like those shown in Figure 17, once reserved for wireless and cable systems, have now become commonplace in optical transmission experiments [20, 21, 22]. In addition, techniques such as polarization multiplexing and pulse shaping are used to maximize the use of the optical spectrum, packing channels densely to achieve the highest spectral efficiency, as shown in Figure 10.

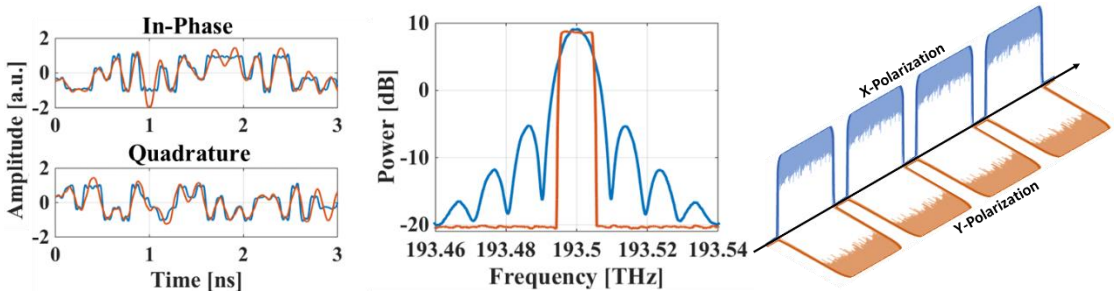

Figure 10. Pulse shaping and Polarization-Multiplexing

2.3.3 Digital Signal Processing

As mentioned previously, the information of the optical field's amplitude, phase and polarization information sampled at Nyquist rate enables a multitude of DSP applications that have greatly enhanced the capacity of optical networks. Impairments such as laser phase noise, chromatic dispersion and polarization-mode dispersion are now typically compensated directly in the digital domain, and pose very little inconvenience in even the longest transmission links.

The typical DSP processing chain in coherent transceivers can be seen in Figure 11. At the transmitter, the first step taken is the mapping of the binary information into the corresponding complex symbols. Following, pulse shaping is applied, typically by means of Finite Impulse Response (FIR), to constrain the spectral occupancy of the modulated signal. Lastly, prior to the digital-to-analog conversion and optical modulation, the signal is preconditioned to correct for any imperfections in the electronic and electro-optic components, namely the frequency limitations or device nonlinearities.

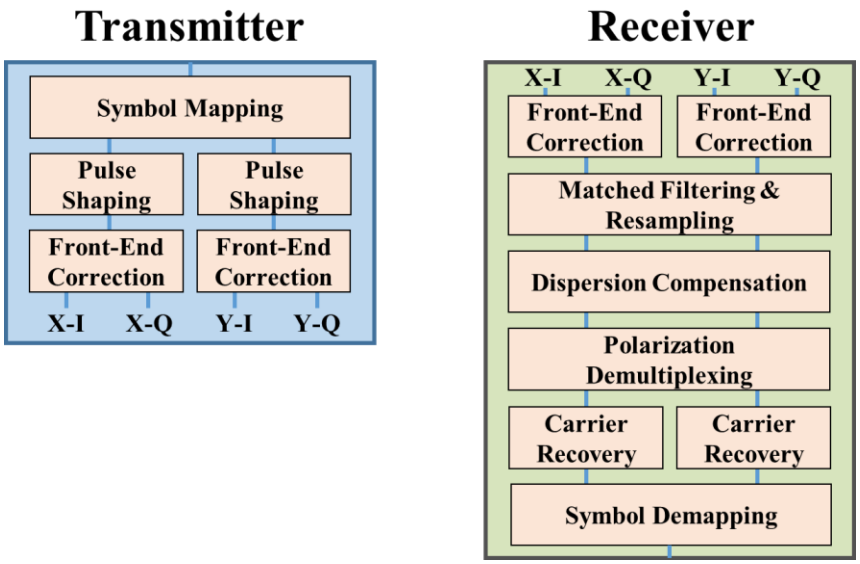

Figure 11. DSP processing chain in coherent transceivers

At the receiver, after the digitization of the electrical signals generated by the coherent receiver, any imperfections in the optoelectronic components are corrected, and the signals are filtered and resampled. Typically, the DSP works with 1.5-2 samples per symbol for the subsequent processing, which consists of dispersion compensation, polarization demultiplexing, carrier recovery and symbol demapping.

To understand how dispersion compensation and polarization demultiplexing are performed, consider for example the case of transmitting a signal in the two polarizations over a system without nonlinearity. The input-output relation will be given by

$$\begin{bmatrix} \tilde{E}_{out,x} \\ \tilde{E}_{out,y} \end{bmatrix} = \boldsymbol{H}(\omega) \begin{bmatrix} \tilde{E}_{in,x} \\ \tilde{E}_{in,y} \end{bmatrix} \tag{2.3.4}$$

where $\boldsymbol{H}(\omega)$ describes the system's chromatic dispersion, polarization mode dispersion and polarization dependent loss (PDL).

$\boldsymbol{H}(\omega)$ consists of the concatenation of a scalar element $H_D(\omega)$ that will account for Chromatic Dispersion, a 2x2 unitary matrix $\boldsymbol{H_{PMD}}(\omega)$ for the first-order polarization mode dispersion, a 2x2 Hermitian matrix $\boldsymbol{H_{PDL}}$ for the polarization dependent loss, and a unitary Jones matrix that will account for the birefringence $\boldsymbol{T}$ [23].

In the case of CD, as explained in Section 2.2.2, the transfer function is given as

$$H_D(\omega) = \frac{\tilde{E}(\mathrm{L})}{\tilde{E}(0)} = e^{-i\frac{\beta_2 L}{2}\omega^2} \tag{2.3.5}$$

which is unitary and invertible and where L is the fiber length, β_2 is the GVD and ω is the angular frequency. The inverse is simply found by taking the complex conjugate, i.e.

$$H_D{}^{-1}(\omega) = \frac{\tilde{E}(\mathrm{L})}{\tilde{E}(0)} = e^{i\frac{\beta_2 L}{2}\omega^2} \tag{2.3.6}.$$

The first-order PMD matrix $\boldsymbol{H_{PMD}}(\omega)$ is given by

$$\boldsymbol{H_{PMD}}(\omega) = \boldsymbol{R}_1^{-1} \begin{bmatrix} e^{i\frac{\Delta\tau}{2}\omega} & 0 \\ 0 & e^{i\frac{\Delta\tau}{2}\omega} \end{bmatrix} \boldsymbol{R}_1 \tag{2.3.7}.$$

where $\Delta\tau$ is the Differential Group Delay (DGD) and R_1 is a unitary axis rotation matrix that converts the two principal states of polarization (PSP) into the x- and y- polarizations.

The global PDL matrix is defined as

$$\boldsymbol{H_{PDL}} = \boldsymbol{R}_2^{-1}\begin{bmatrix}\sqrt{\Gamma_{max}} & 0\\ 0 & \sqrt{\Gamma_{min}}\end{bmatrix}\boldsymbol{R}_2 \tag{2.3.8}$$

where Γ_{max} and Γ_{min} are the maximum and minimum values of the transmission coefficient, respectively, and $\boldsymbol{R}_2$ is an axis rotation matrix that converts the eigen modes of the PDL into the x- and y- polarizations.

To compensate the linear propagation effects, the equalization procedure should estimate a transfer function $\boldsymbol{H_{eq}}$ such that it is the inverse transfer function of the system, i.e.

$$\boldsymbol{H_{eq}} = \boldsymbol{H^{-1}}(\omega) = \begin{bmatrix}h_{xx}(\omega) & h_{xy}(\omega)\\ h_{yx}(\omega) & h_{yy}(\omega)\end{bmatrix} \tag{2.3.9}$$

where the elements of the matrix can be implemented in the time domain by means of a Finite Impulse Response (FIR) filter in a butterfly structure, as shown in Figure 12. The filter tap estimation can be carried out using an adaptive algorithm such as the Constant Modulus Algorithm (CMA), Radius Direct CMA (RD-CMA) [24] or the Least-Mean Squares (LMS) algorithm [25].

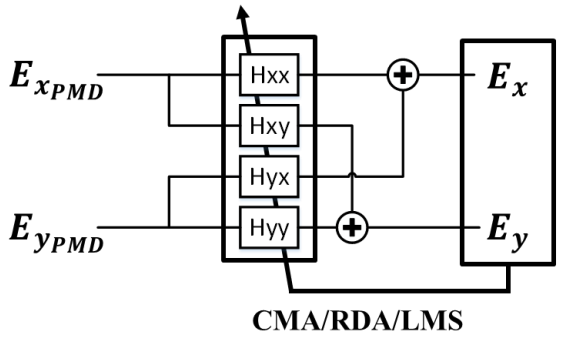

Figure 12. Butterfly equalizer for Polarization Demultiplexing

The last stage of the DSP-chain is to recover the frequency and phase of the optical carrier. Radio frequency (RF) systems, which are driven by oscillators with outstanding

stability, typically rely on Phase Locked Loops (PLLs) to synchronize the transmitter and receiver. In optical systems, however, oscillators are not nearly as stable as their microwave counterparts, and thus would require PLLs with extremely high bandwidths that are much too complex and expensive to deploy. Instead, optical coherent systems carry out the phase locking in the DSP-domain with algorithms that have been adapted from wireless applications. Currently, the most common carrier recovery algorithms are the M^{th} power or the Blind Search algorithms [26].

2.4 Link Architecture

The optical fiber waveguide is the ideal medium to carry out long-distance communications due to its low loss, limited dispersion, and small -albeit finite- nonlinearity. At wavelengths around 1550 nm, optical fibers exhibit propagation losses in the order of 0.2 dB/km [27], which means that the signals, after having travelled over 50 kilometers of fiber (a length corresponding to 10^{10} wavelengths) will still retain one tenth of their original power.

To compensate fiber loss, optical links rely on amplifiers that can regenerate optical signals without significantly degrading the signal quality. Erbium doped fiber amplifiers (EDFA), envisioned in the 1960s and demonstrated successfully in 1987 [4] are by far the most widely adopted in deployed optical networks and, as shown by the measurement in Figure 13, can provide tens of decibels of gain both in the C-band (1535 – 1565 nm) and in the L-band (1565 - 1610 nm), for a total of 10 THz of amplification bandwidth precisely in the window of lowest fiber loss. Due to the millisecond-scale upper-lifetime of Erbium, optical signals modulated at rates beyond 1 GBit/s are essentially amplified as if they were

continuous waves, which makes the EDFA a bit-rate and modulation format agnostic device. In addition, the EDFA can regenerate multiple channels simultaneously without introducing any crosstalk, a key property that enabled the transition from single to multichannel Wavelength Division Multiplexed systems from the 70's and 80's.

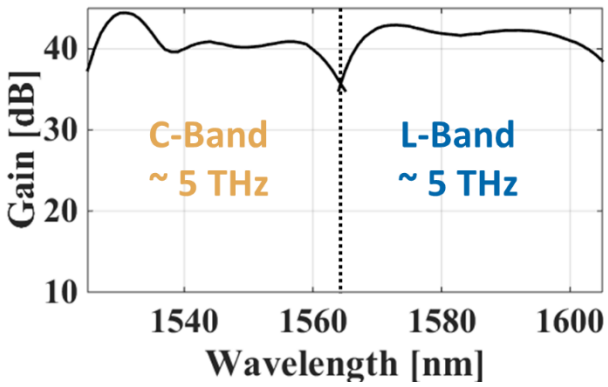

Figure 13. EDFA gain spectrum

Figure 5 shows the typical architecture of an EDFA-amplified WDM link. The combination of a long span of optical fiber and an EDFA forms a primitive cell that can be concatenated a multitude of times to create long (trans-pacific 10,000 km long) links without any intermediate opto-electronic processing or signal regeneration. Typically, the spans will consist of pieces of 50 to 120 km of fiber, whereas the span length will depend on the system requirements. Obviously, shorter spans will accrue less loss, and thus the received OSNR will be higher, but this will increase the system costs due to the higher number of components required.

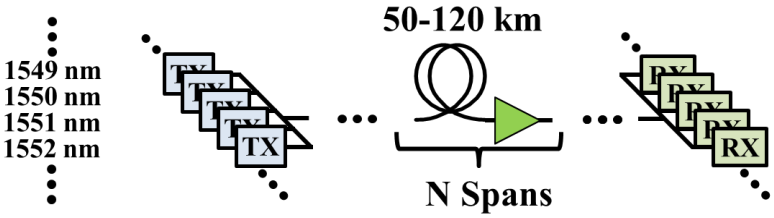

Figure 14. WDM optical link architecture

Two important parameters of EDFAs must be considered in the design of optical links, namely the Gain (G) and Noise Figure (NF), defined as

$$G = \frac{P_{out}}{P_{in}} \tag{2.4.1}$$

$$NF = \frac{OSNR_{out}}{OSNR_{in}} \tag{2.4.2}$$

where P refers to the optical power, typically defined in Watts [W], and $OSNR$ refers to the Optical Signal-to-Noise Ratio (OSNR). The NF, typically expressed in decibels [dB], represents the OSNR degradation that a signal suffers due to increase of the noise level from the Amplified Spontaneous Emission (ASE) occurring in the amplifier.

The OSNR, which can be easily measured with an Optical Spectrum Analyzer (OSA) is analogous to the Signal-to-Noise Ratio (SNR) concept in Communication Theory [18], and is defined as

$$OSNR = \frac{P_{Sig}}{\mathrm{P}_{ASE\,B=12.5\;GHz}} \tag{2.4.3}$$

where P_{Sig} is the total power of the signal and $P_{ASE\,B=12.5\;GHz}$ is the power of the noise in the two polarizations, integrated over a bandwidth B, which by convention is chosen as 12.5 GHz. The OSNR and SNR are thus related by

$$OSNR = SNR \cdot \frac{p \cdot B_{Sig}}{2 \cdot 12.5\;GHz} \tag{2.4.4}$$

where B_{Sig} is the bandwidth of the signal, and p is 1 or 2 depending on whether the signal is single- or dual-polarization, respectively.

The achievable performance of an optical link is closely related to (but, as we will see, not fully defined by) the received signal OSNR. For a quantum-noise-limited signal transmitted through a single-span link, the OSNR at the receiver will be related to the signal launch power P_{launch}, fiber span loss L and amplifier noise figure NF by the following relation

$$OSNR_{rec}\,[dB] = P_{Launch} - P_{Quantum\,Noise} - L - NF \tag{2.4.5}$$

where $P_{Quantum\,Noise}$ is the quantum noise power, defined as

$$P_{Quantum\,Noise} = h\vartheta\Delta\vartheta \tag{2.4.6}$$

and h refers to Plank's constant, ϑ is the photon frequency, and $\Delta\vartheta$ is the reference bandwidth, typically defined as 12.5 GHz.

Per (2.4.5), in order to improve the system performance, it is apparently beneficial to increase the signal launch power, since that increases the OSNR at the receiver. However, while this solution is perfectly feasible in traditional linear channels, in optical fibers, it will not generate the desired effect due to the nonlinear response of the fiber. Namely, at higher powers, the Kerr-effects introduce distortions in the signal that ultimately degrade the BER performance, thereby limiting the maximum signal launch power that can be used in practice.

To support the discussion, we shall rely on a NLSE-based simulation that will be updated and used throughout this thesis to provide practical insight. The model is based on a WDM system with several single-polarization channels spaced at 25 GHz, each carrying 16 GBd 16-QAM signals. The signals are launched into a link that consists of multiple spans of 85 km of SMF amplified by an EDFA with 5 dB NF, wherein the propagation is

emulated with the NLSE. The performance of the received signals is characterized in terms of the Bit-Error Rate performance, and transformed to the previously discussed Q-factor.

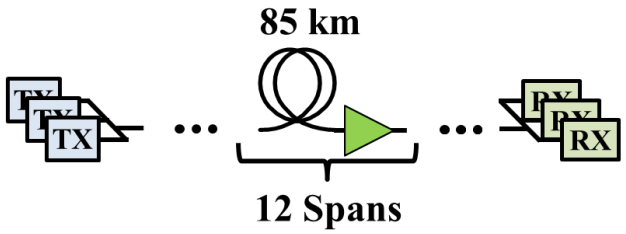

Figure 15. Simulation Schematic

The signal and noise power evolution of the center channel, and its corresponding OSNR are shown in Figure 16. As predicted by the analytical formula, the received OSNR increases dB per dB as the launch power is increased.

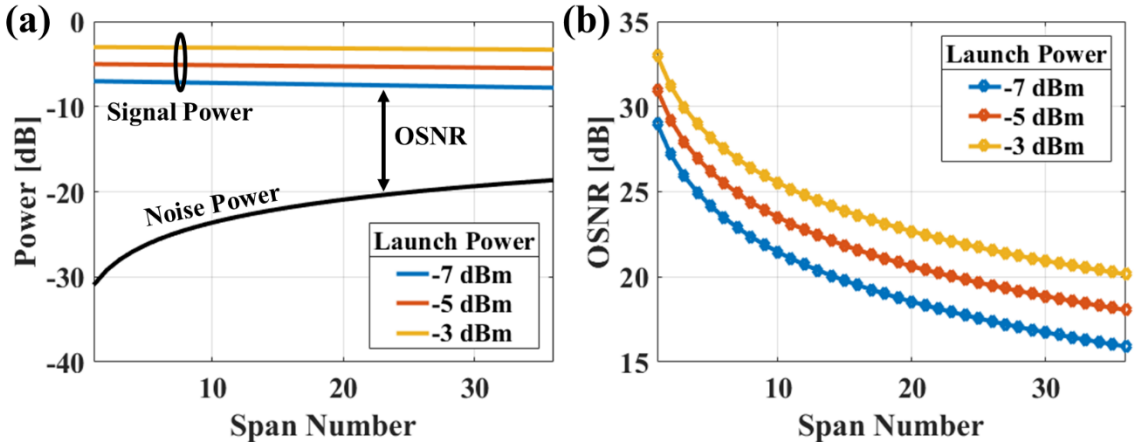

Figure 16. Evolution of (a) Signal and Noise Power (b) OSNR

As previously noted, intuition suggests that this increase in launch power should, at least in a linear system, improve the system performance, given that the received signal power increases, while the noise power stays constant. However, Figure 17 shows that, after transmission over 1020 km, the Q-Factor of the center channel only increases when the launch power is kept below -7 dBm. At higher powers, the Q-factor not only saturates,

but also rapidly falls immediately after reaching the peak performance. This performance degradation is a direct result of the Kerr-induced distortions on the signal, which grow faster than the OSNR increase. Thus, optical links ultimately operate in a regime that is the optimal compromise between the OSNR and nonlinear distortions, and thus, in legacy transmission systems, the powers beyond the optimum become impractical.

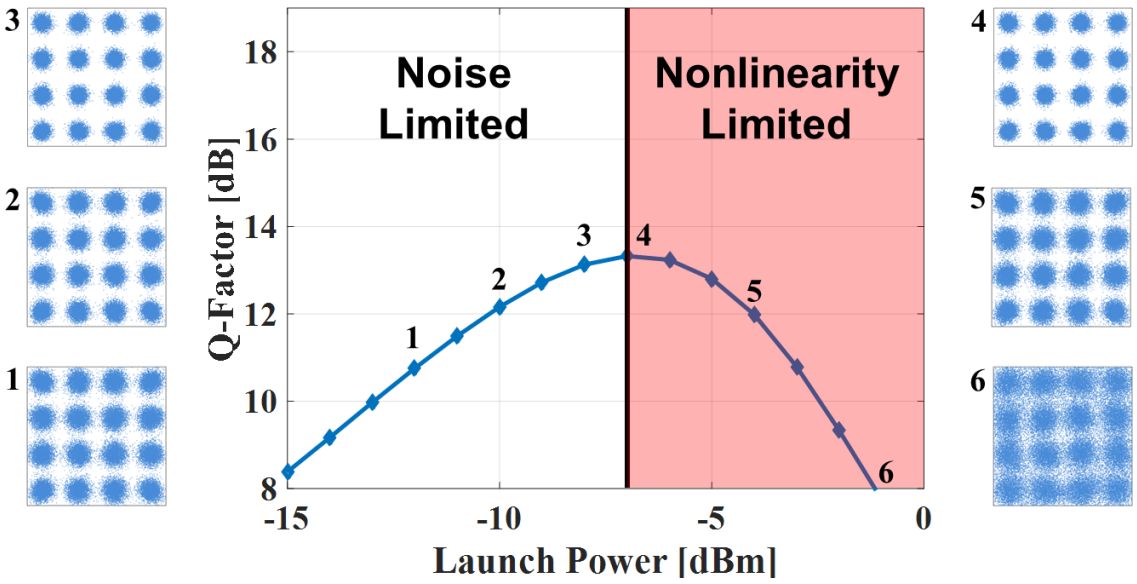

Figure 17. Q-Factor Performance vs. Signal Launch Power

2.5 Fiber Capacity

In 1948, Claude Shannon started the field of Information Theory with his seminal paper titled "A Mathematical Theory of Communications," where he introduced, among other abstract concepts, the bit of information, the information channel and the channel capacity [28]. In his work, Shannon established the notion that any information channel has an upper bound to the rate at which information can be reliably transmitted, which he coined capacity, measured in [bits/s]. In addition, Shannon developed an analytical expression for the capacity of a bandlimited linear channel in the presence of Additive

White Gaussian Noise (AWGN). Shannon's Capacity Formula, also known as the Shannon-Hartley theorem, had the form

$$C = B\log_2(1 + SNR) \tag{2.5.1}$$

where C is the channel capacity, measured in [bits/s], B is the bandwidth of the channel measured in [Hz], and SNR is the Signal-to-Noise Ratio. The resulting capacity curve shown in Figure 18.

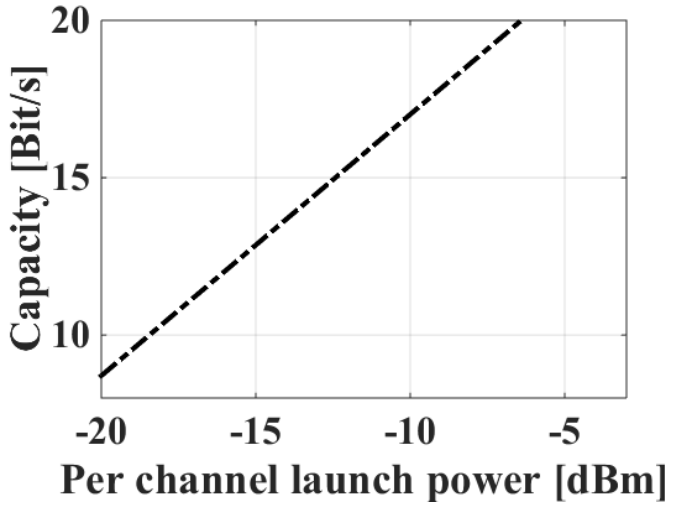

Figure 18. Linear Channel Capacity

Unfortunately, as explained previously, the lightwave channel is nonlinear due to the intensity-dependent index of refraction, and thus, Shannon's formula does not apply to such channels. In this regard, significant efforts have been dedicated to investigate the capacity of light wave channels [10, 29, 30, 31, 32]. The Gaussian Noise (GN) model of nonlinear propagation [32] is a simplified model for the performance in optical fiber transmission that considers the Kerr-induced distortions. Per the GN-model, fiber capacity does not increase monotonically as the channel launch power is increased. Instead the SNR expression is modified to include the effects of fiber nonlinearity [32], taking the form

$$SNR = \frac{P_{Ch}}{P_{ASE} + P_{NLI}} \tag{2.5.2}$$

where P_{NLI} refers to the power of the Nonlinear Interference (NLI) noise, which is related to the signal launch power by

$$P_{NLI} = \eta {P_{Ch}}^3 \tag{2.5.3}$$

where η is a coefficient that depends on the link parameters that is derived in detail in [32].

The GN model indeed predicts that the fiber capacity, instead of growing linearly with the signal launch power, follows a "bell-shaped" curve with a clear maximum, implying that there is an optimum power that achieves maximum capacity. At powers below the optimum, the performance is limited by the ASE noise, whereas at powers above the optimum, the performance is limited by the nonlinear crosstalk. This point of inflexion in the capacity has been coined in the literature as the Nonlinear Capacity Limit [29] and has, as of late, become a constant source of controversy [33, 34, 30, 31, 11].

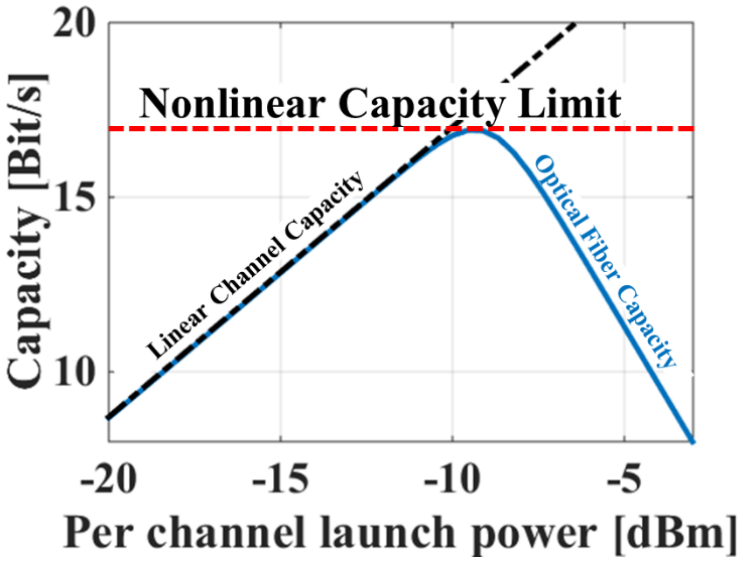

Figure 19. Linear Channel and Optical Fiber Capacity

Currently, in the research community there are two schools of thought regarding the Nonlinear Capacity Limit: on one hand, some think that this limit is insurmountable, and that to accommodate the growing capacity demand we must exploit new transmission dimensions (such as spatial or modal multiplexing) or simply deploy more fibers. On the other hand, another faction argues that, at least in what refers to signal-signal interactions, the crosstalk is a deterministic process and thus should be, at least in principle, cancellable, thereby implying that the capacity limit is significantly higher than what the uncompensated transmission models suggest.

This dissertation aims to prove the latter, supported by the well-established theory of pulse propagation in optical fiber. As seen in Chapter 2, the evolution of deterministic optical waves in an optical fiber must also be deterministic. As such, we argue that any Kerr-mediated interaction among deterministic waves should, in principle, be predictable, and thus, any distortions arising from such interactions should be cancellable.

Chapter 3. Nonlinearity Cancellation with Frequency-Referenced Carriers

3.1 Introduction

As explained in the previous chapter, the nonlinear response in optical fibers gives rise to transmission impairments that do not occur in other well-established communication platforms like the wireless or wireline coaxial channels.

The Kerr effect occurs when an intense light field modifies the refractive index of the material it propagates through, owing to a small, nonlinear polarizability in the material. In most optical devices, and at low optical powers, the refractive-index contribution from the Kerr effect in silica material can be easily neglected. In the spans covered by long-haul fiber networks, however, and given the tight confinement of the optical mode within the fiber, the Kerr effect can seriously degrade signal integrity, especially in modern wavelength division-multiplexed fiber networks, through crosstalk between WDM channels. The degree of degradation depends on the transmitted signal power and the distance over which the signal travels, and the channel spacing. This simple yet powerful notion of WDM crosstalk has shaped both the physical characteristics and the information theory of modern transmission links, which must operate at the threshold of nonlinear distortion, and it also requires that the transmission system designer make fundamental compromises between signal quality and reach.

One obvious way to reduce Kerr effect distortion is to lower the signal power—but that imposes a constraint on the achievable optical-signal-to-noise ratio, and thus, both the capacity and reach of these systems. To get around that limitation, the signal in the majority

of commercial networks is optically re-amplified at periodic intervals using erbium-doped fiber amplifiers. These amplifiers, while greatly extending the physical reach, also generate noise (amplified spontaneous emission) that accumulates along the fiber link, effectively capping the achievable reach or capacity for the transmission for a given acceptable signal quality. To increase the reach, one must increase OSNR, which is possible only by increasing the launch signal power. However, as shown in Figure 17, the launch power level is strictly limited by the nonlinear impairments of the Kerr effect.

Confronted by this nonlinear barrier, transmitting over a longer distance thus requires that the channel be regenerated electronically, by converting photon-encoded bits to electrons and starting all over again. This in turn involves construction of a complex processing chain that first performs fast analog-to-digital conversion, recovers the originally modulated bit stream, and then re-encodes the data onto a laser beam yet again. Effectively, this corresponds to replicating the transmitter and receiver equipment at each point of regeneration. Moreover, each WDM channel requires its own regenerator; hence, for a typical coherent, 100-channel WDM transmission link intended for transcontinental reach, 100 electronic regenerators must be provided, multiple times.

The result, in addition to the obvious capital investment, is greatly increased operating cost, as each channel regenerator consumes 100 W or more in electrical power. Beyond that cost penalty, a more troubling aspect of this trend is the capacity scaling: To increase transmission capacity, channel modulation complexity must also increase, mandating shorter optical reach, higher regenerator cost, or both.

This vicious cycle has spawned an intense search for practical alternatives to electronic regeneration in modern, high-capacity and long reach fiber optic links. One

obvious approach is to reduce amplifier noise through techniques such as distributed Raman amplification, but Raman and hybrid Raman/EDFA links can still carry high costs of operation and deployment. Another approach is to work toward circumventing the Kerr-imposed optical-power limit per channel by increasing the number of spatial modes carried in the fiber. This notion underlies the current, active research emphasis on Space-Division Multiplexing (SDM) to address the growing capacity demand in optical communications.

While advanced SDM has been validated and remains a credible and complementary path for capacity scaling, our lab has focused on a much simpler question: How can the Kerr imposed distortion and corresponding signal power limit be overcome in conventional single-mode fiber?

The Kerr-mediated signal-signal interaction (that is, WDM channel crosstalk) - although a major contributing factor to the so-called nonlinear capacity limit- should not necessarily impose a fundamental limit on the fiber information capacity. Noise-signal nonlinear exchange does limit theoretical capacity, but modern fiber transmission is operating far from that regime. Thus, decoupling Kerr-mediated distortion from the capacity bound begins with addressing the nonlinear signal-signal exchange among WDM channels.

The nonlinear channel interaction in silica fiber can be described accurately, which in principle at least, offers the opportunity to reverse the effect of Kerr distortion. This reasoning has motivated substantial research on Nonlinearity Cancellation (NLC) during the last decade, which has resulted in both physical and computational approaches to invert WDM channel crosstalk. Physical demonstrations based on phase conjugation have proved

to be a robust NLC method, but until now, attempts relying only on DSP-based NLC have been only marginally successful.

3.2 Digital Back Propagation

3.2.1 Principle

Digital Back Propagation (DBP) is one such DSP-based technique that enables the cancellation of linear and nonlinear propagation impairments. As its name indicates, DBP consist of numerically inverting the propagation, in an attempt to reverse the effects of the Kerr interaction. From the perspective of the NLSE, the latter is tantamount to digitally propagating the field in the backwards direction over a virtual link that is a mirror image of the real link [35, 36], in terms of its physical properties and/or evolution.

To develop an intuitive understanding of such method, let us imagine (since it is physically unrealizable) that we can manufacture a fiber with negative parameters to those of SMF, namely negative attenuation (i.e. gain), positive dispersion and negative nonlinearity. If we were to concatenate a regular piece of fiber with this imaginary counterpart, as seen in Figure 20, then any effects occurring in the first piece would essentially be undone in the second, and the transmitted signals would arrive in the same state as they were launched at the beginning of the link.

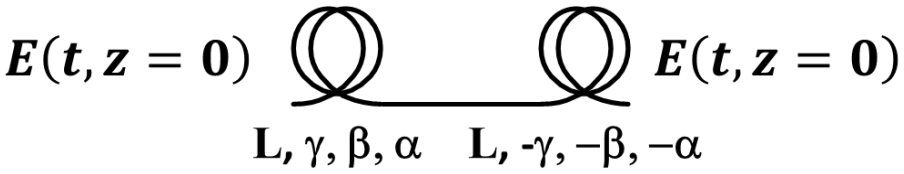

Figure 20. Physical implementation analogy of Digital Back Propagation

In the digital domain, this scenario can be emulated using the Nonlinear Schrodinger Equation [37], which was introduced in Section 2.2, and in the forward direction has the form

$$\frac{\partial A_i}{\partial z} + \frac{1}{v_{gi}(\omega_i)}\frac{\partial A_i}{\partial t} - j\sum_n (-i)^n \frac{\beta_{\mathrm{ni}}}{n!}\frac{\partial^{\mathrm{n}} A_i}{\partial t^{\mathrm{n}}} + \frac{\alpha_i}{2}A_i = j\gamma\left(|A_i|^2 + 2\sum_{m\neq l}|A_i|^2\right)A_i \tag{3.2.1}$$

where i represents the i^{th} channel, A_i represents the mode complex amplitude (each having ω_i carrier frequency), γ is the nonlinear coefficient, while α_i, v_{gi} and β_{n} are mode attenuation, group velocities and dispersion orders, respectively. The latter is defined by the standard expansion: $\beta_{\mathrm{n}} = \frac{d^k n(\omega)}{d\omega^k}$, with n being the effective waveguide refractive index [13].

The propagation in the backwards direction can be performed by taking the following transformations

$$\alpha \rightarrow -\alpha \tag{3.2.2}$$

$$\beta_{\mathrm{n}} \rightarrow -\beta_{\mathrm{n}} \tag{3.2.3}$$

$$\gamma \rightarrow -\gamma \tag{3.2.4}$$

which is essentially the same as inverting the fiber parameters.

It is worth noting that Electronic Dispersion Compensation (EDC) is a special case of DBP in which the virtual link only accounts for fiber dispersion. In the physical implementation analogy, the fiber piece with inverted parameters would simply have negative dispersion, which has actually been realized in practice in the form of Dispersion Compensating Fibers (DCF) or Dispersion Compensating Modules (DCM) [38, 39, 40].

However, there are significant differences between EDC and NLC in their digital implementation. First, because dispersion is a linear effect, the compensation can be done in a per-channel basis. In contrast, the compensation of inter-channel nonlinearities must be performed by processing the full wideband field including all the propagating channels. In addition, given that DBP requires numerically solving the Nonlinear Schrodinger Equation using the Split-Step Fourier Method, the equalization requires multiple steps.

Returning to the system simulation initiated in Section 2.4, we now implement Digital Back Propagation and characterize the performance of the center channel. As shown by the red curve in Figure 21, DBP enables the use of higher launch powers without incurring in a penalty. At a launch power of -1 dBm, the Q-factor improves by over 9 dB, thereby overcoming the performance limit imposed by fiber nonlinearity.

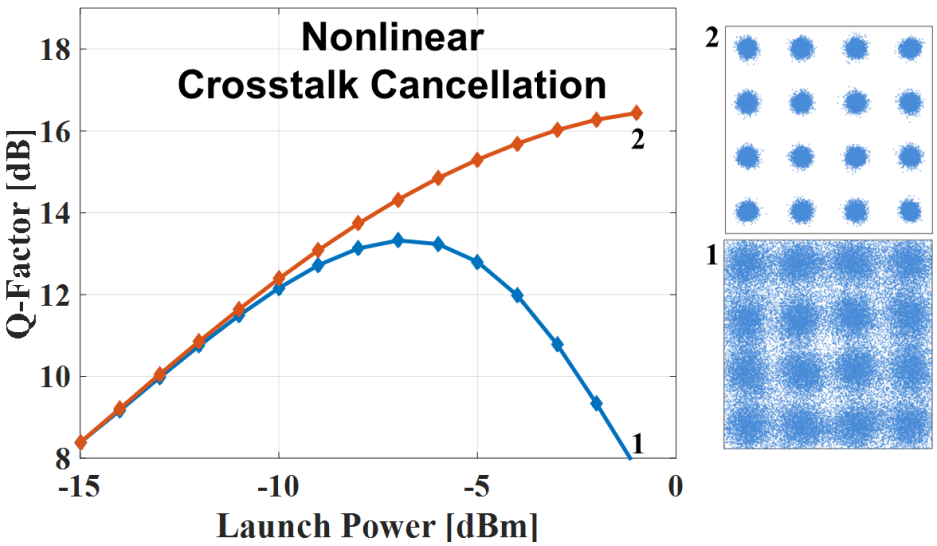

Figure 21. Center channel performance with and without Digital Back Propagation

3.2.2 Challenges

To date, DBP has been demonstrated with significant success only in single-channel systems. In the few experiment-based demonstrations of DBP in multichannel

systems so far, there has been limited success for a variety of reasons. When single-channel DBP was implemented in a multichannel system, the improvement was severely limited because of the lack of compensation of the crosstalk arising from the other channels. More surprisingly, however, in multichannel systems in which the DBP operation accounted for all the propagating channels, only a modest performance improvement was reported [41].

One interesting characteristic of these past multichannel efforts is that they all have mimicked a conventional WDM system, that is, one that uses independent laser emitters. The frequency of each free-running laser fluctuates with respect to all other channels in an uncorrelated, stochastic manner, which according to equation (3.2.1) directly implies that the physical propagation speed in the channel also fluctuates randomly. That random element, in turn, results in unpredictable walk-off rates among interacting information carriers, which eliminates, even in principle, any prospect for reversing nonlinear interaction along the fiber length [11].

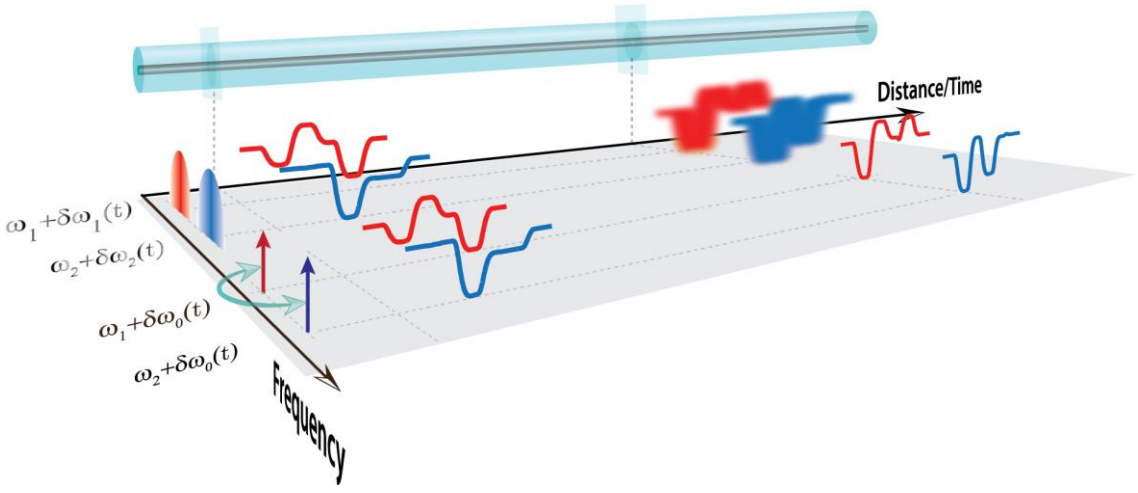

Figure 22. Physical mechanism illustration

Thus, to implement an effective NLC scheme using a theoretical model of the Kerr-mediated interaction, the key step is eliminating this physical uncertainty by seeking a

stable frequency reference frame for all WDM carriers [11]. The frequency reference thus acts as a “railway track” in the WDM system, preventing random frequency walk and ensuring that nonlinear interaction can be predicted and computationally reversed at the end of the path. The most natural approach to providing a “railway track” is one that incorporates an Optical Frequency Comb (OFC).

Optical Frequency Combs have been the subject of intense non-telecom-related research for decades, but practically useful combs have become available commercially only recently. In contrast to conventional, highly stabilized, cavity-defined combs that adhere to a rigid frequency plan, a new class of combs has emerged based on travelling-wave mixers that can be freely tuned, cover the spectral range well wider than C- and L-bands, and use Continuous-Wave (CW) telecom diodes rather than pulsed, research-class lasers. The quality of the carriers derived from these new comb emitters is comparable to a kHz-linewidth, shot-noise-limited CW source, and is substantially higher than that of a common mode-locked laser. In fact, multiple experimental demonstrations have validated these combs as outstanding carriers for coherent modulation formats [42, 43].

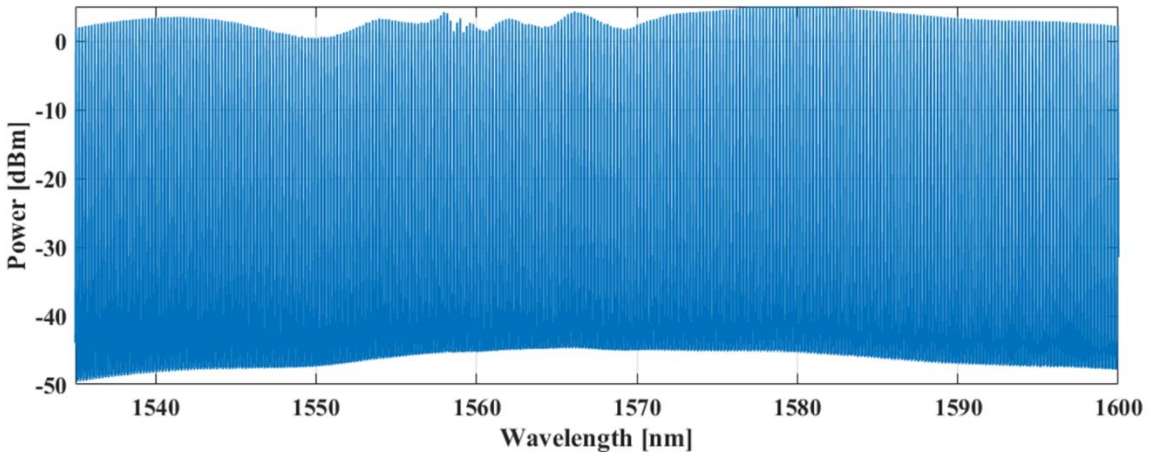

Figure 23. Optical Frequency Comb spectrum

In the context of fiber communications, such a frequency comb, by acting as a physical WDM channel grid, can provide equidistant tones that can act either as information carriers or, at either end of the coherent transmission link, as local oscillators. Once that frequency frame is established, an effective NLC can be accomplished at the transmitter side (pre-compensation), receiver side (post-compensation) or partially at both ends of the transmission system.

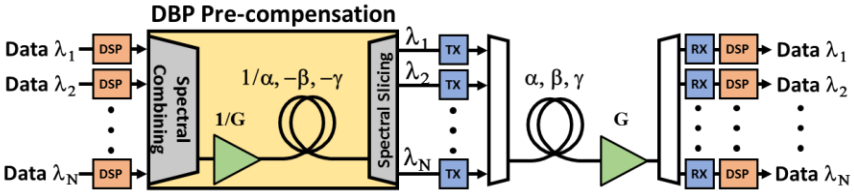

Figure 24. Nonlinearity Cancellation at the transmitter-side

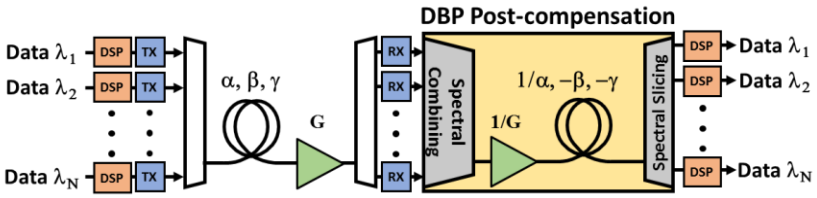

Figure 25. Nonlinearity Cancellation at the receiver-side

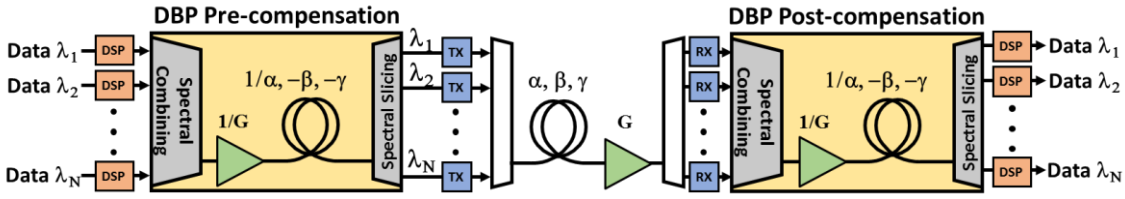

Figure 26. Nonlinearity Cancellation split between the transmitter- and receiver-sides

Regardless of the specific choice for NLC deployment, a successful implementation should comprise two critical components: Frequency-Referenced Carriers (FRCs) and an inverse calculation engine. In the most straightforward implementation, the inverse calculation is performed numerically, by retracing the propagation along the fiber

link in which the impairment was incurred. In simple terms, this back-propagation "untangles" the trajectories through which the information channels passed while their information content. More specifically, by calculating the inverse solution of the nonlinear Schrodinger equation that governs the propagation, one can recover the physical WDM channels substantially free of nonlinear crosstalk. The FRCs, meanwhile, ensure that a unique correspondence exists between the virtual link in which the inverse NLSE solution is calculated and the physical one in which actual propagation takes place.

3.2.3 Frequency Referenced Carriers

As explained in the previous section, the precise knowledge of the optical carrier frequency is critical for the inversion of nonlinear interaction effects. To clarify this important requirement, consider N co-polarized frequency modes, described by the equation

$$E(t, z = 0) = \sum_{m=1}^{N} e^{-i\omega_m t} \sum_{k} A_{mk} p(t - kT) \tag{3.2.5}$$

where the index m represents the m^{th} channel, ω_m is the channel's carrier frequency, A_{mk} is the k^{th} symbol's complex amplitude, and $p(t - kT)$ represents the pulse shape. In a single-mode waveguide, the interaction will be fully described by a set of coupled scalar nonlinear Schrödinger Equation (3.2.1) [9].

The wave interaction defined by Equation (3.2.1) is deterministic and stable [15, 16] allowing, in principle, the computational inversion of dispersion and any distributed Kerr interaction. Indeed, this notion was the basis for recent nonlinear cancellation effort that solves inverse-propagating NLS relation [35, 36] by means of Digital Back

Propagation, as described in Section 3.2. However, in practice these attempts have led to limited impairment suppression [44, 45, 41].

As pointed out in Section 3.2.2, NLC that relies on the inversion of Equation (3.2.1) faces a fundamental challenge that was not addressed in prior experimental studies; the NLS inversion requires precise knowledge of modal carrier frequencies, which has only recently been investigated by a theoretical study [11].

Let us now consider the propagation of N co-polarized frequency modes where each mode is known to deviate from its center frequency. In this case, the equation describing these modes becomes

$$E(t, z = 0) = \sum_{m=1}^{N} e^{-i(\omega_m + \delta\omega_m(t))t} \sum_{k} A_{mk} p(t - kT) \tag{3.2.6}$$

where $\delta\omega_m(t)$ represents the carrier's random time-dependent frequency deviation with respect to its center frequency ω_m. During propagation, the stochastic carrier frequency uncertainty is mapped to a mode velocity ambiguity via waveguide chromatic dispersion [11], and, while the Kerr-mediated process is deterministic, the resulting nonlinear interaction appears random. Indeed, experimental demonstrations to date [44, 45] have relied on uncorrelated (free-running) emitters, inherently reducing the modal frequency (and phase) stability. In this case, the carrier frequency uncertainty is transformed to stochastically varying walk-off rate between the modes, leading to diverging inversion of Eq. (3.2.1).

Returning to the system simulation initiated in Section 2.4 and expanded in Section 3.2.1, we simulate the effect of a frequency deviation in the center channel of a 7-channel system that employs Digital Back Propagation. Figure 27 shows the performance of the

center channel, where the ideal DBP performance is represented by the red curve (DBP – 0 MHz), and the other curves represent the performance when the frequency of the center channel in the physical transmission system deviates from its ideal value.

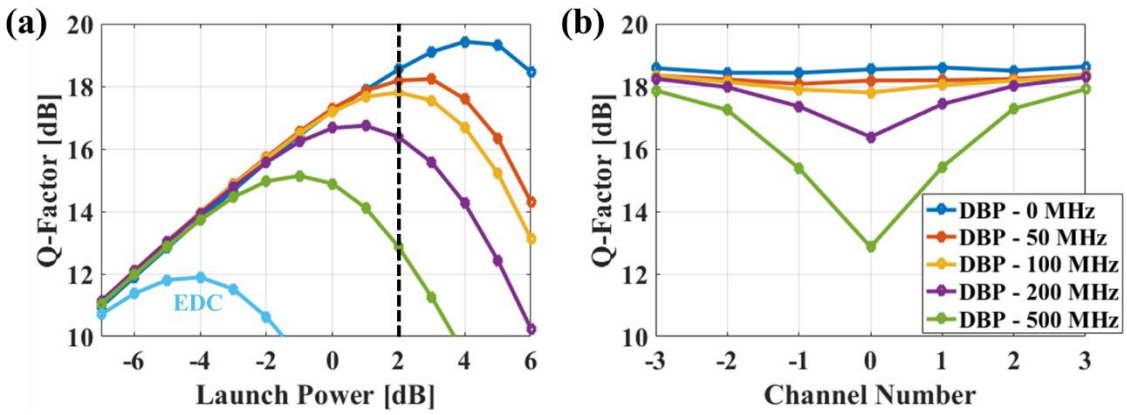

Figure 27. Penalties in Digital Back Propagation due to laser frequency uncertainty (a) Q-Factor vs. Launch Power (b) Q-Factor vs. Channel number

It is apparent from Figure 27 that even the smallest carrier frequency deviations have catastrophic effects in the NLC process. This issue becomes particularly worrisome if we consider that state-of-the-art External Cavity Lasers (ECL) recommended by the International Telecommunication Union (ITU), namely the Integrated Tunable Laser Assembly (iTLA) are specified with an end-of-life frequency accuracy of 1.5-3 GHz. Consequently, system implementations that rely on the reversibility of multichannel nonlinear interaction will require a lightwave source that can generate carriers with high degree of mutual coherence and precise control of the carrier spacing.

As proposed in Section 3.2.2, the optical frequency comb is the ideal instrument to guarantee a static carrier spacing. It is important to recognize that optical frequency combs are not perfectly stable since after all, optical frequency combs are also derived from an optical seed that will suffer the same stochastic center-frequency variations. However,

while the center frequency of the comb may vary, the carrier spacing, which is ultimately determined by Radio-Frequency (RF) oscillators that are orders of magnitude more stable than optical oscillators, will be strictly maintained.

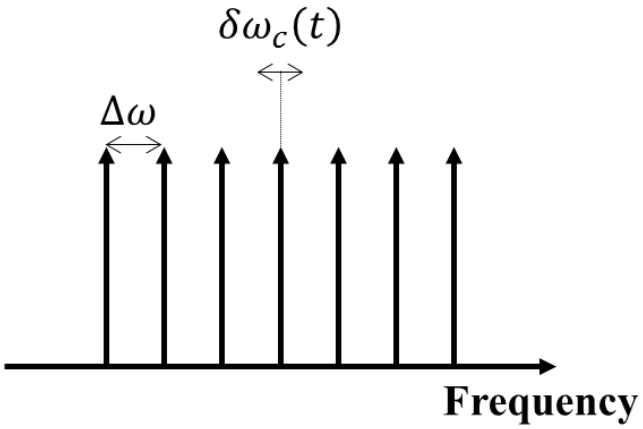

Figure 28. Comb center frequency deviation and fixed carrier spacing

To illustrate the last point quantitively, let us consider the transmission of N co-polarized frequency modes extracted from an optical frequency comb centered at ω_0. In this case, the equation describing these modes becomes

$$E(t, z=0) = e^{-i(\omega_0+\delta\omega_c(t))t} \sum_{m=-\frac{N}{2}}^{\frac{N}{2}} e^{-i(m\cdot\Delta\omega)t} \sum_k A_{mk} p(t-kT) \tag{3.2.7}$$

where $\delta\omega_c(t)$ represents the comb's center frequency deviation and $\Delta\omega$ is the comb pitch. In this case, the center frequency of the comb deviates, but it affects all channels equally, and thus, the channel frequency spacing is maintained constant, as is the relative walk-off between the channel, to the first order, or more specifically, defined by the curvature of the dispersion characteristics, defined by the β_3 parameter. Thus, the nonlinear interaction remains deterministic and can still be accurately predicted. The comb center frequency

deviations only become significant when they reach tens of GHz, or in systems with large dispersion slope, which is rarely the case and certainly not an issue in SMF-based links.

Recognizing this basic requirement, we devised a set of three NLC experiments to quantify the role of mutually frequency-correlated emitters. Specifically, the carriers were directly derived from a parametric frequency comb seeded by a single, continuous-wave master oscillator [46].

3.3 Experimental Demonstration 1: Noise-Unimpaired Nonlinearity Cancellation

As with any Kerr-mediated interaction, the presence of noise limits the reversal of the crosstalk-induced distortion. The first experiment illustrates Kerr-inversion physics and nonlinear reversal in a pump-probe configuration that is practically noise unimpaired. Both the intense (pump) and weak (probe) waves had very high signal-to-noise-ratio (SNR) and propagated over a short, nearly lossless, Highly Nonlinear Fiber (HNLF) segment to guarantee that Kerr-induced impairments dominate over stochastic, noise-induced distortions. Both pump and probe waves, separated by 30 nm, were derived from a parametric comb source and had OSNRs in excess of 40 dB. The probe, which experienced severe distortions due to the Kerr-induced crosstalk from the pump, was then precompensated to achieve a distortion-free reception.

3.3.1 Experimental Setup

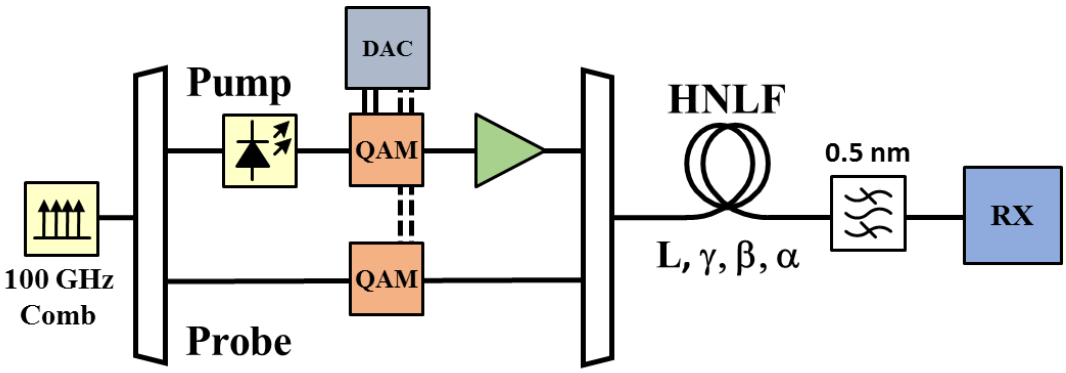

Figure 29. Pump-probe cross-phase modulation pre-compensation schematic

The pump-probe setup is shown in Figure 29. The co-polarized pump and probe modulated waves, centered at 1588 and 1558 nm, respectively, were launched into a 1100 m-long HNLF. To ensure the necessary mutual coherence between the two waves, they were extracted from a 100 GHz-pitched parametric optical frequency comb. The OSNR of the pump was maximized by injection-locking a 100-mW Distributed Feedback (DFB) to the comb line at 1588 nm prior to being modulated and amplified by an EDFA booster. To suppress an onset of the Stimulated Brillouin Scattering (SBS) threshold in the HNLF, the pump was also phase-modulated with pseudo-random multi-level pattern. Figure 30 demonstrates the effective suppression of SBS, wherein a threshold cannot be observed even at maximum pump powers.

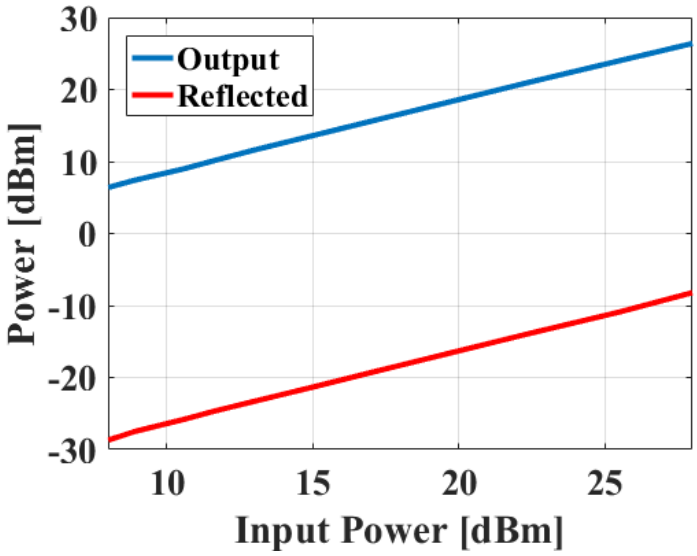

Figure 30. SBS measurement for HNLF

Considering the relatively short interaction length in this experiment (1100 m), and the correspondingly constrained walk-off between the two waves, the full NLSE inverse calculation was found to be superfluous in this case. Rather, a direct precompensation was performed on the signal, whereby, upon successful coherent detection, the signal was pre-distorted in real-time by adjusting its waveform amplitude and phase (on a point-by-point basis) by subtracting the XPM generated distortion from the input waveform. In effect, the applied pre-distortion profile was the difference between the launched and detected waveforms (for both imaginary parts of the electric field), ultimately allowing a full restoration of the ideal signal waveform.

It ought to be emphasized that, while the described setting might have no direct bearing on optical communication systems, this experiment was nevertheless of interest from a fundamental scientific perspective, and may become useful in several sensing and high speed all-optical signal processing applications, where the dynamic range and/or sensitivity are limited by the waveguide nonlinear response.

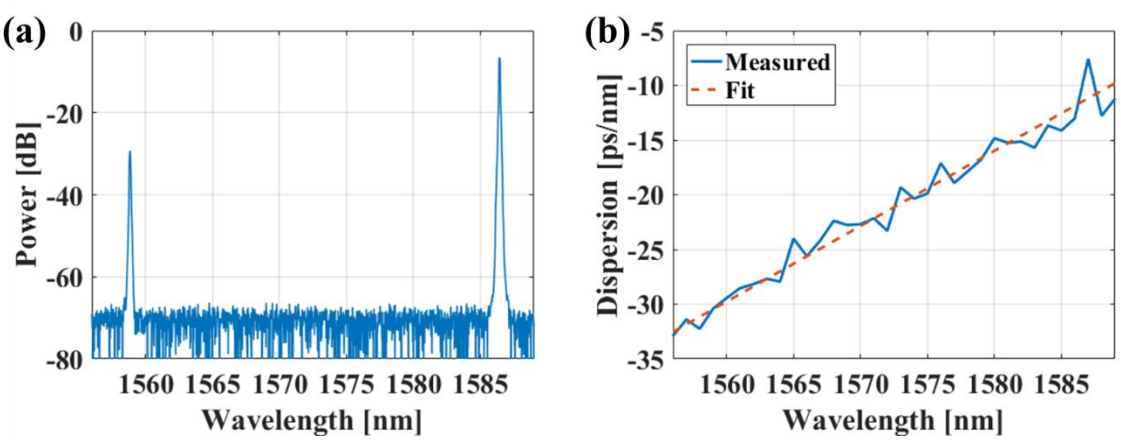

Figure 31. (a) Pump and probe spectrum (b) HNLF dispersion profile

The pump and the probe were launched into 1100 m long HNLF with nonlinear parameter of 7 $W^{-1}km^{-1}$, dispersive parameters β_2 = 37.9 ps^2/km, β_3 = -0.06 ps^3/km and transmission loss of α = 0.6 dB/km. This segment was specifically selected to guarantee sufficient walk-off between pump and probe and provide clear distinction among the nonlinear interaction mechanisms. As shown in Figure 31, the pump beam, centered at 1588 nm, was amplified to 250 mW power level and was amplitude modulated to achieve strong cross phase modulation (XPM). The signal wave, centered at 1558 nm and co-polarized with the pump had two orders of magnitude lower power (1 mW) and was amplitude modulated.

3.3.2 Results

The weak wave (probe) experienced significant distortion (red curve in Figure 32) that can be completely reversed by NLC in the high SNR regime, eliminating any distinction between the launched (black) and compensated (green) waveform. This contrast is even more apparent in the spectral domain, as shown in Figure 32.

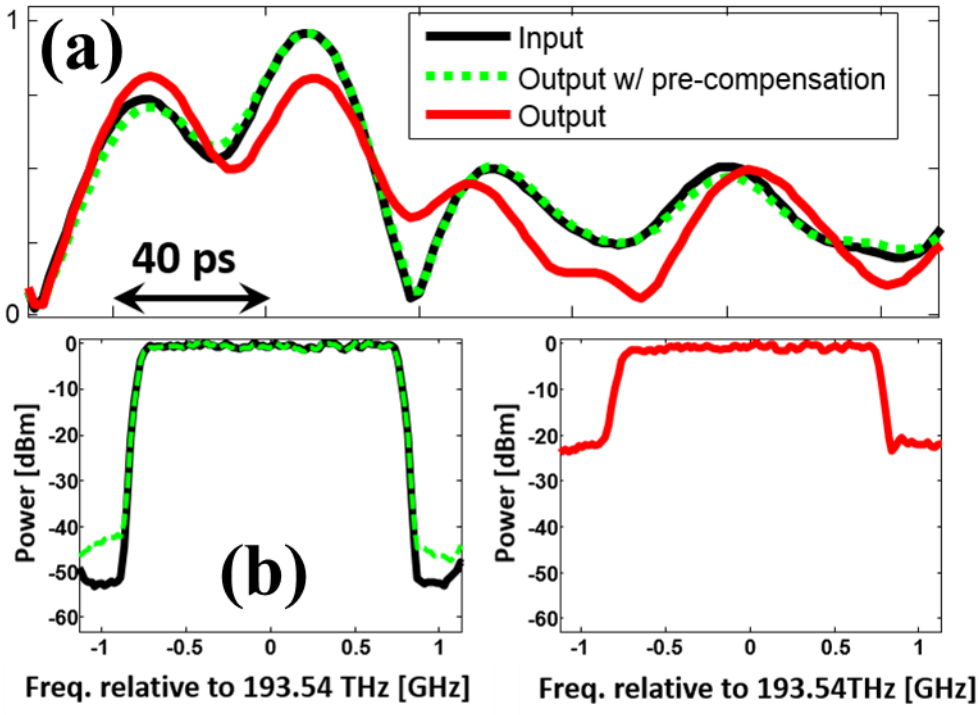

Figure 32. Pump-probe cross-phase modulation compensation
(a) Time domain response (b) Spectra with same color-coding scheme

3.4 Experimental Demonstration 2: Nonlinearity Cancellation in Long-Haul Transmission

In the second experiment, we demonstrate the reversal of non-linear crosstalk in coherent Wavelength Division Multiplexed transmission. In this case, the transmission is performed in a recirculating loop [47] emulating a modern communication link with three WDM channels; the signals are transmitted over 1000 km and reamplified periodically after each span of 85km of standard single mode fiber. Due to the long transmission length and the significant accrued dispersion, the NLC is performed by precompensating the signals using multichannel DBP.

3.4.1 Experimental Setup

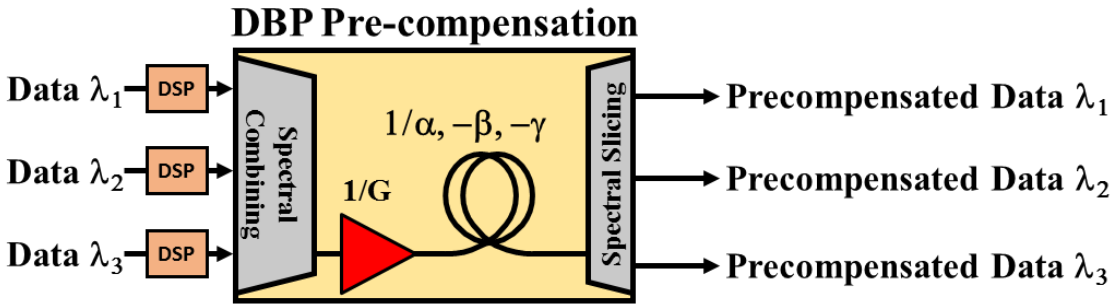

Figure 33. Digital Back Propagation block

The detail of the DBP block is shown in Figure 33. The data to be transmitted on each of the WDM channels are mapped to a desired modulation format and subsequently combined and passed to a full-field (back-propagating) NLSE engine taking into account the transmission link parameters. Subsequently, the NLSE full-field output is channelized into spectral slices and independent, but fully-synchronously pre-distorted waveforms are generated for each channel. In this experiment, an internally developed graphics processing unit (GPU)-assisted NLSE solver was used as the DBP computational engine [11]. The DBP engine served to calculate the inverse to the actual propagation in the physical link – thus mirror-imaged power evolution (to that of the physical link) and taking into account opposite signed fiber parameters (dispersion and nonlinearity), as well as reciprocals of amplifier gain and attenuation, as explained in detail in [11]. The calculation was based on a symmetric split-step NLSE solver with 0.01 degrees allowed phase variation in the nonlinear step, wherein blocks of 216 symbols were processed using 4 samples per symbol, a frequency resolution of ~48 kHz and a time resolution of ~7.8 fs. The full schematic of a system employing transmitter-side DBP is shown in Figure 34.

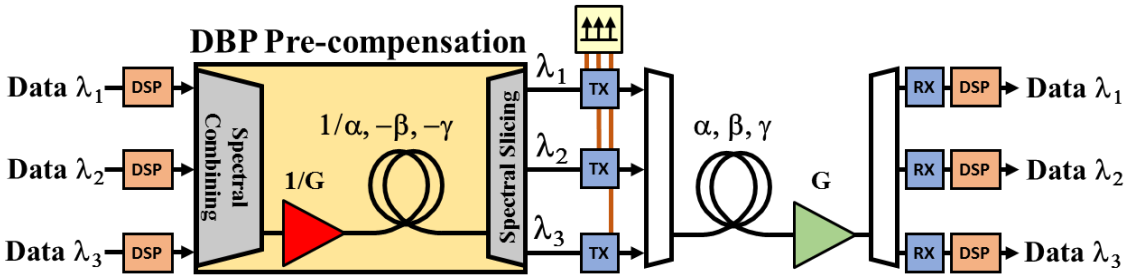

Figure 34. WDM Transmitter-side DBP implementation

The 3-channel WDM DBP-transmitter implementation is presented in Figure 35. A 25 GHz-pitched narrowband parametric frequency comb was generated following the guidelines found in [46]. Two Distributed Feedback lasers served as comb seeds that were injection locked to spectral lines of a phase-modulated External Cavity Laser with 3 kHz linewidth. The optical comb was demultiplexed using a Waveshaper Optical Processor (OP), availing mutually coherent optical carriers with OSNRs in excess of 45 dB and sub-5 kHz linewidth. Different shift-register initial conditions were used to generate three Pseudo-Random Bit Sequences (PRBS) that were subsequently gray mapped to 16-Quadrature Amplitude Modulation symbols. Transmitter DSP consisted of raised-cosine filtering using 4 samples-per-symbol, 128 filter taps and roll-off factor of 0.1 was applied prior to the DBP computation to constrain the spectral occupancy. Three Digital to Analog Converters (DAC) [19] were used to generate the electrical pre-distorted signals at the rate of 64 GS/s. The DACs exhibited clock feed through, which generated a tone at 16 GHz that was filtered using 4th order electrical Bessel filters. The pre-distorted 16 GBaud 16-QAM signals were cast onto the optical carriers by means of nested Mach-Zehnder modulators (NMZM), passively coupled, and a Polarization Beam Splitter (PBS) was used to ensure that all channels were co-polarized. The time alignment of all channels was controlled to within 5 ps and was accomplished by means of optical delay lines and

synchronous triggering of the DACs. It is important to note that all carriers were frequency referenced but no effort was made to control the channel's relative optical phases [11].

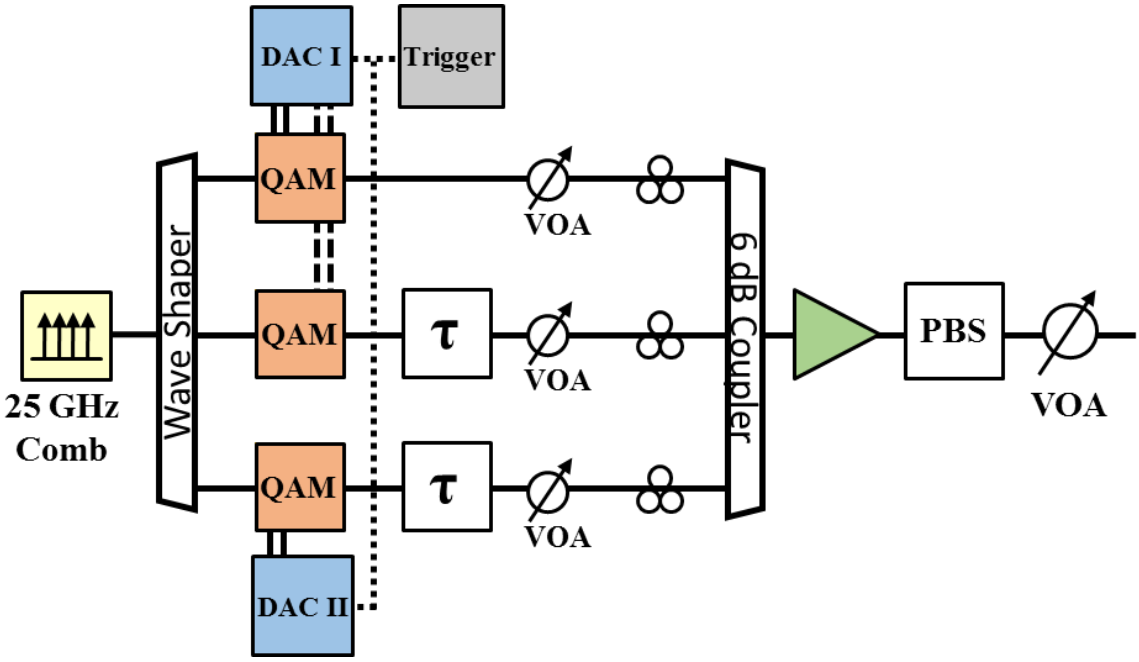

Figure 35. WDM Frequency-Referenced Transmitter implementation
DAC: Digital-to-Analog Converter QAM: Quadrature-Amplitude Modulator. τ: Variable optical delay line. PBS: Polarization beam splitter. VOA: Variable optical attenuator.

The transmitter was optimized to accurately replicate the full-field output of the DBP-block. To characterize the back-to-back performance, the generated pre-compensated optical waveforms of all channels were asynchronously acquired using a coherent receiver in homodyne configuration. Subsequently, the full optical field was digitally reconstructed and virtually propagated using the same NLSE computation as in the DBP-block. The constellations generated by virtual propagation, were then characterized in terms of the worst-case Q-factor, and an optimum pre-emphasis profile was found and applied to correct any non-ideal frequency and phase responses of the filters, electrical amplifiers and electro-optic modulators [48].

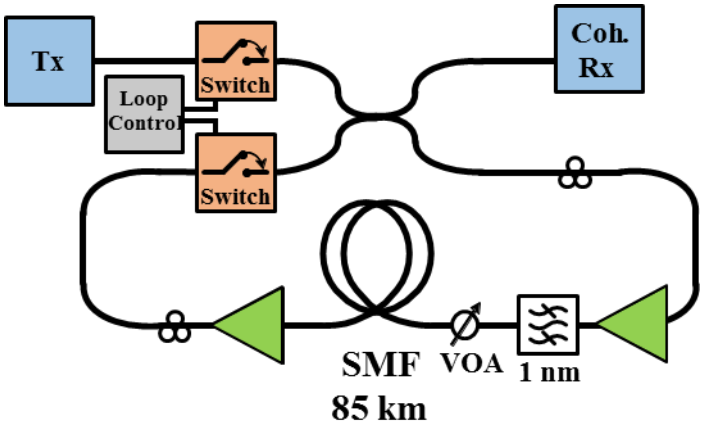

Figure 36. Recirculating loop
TX: Frequency Referenced Transmitter. VOA: Variable Optical Attenuator. SMF: Single-Mode Fiber. Coherent RX: Coherent Receiver

The transmission experiment was performed in a recirculating loop implemented as shown in Figure 36. A single 85 km span of Standard Single-Mode Fiber (SSMF) with 16 ps/nm/km dispersion, nonlinear coefficient of 1.22 $W^{-1}km^{-1}$ and total attenuation of 15.95 dB served as the transmission fiber inside the loop. Fiber loss was compensated by an Erbium Doped Fiber Amplifier with 4.5 dB noise figure and a second EDFA was employed to compensate the loop-associated losses and allow a wide range of launch powers. A 1 nm-wide WDM Optical Filter was used to remove the out-of-band ASE noise before launching the signals into the fiber. The combined loss of the loop components from amplifier B to amplifier A was 9.5 dB and the loop-associated optical signal-to-noise ratio with respect to the channel launch power and number of loops are shown in Figure 38.

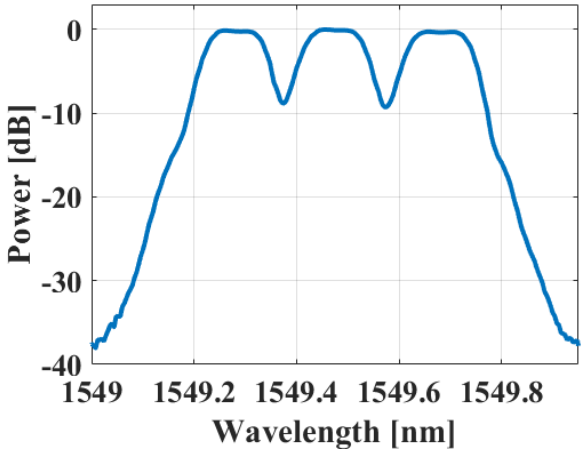

Figure 37. Three-channel spectrum before transmission

After transmission, the signals were independently filtered, down converted using a local oscillator (LO) with <100 kHz linewidth and were coherently detected. The coherent receiver consisted of an integrated 90-degree hybrid and a pair of balanced detectors with 40 GHz Bandwidth. The electrical signals were digitized using a real-time oscilloscope at the rate of 100 GS/s and offline processing was performed on a personal computer running MATLAB. Receiver DSP operated on blocks of 216 symbols using 4 samples per symbol and consisted of the standard filtering chain for coherent receivers [26], including receiver front-end correction, timing recovery, carrier frequency and phase estimation and least mean squares adaptive equalization relying on the constant modulus algorithm for pre-convergence. The bit-error rate measurements were performed by error counting in a sufficient collection of samples satisfying the 90% confidence interval [49], and Q-factors were extracted from BER measurements.

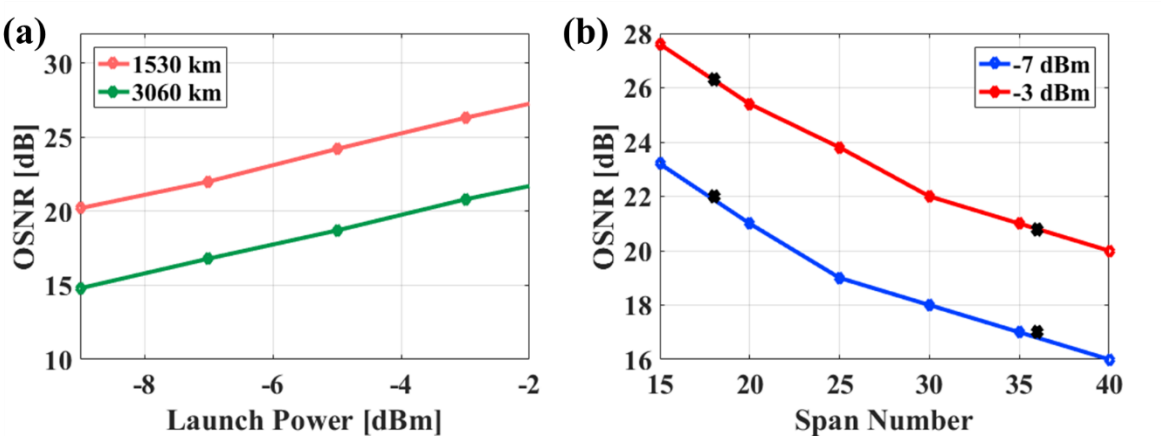

Figure 38. Measured OSNR at linear and nonlinear reach

To gauge the role of frequency stabilization in nonlinear inversion of Equation (3.2.1) the performance of three different configurations was tested, as shown in Figure 39. The first measurement was performed with lasers with uncorrelated carrier frequencies, i.e. free-running. The second measurement was performed with two mutually coherent channels, where the side carriers were derived from a frequency comb centered at 1549.3 nm and separated by 75 GHz, whereas the center channel was derived from a free-running laser. Lastly, a third measurement was performed with all three channels derived from a frequency comb, thus guaranteeing full mutual coherence.

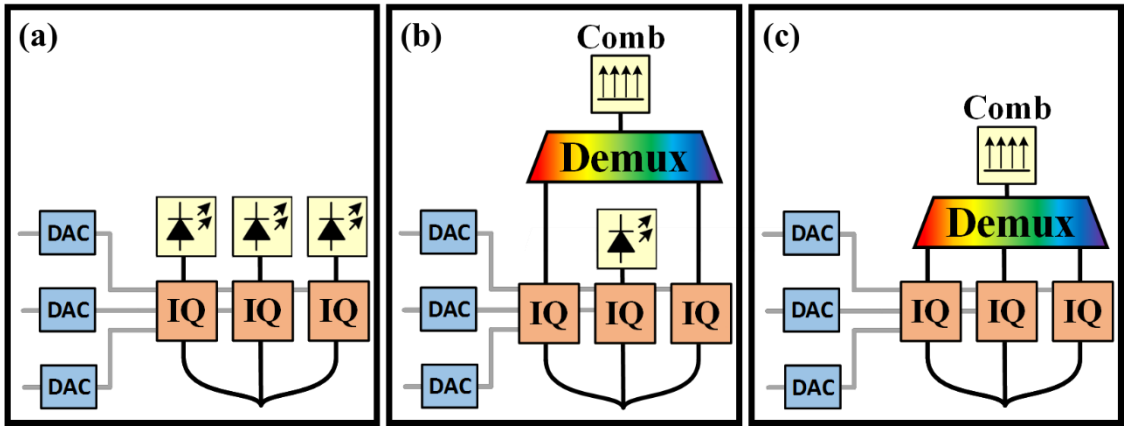

Figure 39. Transmitter schematic with three mutual-coherence configurations
(a) Free-running lasers (b) Two mutually-coherent carriers and one free-running laser
(c) Three mutually-coherent carriers

To illustrate the scalability of the nonlinearity pre-compensation principle, additional experiments were performed with 5 channels, with some constraint on the quality of the available equipment. In this experiment, five lines were extracted from a 25 GHz pitched frequency comb and were used as carriers in the transmission and the same three degrees of coherence between the carriers shown in Figure 39 were investigated.

3.4.2 Results

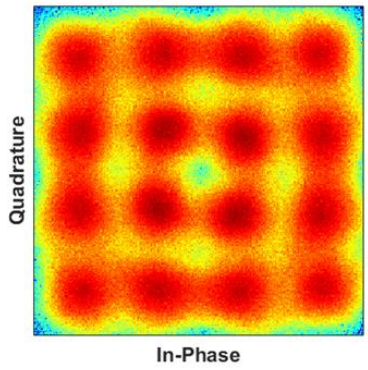

Figure 40. Center channel constellation for 2 dBm launch and EDC-based transmission

The constellation of the center channel for a launch power of 2 dBm when EDC is employed with the comb-derived carriers is shown in Figure 40, exemplifying the significant Kerr-induced distortions that occur at such high power. The measurements in Figure 41 clearly demonstrate the effective suppression of the nonlinear interaction; even after the distributed 1020 km-long nonlinear interaction and ten-fold increase in the signal launch power beyond the optimum, the transmission quality (determined in terms of Q-Factor) is maintained. The saturation in performance and its eventual decline are attributed to the Kerr-induced signal-noise interaction [50] (which is an inherent fundamental limit on the achievable performance), as well as the limitations of the experimental setup,

particularly, the fast arbitrary waveform shaping necessary to launch the inverted NLSE solution, which have become available only recently [19].

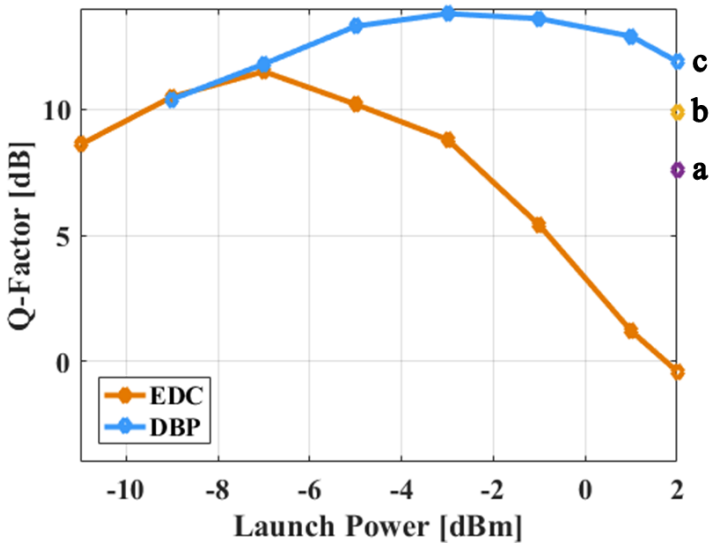

Figure 41. Measured performance of the central channel with and without the nonlinear cancellation based in a three-channel system

As explained in Section 3.4.1, to further corroborate the critical importance of frequency referencing and its impact on the nonlinearity compensation ability, the performance was measured with three frequency-uncorrelated (free-running) carriers, and with a combination of correlated and uncorrelated carriers, whereas the latter was realized by two comb-referenced channels, while substituting the middle carrier by a single free-running laser. The performance of the three different carrier coherency configurations at launch power of 1.6 mW (2 dBm) is shown in Figure 41, and the resulting constellation diagrams are given in Figure 42.

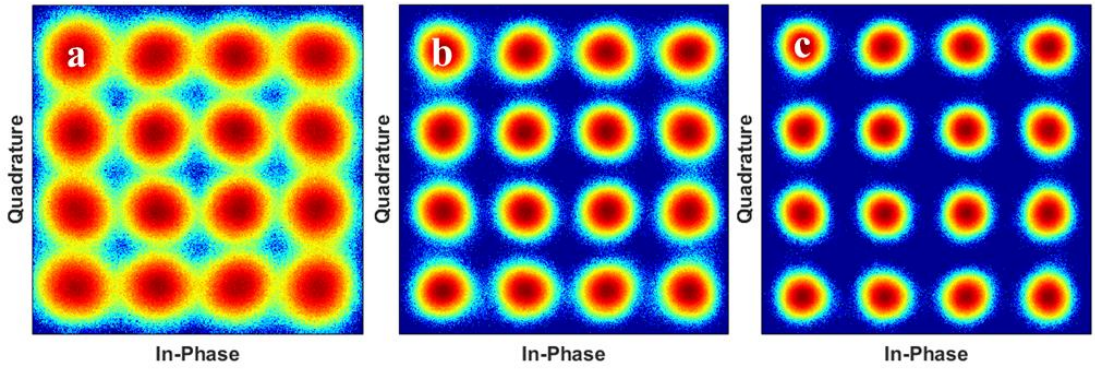

Figure 42. Center channel constellations with DBP-based transmission for 2 dBm launch power per channel in a three-channel system with (a) Uncorrelated carriers (b) Two mutually coherent side carriers and middle uncorrelated carrier (c) All three mutually coherent carriers

The results in Figure 42 clearly show that as the level of the mutual coherence between the interacting waves is increased (i.e. from the complete lack of coherence for three free-running oscillators, all the way to the full frequency referenced system), a qualitative improvement of the signal restoration is obtained, fully attesting to the gradual increase in the ability of the ensuing nonlinear interaction reversal. Particularly, when compared with the fully referenced system, the frequency uncertainty of only the middle carrier suffices to prevent a stable nonlinear compensation.

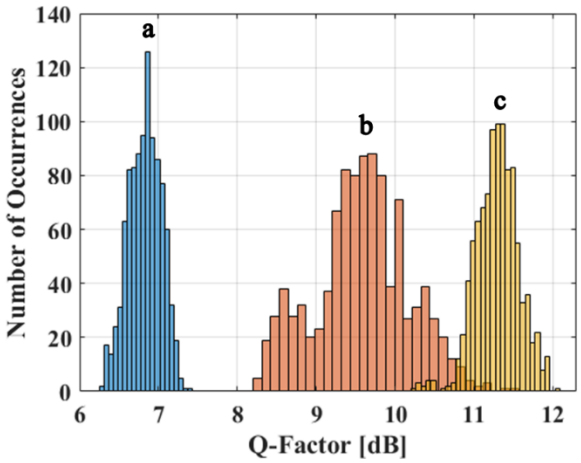

Figure 43. Center channel performance histogram over 2200 measurements for 2 dBm launch power per channel for three mutual coherence configurations in a three-channel system
Blue –Uncorrelated carriers; Pink –Two mutually coherent side carriers and (middle) one uncorrelated carrier; Yellow –All three mutually coherent carriers.

Indeed, we observed a considerable variation of the output signal condition that is reflected by a widely varying figure of merit accumulated over 2200 measurements, as shown by the histogram in Figure 42. We emphasize that, contrary to the widespread opinion that nonlinear interaction reversal is only a matter of computation, presented results clearly demonstrate that no amount of computational complexity can make up for the mutual coherence of the modes (in the interaction reversal).

We note that information capacity in the strict sense [28] cannot be measured experimentally. However, the experiments attest to the capacity increase beyond the presently accepted limits by demonstrating reversal of signal-signal interactions, assumed to be non-viable in previous information capacity treatments [10, 29].

The Q-factor vs. launch power results for the five-channel system are shown in Figure 44, wherein, except for at the very high launch powers, these results fully quantitatively replicate the measurements obtained with three channels. The observed quantitative departure in performance in the range of high launch powers is attributed to the limitations of the equipment available at the time of experimentation. Figure 45 shows the resulting constellations, and Figure 46 shows the performance histograms, from which the same conclusions as in the three-channel experiment can be drawn.

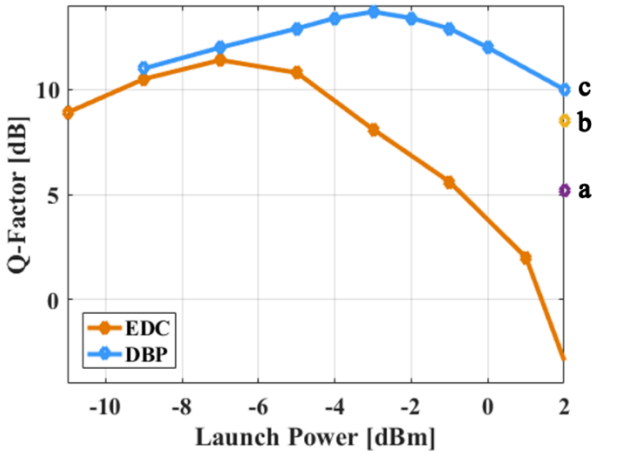

Figure 44. Measured performance of the central channel with and without the nonlinear cancellation based in a five-channel system

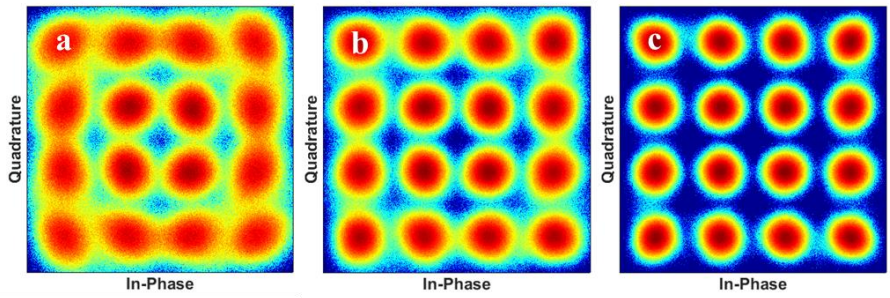

Figure 45. Center channel constellations with DBP-based transmission for 2 dBm launch power per channel for five-channel system with (a) Uncorrelated carriers (b) Two mutually coherent side carriers and middle uncorrelated carrier (c) All three mutually coherent carriers

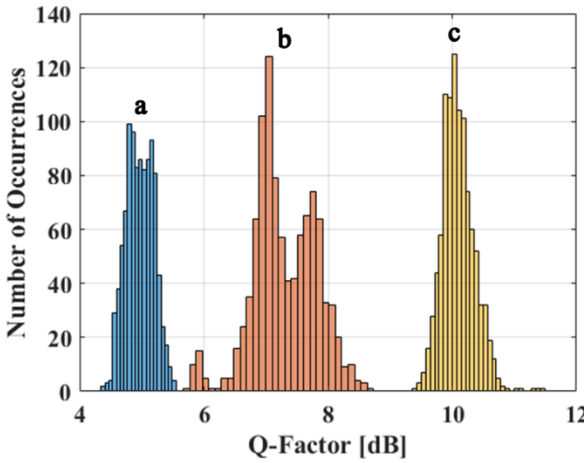

Figure 46. Center channel performance and its variation over 2200 measurements for 2 dBm launch power per channel for three mutual coherence configurations in a five-channel system
Blue –Uncorrelated carriers; Pink –Two mutually coherent side carriers and (middle) one uncorrelated carrier; Yellow –All three mutually coherent carriers.

3.5 Experimental Demonstration 3: The First Demonstration of a Two-Fold Transmission Reach Enhancement

In the third experiment, we demonstrate the reversal of non-linear distortion in coherent wavelength division multiplexed transmission employed to extend the system reach. As in Section 3.4.1, the transmission is performed in a loop emulating a modern communication link with three WDM channels. Again, due to the long transmission length and the significant accrued dispersion, the NLC is performed by precompensation the signals using multichannel DBP.

3.5.1 Experimental Setup

The experimental setup used in this demonstration is identical to that in Section 3.4.1. Firstly, the performance of the system is compared with and without the compensation of the non-ideal transfer function of the transmitter components.

Subsequently, the three channels are transmitted to the maximum distance possible that would achieve a Q-factor performance that satisfies the Forward Error Correction (FEC) threshold. In this experiment, the chosen FEC BER threshold was 10^{-3} (Q^2 = 9.8 dB), corresponding to a simple Reed-Solomon (255,233) code. Two transmission scenarios were investigated. In the first case, only linear impairment compensation was applied, i.e. the DBP pre-compensation block at the transmitter was disabled and Electronic Dispersion Compensation was applied at the receiver by means of a T/2-spaced finite impulse response filter (where T is the symbol period), with the number of taps chosen following the guidelines found in [26]. In the second case, both linear and nonlinear impairment

compensation was employed at the transmitter side, i.e. the DBP pre-compensation block was enabled, leaving no need for any further dispersion compensation at the receiver.

3.5.2 Results

A comparison between the spectra of the ideal signal and the modulator output is presented in Figure 47. The waveform shown corresponds to the center channel pre-distorted signal for transmission over 3000 km and 1 dBm launch power. The spectrum of the modulator output without digital pre-emphasis is shown in Figure 47 (a). The frequency response of the components in the transmitter exhibit a roll-off that attenuates the signal at high frequencies. Figure 47 (b) shows the spectrum of the output of the modulator for the appropriate pre-emphasis fully matching the ideal numerically calculated pre-distortion spectrum. It is worth noting that the example shown is that for a highest power tried in the experiment, where the nonlinear pre-distortion departs the most from the EDC-only counterpart. Furthermore, Figure 48 shows the back-to-back constellations before and after successful application of the pre-emphasis. Quantitatively, the pre-emphasis yielded 9.3 dB of performance improvement. The results shown in Figure 47 and Figure 48 are utmost important for NLC and serve to evaluate the ability of precise waveform shaping, which plays a crucial role in the pre-compensation of nonlinear effects.

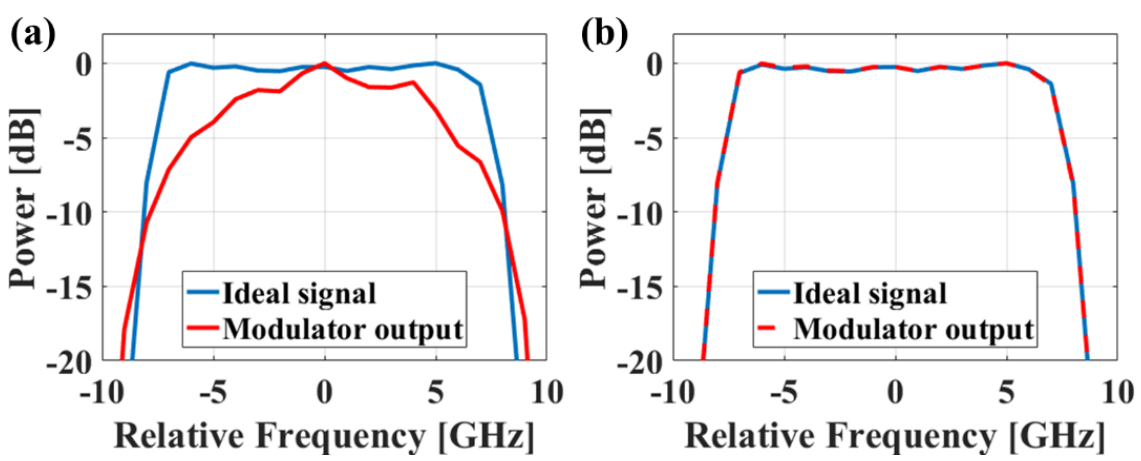

Figure 47. Spectra of (a) Generated optical signal without digital pre-emphasis (b) Generated optical signal with digital pre-emphasis.

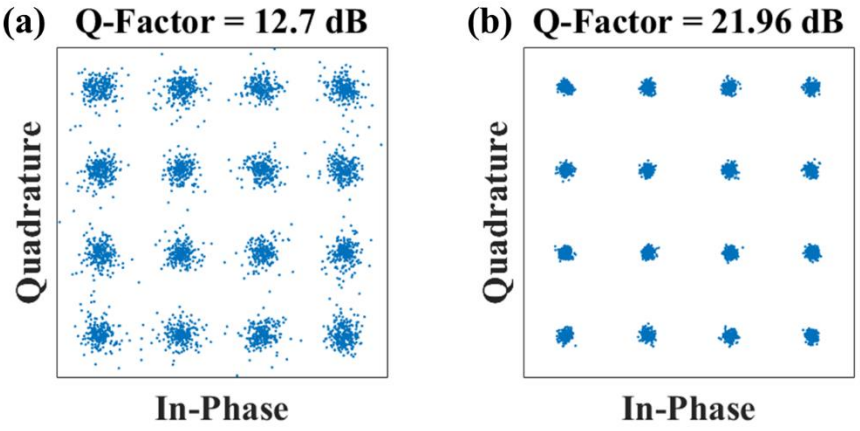

Figure 48. Back-to-back constellations of (a) Signal without transmitter compensation after virtual propagation (b) Signal with transmitter compensation after virtual propagation.

The transmission performance for all channels is presented in Figure 49 and Figure 50. The linear reach (i.e. using EDC only) for the chosen FEC threshold was 1530 km, whereas the optimum launch power per channel was -7 dBm. At this distance the improvement in Q-factor provided by DBP was 2.3 dB for the center channel, while the optimum launch power per channel was found to be -3 dBm.

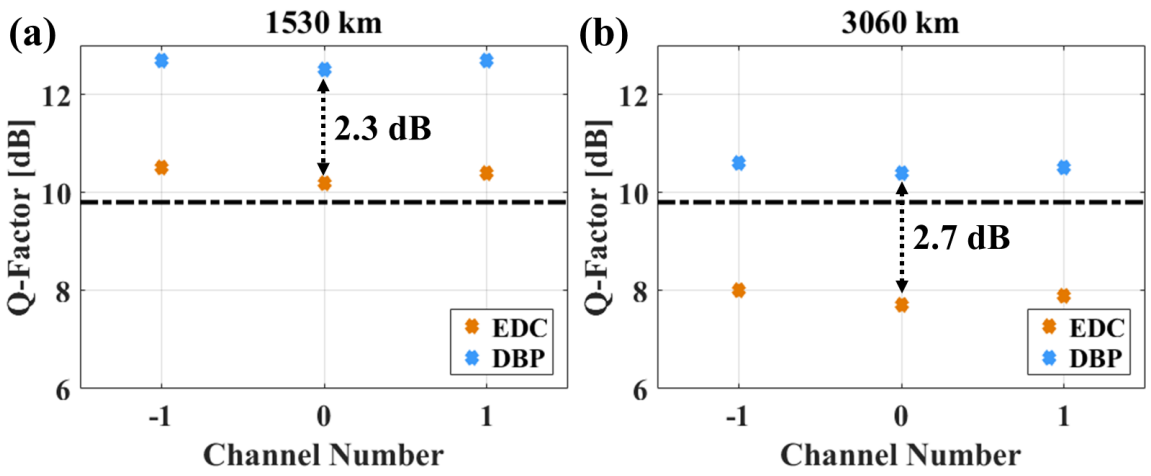

Figure 49. Q-factors for transmission distances of (a) 1530 km (b) 3060 km.

The attempt to double the transmission distance to 3060 km at the former optimum average power level (effectively in the linear regime) resulted in the measured performance of the center channel corresponding to the Q-factor of 7.7 dB, i.e. below the required forward error correction threshold of 9.8 dB. In sharp contrast, employing DBP improved the Q-factor to 10.4 dB, for the optimum launch power per channel increased from -9 dBm to -3 dBm. We can conclude that DBP effectively enabled the transmission within the nonlinear propagation regime, and could take advantage of the increased OSNR provided by the higher launch power. Figure 51 shows a comparison between the constellations and eye diagrams captured at 1530 km using EDC and at 3060 km obtained by the DBP with FRC's, exhibiting virtually the same performance at twice as long a distance, which was made possible by digital NLC for the first time, to the best of our knowledge and is in full agreement with theoretical predictions from [11].

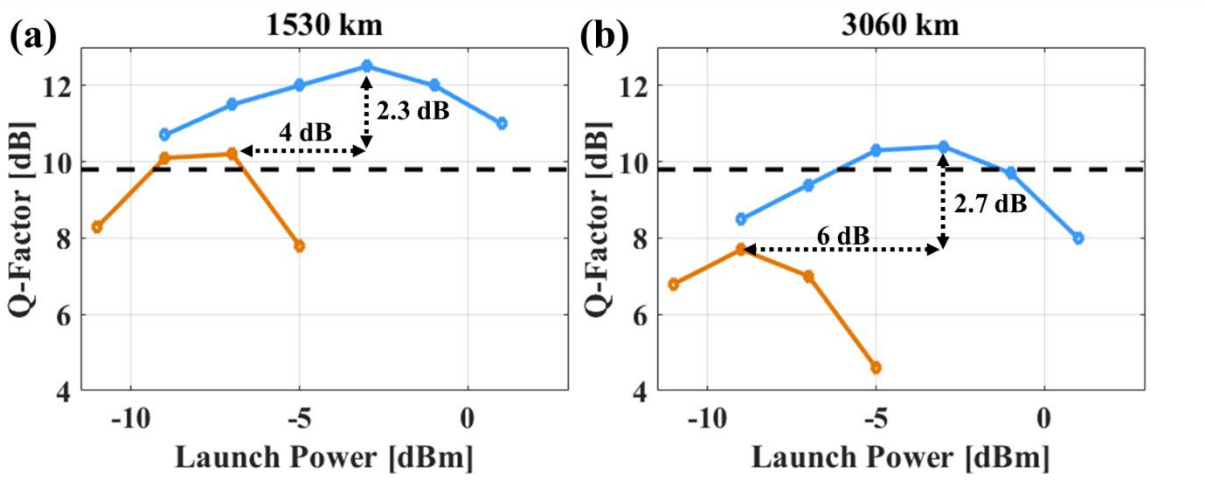

Figure 50. Center channel Q-factor vs. Launch Power per channel for transmission distances of (a) 1530 km (b) 3060 km.

The important ramifications of this demonstration are three-fold: First, the obtained result without a doubt demonstrates the ability of reversing signal-signal interaction in propagation. Second, given that phases of the transmitted channels have not been tracked, nor controlled, these results further corroborate the prediction of [30] that phase stability plays a minor role in NLC. Third, although not directly aimed at in the particularly realized setting, this experimental result also clearly warrants the re-definition of the established capacity bounds in fiber optic transmission, which nearly universally considered the nonlinear interaction as an irreversible impairment. Finally, it must be observed that the 100% reach extension (with respect to the ordinary EDC-only transmission), i.e. doubling of the linear reach, was made possible by the full-complexity NLS calculation, which is prohibitively complex for real-time implementation. Nevertheless, this results represents a strong motivation for an active pursuit of more efficient methods for NLS integration amenable to application specific integrated circuits (ASIC) implementation.

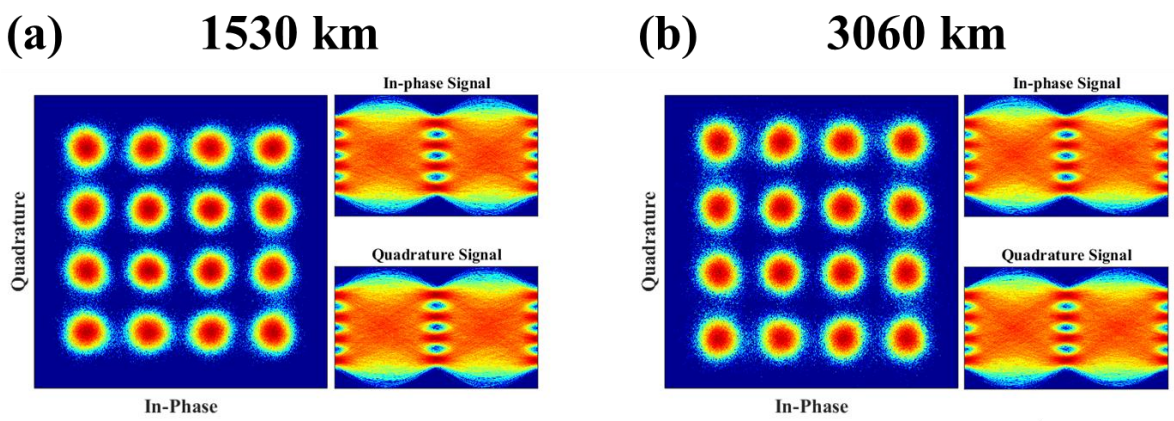

Figure 51. Center channel constellations and eye diagrams for transmission over (a) 1530 km employing EDC (b) 3060 km employing DBP.

3.6 Summary

In this chapter, we have, for the first time, rigorously demonstrated the importance of employing frequency referenced carriers for the compensation of nonlinearities using DSP-based techniques. We devised a set of three NLC experiments to strictly quantify the role of mutually frequency-correlated emitters. Specifically, the carriers were referenced by a parametric frequency comb derived from a single, continuous-wave master oscillator [46].

In the first experimental demonstration, we detailed the application of nonlinearity cancellation in a noiseless system, where frequency-referenced pump and probe waves were propagated through a short piece of HNLF to ensure high nonlinear interaction with negligible noise effects. The pump, whose power was orders of magnitude larger than the probe, generated significant crosstalk on the uncompensated probe, and distorted it from its original form. In sharp contrast, when the probe was precompensated for the predicted crosstalk, the probe arrived at the receiver without any distortion.

In the second experimental demonstration, three 16 GBd 16-QAM WDM channels spaced at 25 GHz were transmitted over 1020 km of SMF, at 2 dBm per channel, a power that was far higher than the optimum level. Such conditions elicited significant nonlinear crosstalk, and severely distorted the constellation of the center channel. In the experiment, the performance of the Nonlinearity Cancellation was investigated with three different configurations with varying degrees of mutual coherence among the propagating carriers. It was seen that when the center channel was carrier by a free-running laser, the performance of the nonlinearity cancellation suffered significantly. Similarly, when the two side channels were free-running, the performance dropped even further. Lastly, when all the channels lack reference, the cancellation failed completely. Additionally, the same demonstration was extended to a system that carried 5 channels, where again it was observed that the nonlinearity cancellation was only successful when all channels were frequency-referenced.

In the last experiment, the linear reach of the same three-channel system, measured at 1530 km, was doubled to 3060 km by compensating the nonlinear crosstalk. The reliance on FRC's allowed the transmission to occur in the previously forbidden nonlinear regime. Nonlinearity cancellation enabled us to take advantage of the increased signal OSNR provided by a higher launch power without incurring in a penalty due to the crosstalk. Although the demonstration was based on only three channels, its extension to a larger channel count (as shown in the previous experimental demonstration), as well as polarization-multiplexed systems is straightforward.

The experiments exposed in this chapter directly confirmed the attainability of higher information capacities in fiber optic links than those currently established. As

implied by the physical channel interaction and the joint processing necessary for its reversal, the pursuit for capacity increase needs to rely on multi-user / Multiple Input–Multiple Output (MIMO) cooperative processing [51].

Chapter 3, in part is a reprint of the material as it appears in Optics and Photonics News, vol. 27, no. 3, pp. 30-37, (2016), titled "Beating the nonlinear capacity limit," by Eduardo Temprana, Nikola Alic, Bill P.-P. Kuo, and Stojan Radic. In addition, Chapter 3 in part is a reprint of the material as it appears in Science, vol. 348, no. 6242, pp. 1445-1448, (2015), titled "Overcoming Kerr-induced capacity limit in optical fiber transmission," by Eduardo Temprana, Evgeny Myslivets, Bill P.-P. Kuo, Lan Liu, Vahid Ataie, Nikola Alic, and Stojan Radic. Lastly, Chapter 3 in part is a reprint of the material as it appears in Optics Express, vol. 23, no. 16, pp. 20774-20783, (2015), titled “Two-fold transmission reach enhancement enabled by transmitter-side digital backpropagation and optical frequency comb-derived information carriers,” by Eduardo Temprana, Evgeny Myslivets, Lan Liu, Vahid Ataie, Andreas O.J. Wiberg, Bill P.-P. Kuo, Nikola Alic, and Stojan Radic. The dissertation author was the primary investigator, and the primary author of these articles.

Chapter 4. Alternative Architectures for Frequency Referenced Transmitters

4.1 Introduction

A natural response to the relentless data growth in today's information-centered society is that of a quest for low cost photonics technology. In optical networks, system cost is driven by two factors: firstly, the complex and high power dissipating transceivers that have become ubiquitous in the high-speed fiber optic transmission systems and secondly, the nonlinear capacity constraint in standard transmission systems, which imposes a strict limit on the information density and reach that can be transported over a fiber optic link. As a solution, in this section we propose two architectures that successfully solve both impediments in transmission systems. On one hand, following the groundwork developed in the previous chapter, we demonstrate successful nonlinearity cancellation that enables transmission beyond the nonlinear limit. On the other hand, we propose and demonstrate two alternative frequency-referenced transmitter architectures with components.

In Chapter 3, a system implementation that relied on frequency (but not phase) referenced carriers extracted from a on optical frequency comb was proposed and a 100% reach extension was demonstrated in a long-haul transmission experiment. In this chapter, we extend the notion of FRCs for nonlinearity cancellation by employing injection locked (IL) distributed feedback lasers referenced to an OFC generated in the RF domain, wherein the IL lasers serve to regenerate the limited OSNR of the demultiplexed comb lines while practically preserving the linewidth of the master oscillator. This scalable architecture is

an attractive alternative to the parametric OFC used in Chapter 3 that similarly allows to generate independent high-OSNR, narrow-linewidth frequency referenced carriers. To validate the new architecture, we demonstrate a 100% increase in system reach of a four-channel single-polarization coherent link, and show that it is only achievable when the carriers are frequency referenced.

In addition, in a second experimental demonstration, we demonstrate high speed coherent transmission based on an ultra-low-cost non-temperature controlled Fabry-Perot laser, which again was injection-locked to a reference optical frequency comb. In this case, the reach of the 50 GBaud 16-QAM channel is extended to more than 2000 km, breaching the nonlinear capacity limit using nonlinearity cancellation [36].

4.2 Experimental Demonstration 4: Injection-Locked Distributed Feedback Lasers as Frequency Referenced Carriers

4.2.1 Experimental Setup

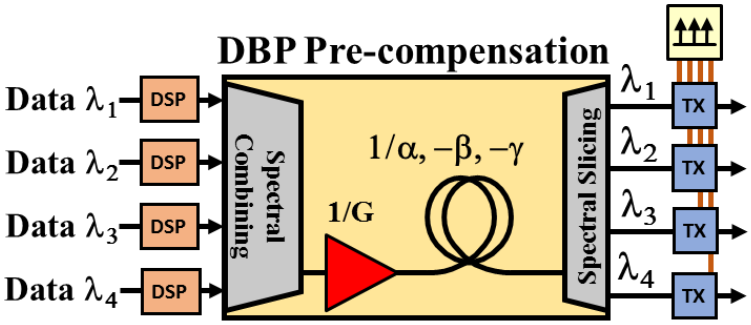

Figure 52. Transmitter-Side Digital Back Propagation relying on frequency referenced carriers

The block diagram of the DBP transmitter is shown in Figure 52. The data to be transmitted on each of the WDM channels is mapped to a desired modulation format, replicating the method described in detail in Chapter 3, spectrally combined, and passed to

a full-field back-propagating NLSE engine considering the transmission link parameters. Subsequently, the NLSE full-field output is channelized into spectral slices and independent, but fully-synchronous pre-distorted waveforms were generated for each channel. The DBP engine served to calculate the inverse to the actual propagation in the physical link with mirror-imaged power evolution (to that of the physical link) and considering oppositely signed fiber parameters (dispersion and nonlinearity), as well as reciprocals of amplifier gain and fiber attenuation, as explained in detail in [52]. The fiber dispersion, dispersion slope and nonlinear parameter of the virtual fiber were acquired by direct measurement and optimized by repetitive training of the transmission system.

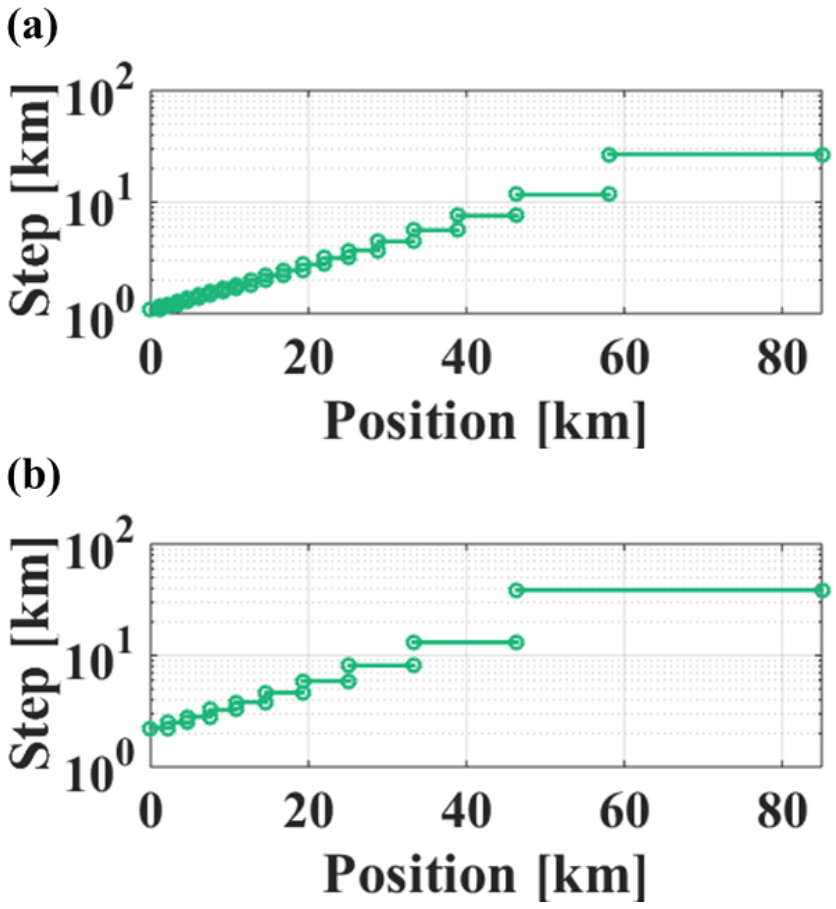

Figure 53. Step size distribution used in the NLSE solver for a transmission distance of 3060 km and -3 dBm launch power (a) 20 steps-per-span and (b) 10 steps per span.

The spatial resolution in the NLSE solver was initially chosen to achieve maximum accuracy by restricting the amount of nonlinear phase shift in each step to 0.01 degrees. In addition, an implementation with limited complexity was investigated by limiting the number of steps-per-span to 10 and 20. Figure 53 shows the step-size distribution for the case of a transmission distance of 3060 km and -3 dBm launch power. In contrast to the case of equidistant steps, when the number of steps is limited, the distribution becomes denser in the initial section of the fiber, as dictated by the exponential decay of the signal power in propagation, as implied by the notion of accuracy and nonlinear phase accumulation in the SSFM.

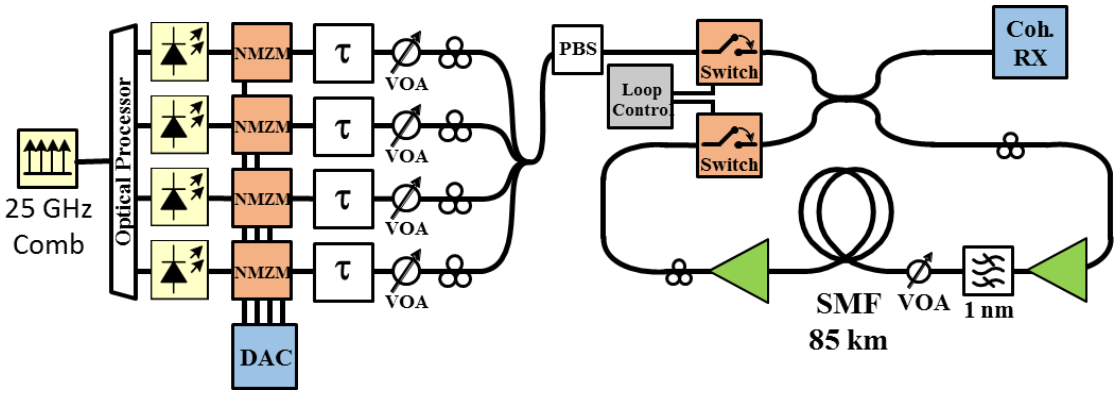

Figure 54. TS-NLC experimental implementation and recirculating transmission loop
DAC: Digital-to-Analog Converter. QAM: Quadrature Amplitude Modulator. VOA: Variable Optical Delay Line. VOA: Variable Optical Attenuator. PBS: Polarization Beam Splitter. SMF: Single-Mode Fiber. Coh. RX: Coherent receiver.

The four-channel frequency referenced transmitter implementation is shown in Figure 54. A 25 GHz-pitched OFC was seeded by a continuous-wave external cavity laser with 3 kHz linewidth serving as the master oscillator. The OFC provided spectral tones with ~35 dB OSNR, i.e. 20 dB lower than the parametric OFC used in [53, 54]. The comb lines were demultiplexed by an optical processor and used to injection-lock four DFB lasers with an injection ratio of -15 dB. We again emphasize that, as before, the path lengths of

the demultiplexed comb lines were not matched and that the optical phases of the lasers were not stabilized nor controlled during the experiment. Injection locking combines the best of the two laser sources' properties – the high coherence of the master oscillator and the high power of the DFBs, directly availing a high launch OSNR of the system, normally not obtainable by OFCs, except in the case of parametric combs [53, 54, 46]. The spectral line shape of the master and injection-locked lasers were measured utilizing self-heterodyne beating with a decorrelation length of 20 km. As seen in Figure 55, the injection locked DFB lasers practically preserved the linewidth of the master lasers for injection ratios as low as -15 dB.

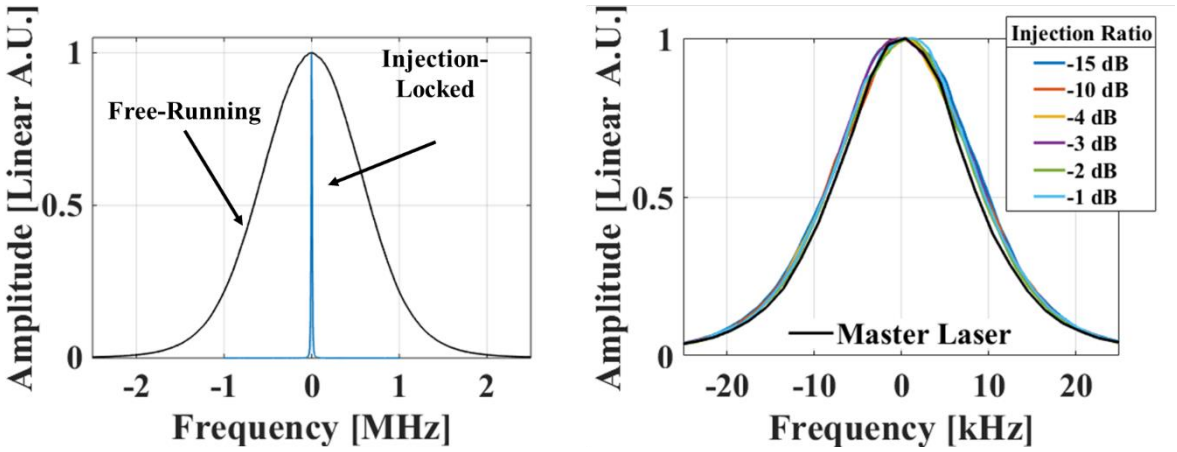

Figure 55. DFB laser in free-running and injection locked conditions

Different shift-register initial conditions were used to generate four pseudo-random bit sequences that were subsequently gray mapped to 16-Quadrature Amplitude Modulation symbols. Raised-cosine filtering using 4 samples-per-symbol, 512 filter taps and roll-off factor of 0.01 was applied to constrain the spectral occupancy. The DBP computation was based on a symmetric split-step NLSE solver over a total bandwidth of ~128 GHz, wherein blocks of 216 symbols were processed with a frequency resolution of ~48 kHz and a time resolution of ~7.8 fs.

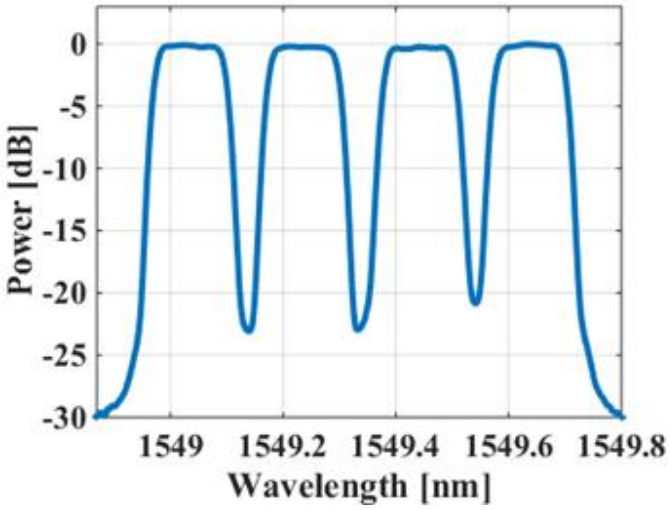

Figure 56. Four-channel spectrum before transmission

Four pairs of digital-to-analog converters with 5 Effective Number of Bits (ENOB) [19] were used to generate electrical signals at the rate of 65 GS/s. The 16 GBaud 16-QAM signals were imprinted onto the optical carriers by means of nested Mach-Zehnder modulators, passively multiplexed and a polarization beam splitter was employed to ensure that all channels were co-polarized. The precise time alignment of the data sequences of all channels was accomplished to within 1 ps by means of optical delay lines and synchronous triggering of the DACs.

The transmission experiment was performed in the recirculating loop shown in Figure 54, which consisted of a single 85 km span of Single-Mode Fiber with 16.53 ps/nm/km dispersion, nonlinear coefficient of 1.22 $W^{-1}km^{-1}$ and total attenuation of 15.95 dB that was compensated by an Erbium Doped Fiber Amplifier with 4.5 dB noise figure. The spectrum showing the four channels before transmission is pictured in Figure 56. After transmission, the signals were independently filtered and detected using a coherent receiver that consisted of a 90-degree hybrid and a pair of balanced detectors with 40 GHz-

bandwidth. The electrical signals were digitized using a real-time oscilloscope operating at 100 GS/s sampling rate, and subsequent processing was performed offline on a personal computer. The receiver DSP consisted of the standard processing chain [26] that includes receiver front-end correction, symbol timing recovery, matched filtering, carrier frequency and phase estimation and least mean squares adaptive equalization. The assumed FEC was a standard Reed-Salomon (RS) 255,233 code with a BER threshold of 10^{-3} (Q-factor = 9.8 dB).

The performance of the system was characterized in two configurations: initially, only Electronic Dispersion Compensation was applied as the first step of the receiver DSP by means of an ideal correction of the quadratic phase in the frequency domain. Subsequently, only DBP was applied at the transmitter to precompensate both for dispersion and nonlinearities. To achieve the maximum nonlinearity compensation, the spatial resolution of the NLSE solver was chosen such that the maximum nonlinear phase shift in each step did not exceed 0.01 degrees.

In addition, the performance of an implementation with limited complexity was investigated by restricting the maximum number of steps-per-span taken in the NLSE solver and optimizing the step size by following the signal power evolution.

Lastly, the performance of a DBP implementation that relies on an inaccurate fiber model was investigated by introducing a 0.5% and 1% mismatches between the dispersion parameter of the DBP block (D_{DBP}) and the exact fiber dispersion value (D_{REAL}).

4.2.2 Results

The BER-derived Q-factors for varying launch powers are shown in Figure 58a. For the chosen FEC threshold (Q = 9.8 dB), the linear reach was 1530 km. The optimum launch power when employing EDC only was -7 dBm and an inner (worst) channel Q-factor was 10.2 dB. Attempting EDC-based transmission over twice the linear reach (3060 km) resulted in a Q-factor penalty of 2.1 dB, which fell far below the required threshold and would require higher FEC overhead. Nevertheless, as shown in Figure 58b, at 3060 km, DBP with FRCs yielded a 4 dB increase in signal launch power and a corresponding improvement in the inner channel Q-factor of 2.3 dB. The constellations for optimum launch power conditions are shown in Figure 59. As demonstrated, operating in the nonlinear transmission regime and relying on TS-NLC with FRCs enabled a two-fold system reach expansion with an ample margin over the FEC threshold.

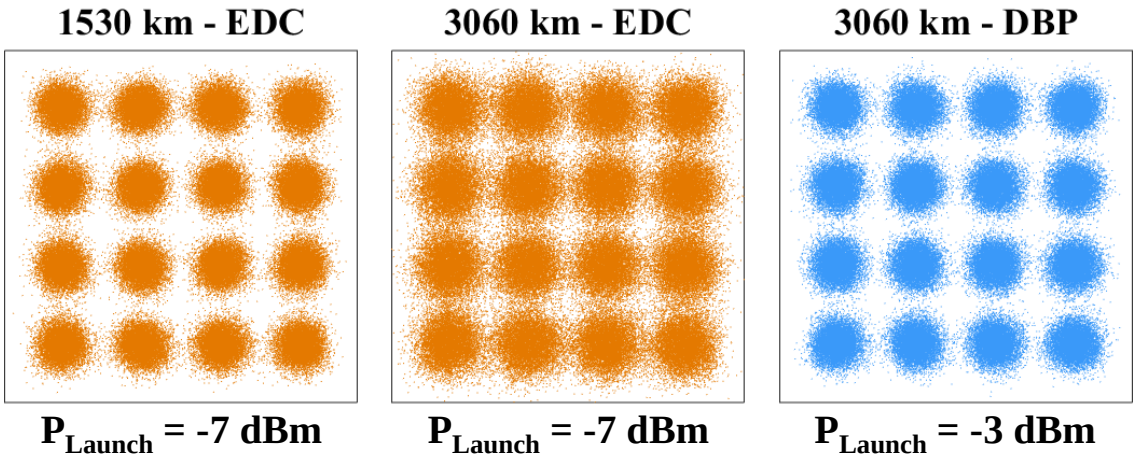

Figure 57. Inner (worst) channel constellations at optimum launch power for the linear and nonlinear reach.

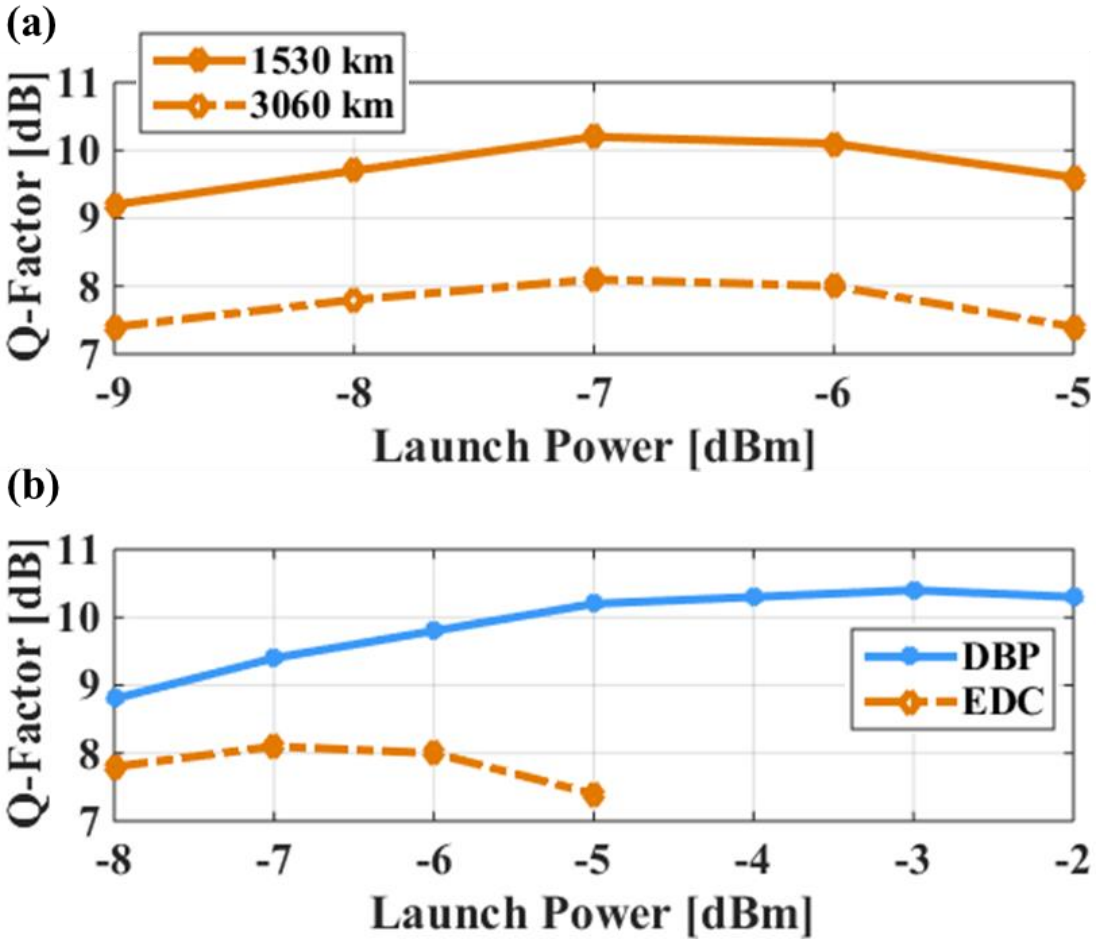

Figure 58. Q-factor vs. Launch Power for (a) EDC-only based transmission with FRCs at 1530 and 3060 km (b) EDC-only and DBP-only based transmission with FRCs at 3060 km.

It is important still important to emphasize the role of the frequency reference in the results. Namely, note that unlike any previously published work, here we used injection-locking as an indirect frequency reference technique, emphasizing the single most important property of the mutual coherence of the channel carriers postulated in [11]. The comparison of the system performance with and without FRCs is shown in Figure 59. When IL was not used as a frequency reference, the wavelength of the free-running DFB lasers was finely tuned to match the OFC using an Optical Spectrum Analyzer (OSA) with 0.1 nm resolution bandwidth. EDC-based transmission without FRCs exhibited a small

penalty that was mainly attributed to the broader linewidth of the free-running DFB lasers. In sharp contrast, the performance of TS-NLC was severely degraded in the system without FRCs, which demonstrated the importance of having a stable frequency reference to achieve significant NLC.

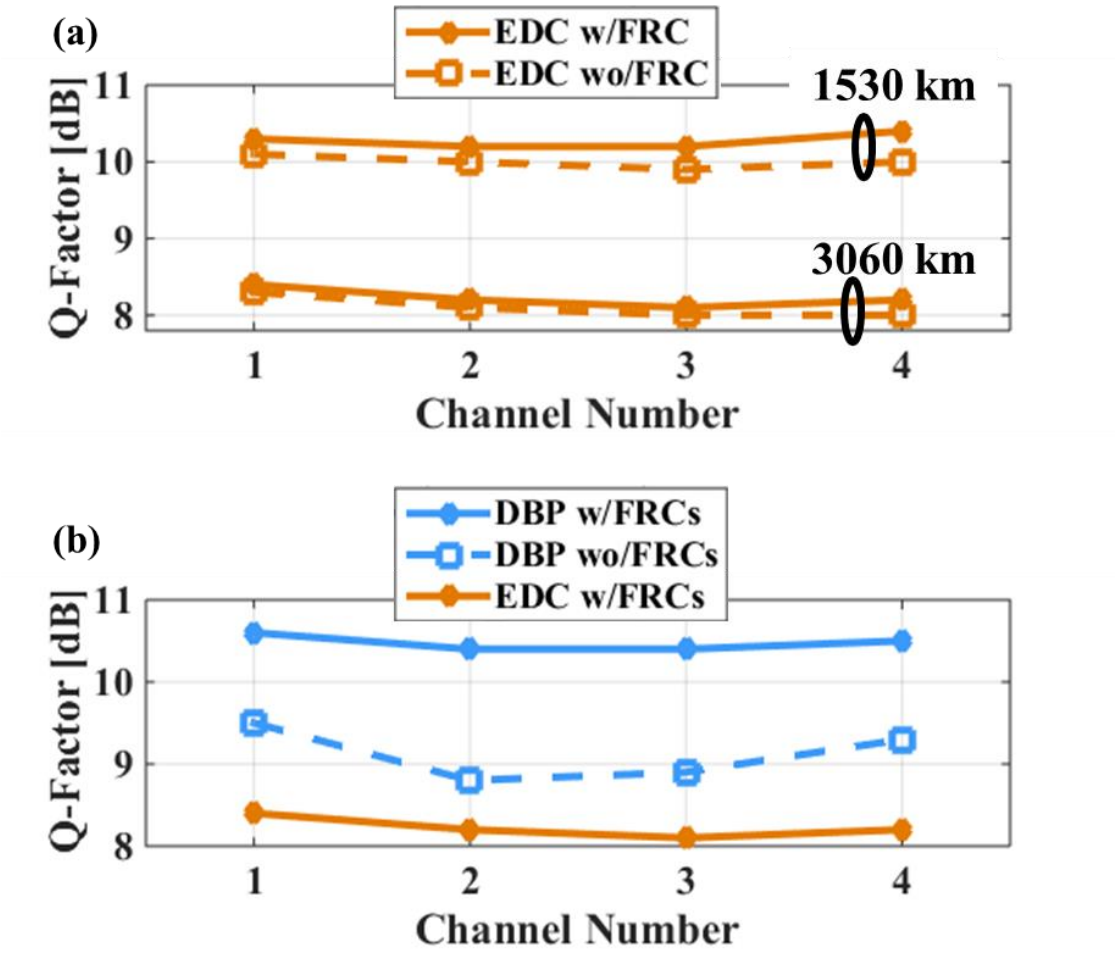

Figure 59. Q-factor vs. Channel Number at optimum launch power for (a) EDC-only based transmission at 1530 and 3060 km with and without FRCs (b) EDC-only and DBP-only based transmission at 3060 km with and without FRCs.

The comparison between the full-complexity DBP and the implementation with limited steps-per-span is shown in Figure 60. In the case of DBP with unlimited steps-per-span, the optimum launch power was -3 dBm. Limiting the number of steps to 20 resulted in a small Q-factor penalty, but still enabled a doubling of the system reach. In contrast,

the use of 10 steps-per-span reduced the optimum signal launch power to -4 dBm, which in turn generated a Q-factor penalty of 0.4 dB.

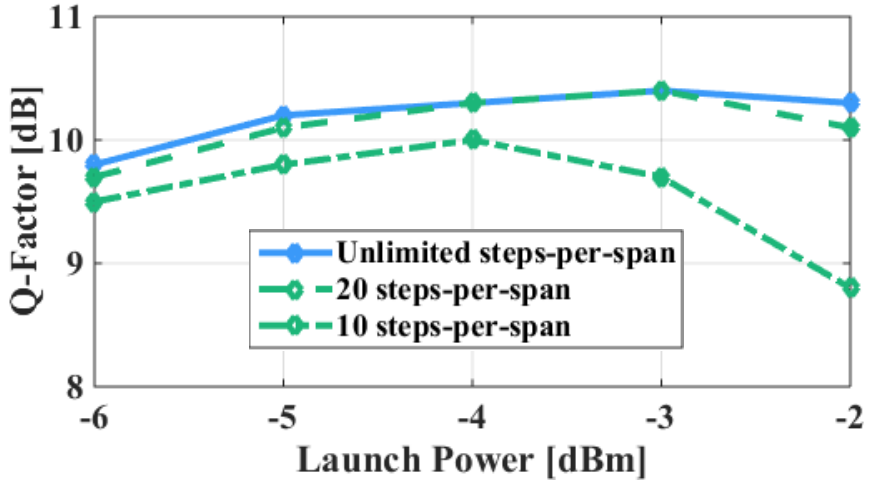

Figure 60. Inner (worst) channel Q-factor vs. launch power per channel for different choices of the spatial resolution used in the NLSE solver.

The effect of a model inaccuracy in the fiber dispersion parameter can be seen in Figure 61, a 0.5% mismatch lead to a reduction of the optimum signal launch power by 1 dB and a corresponding Q-factor penalty of 0.5 dB. Furthermore, a 1% mismatch lead to a penalty of ~2 dB, which severely limited the gain yielded by DBP.

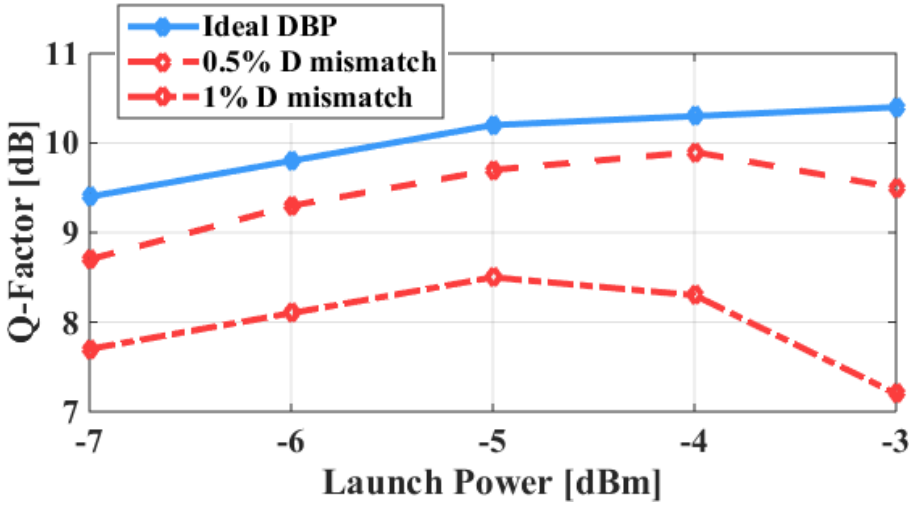

Figure 61. Inner (worst) channel Q-factor vs. launch power per channel for DBP with different model accuracies.

4.3 Experimental Demonstration 5: Injection-Locked Fabry-Perot Laser as Frequency Referenced Carrier

4.3.1 Experimental Setup

The experimental setup is presented in Figure 62. An RF-generated optical frequency comb (OFC) was derived from an External Cavity Laser with 3 kHz linewidth [55] and an isolated comb line was used to injection lock a low-cost Fabry-Perot Laser (FPL) with an injection ratio of -5 dB. The FPL had an output power of 1 dBm and was subsequently amplified by an Erbium Doped Fiber Amplifier to 14 dBm. A 50 GBaud 16-Quadrature Amplitude Modulation signal was imprinted on the FPL carrier by an IQ modulator driven by two amplified Digital-to-Analog Converters [19] with 16 GHz 3 dB-bandwidth and a sample rate of 65 GS/s. Raised-cosine filtering with 0.2 roll-off factor was employed to constrain spectral occupancy and digital pre-emphasis was applied to compensate for the non-ideal responses of the electronic and electro-optic transmitter components.

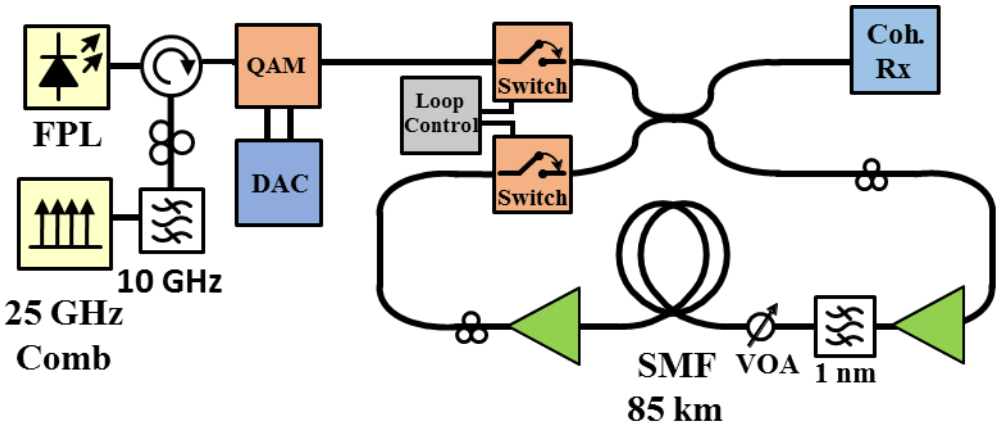

Figure 62. Injection-Locked Fabry-Perot Laser transmission schematic

Long-haul transmission was emulated in a recirculating loop that consisted of an 85-km span of Single-Mode Fiber with 16 ps/nm/km dispersion, a nonlinear coefficient of 1.22 $W^{-1}km^{-1}$ and a total attenuation of 15.95 dB, which was compensated by a 4.5 dB noise figure EDFA. After transmission, the signal was detected using a coherent receiver with 40 GHz bandwidth and a local oscillator ECL with 100 kHz linewidth. The electrical signals from the balanced detectors were digitized at the rate of 100 GS/s using a real-time oscilloscope with 33 GHz bandwidth and offline processing was performed on a personal computer. Linear and nonlinear transmission impairments were compensated using Digital Back Propagation [36] with 5 steps-per-span and subsequent DSP consisted of receiver front-end correction, symbol timing recovery, carrier frequency-and-phase estimation and Least Mean Squares adaptive equalization [26]. Bit-error rate measurements were performed by error counting in the same rigorous manner as the previously described experiments.

4.3.2 Results

The optical spectrum of the free-running FPL is presented in Figure 63 (a), showing the typical multi-mode operation and excessive spectral width of the FPL. In contrast, as shown in Figure 63 (b), under OIL with an injection ratio of -5 dB, the locked mode dominates and the sideband become suppressed by over 30 dB. In addition, as shown in Figure 63 (c), the FPL could be injection-locked to several modes away from the center.

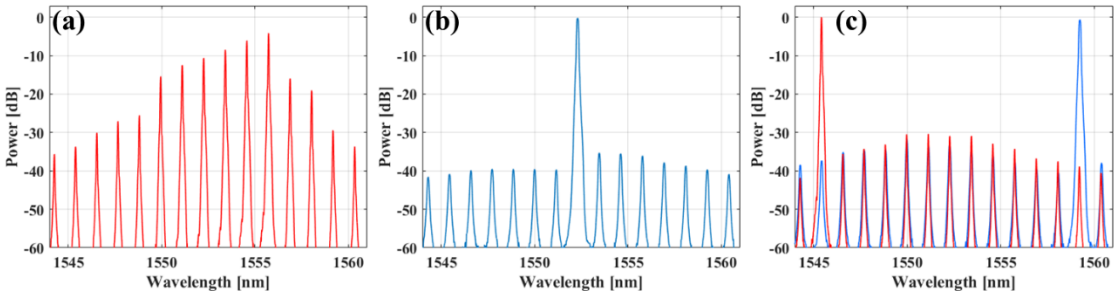

Figure 63. Fabry-Pero Laser Spectrum (a) Free running (b) Injection-locked to center mode (c) Injection-locked to side-modes

The locked-mode linewidth closely follows that of the injected tone, with a small increment caused by the Amplified Spontaneous Emission introduced by the FPL. The dependence of the linewidth with respect to the injection ratio can be seen in Figure 64 (a). The optical spectrum and the constellation measured at back-to-back are shown in Figure 64 (b).

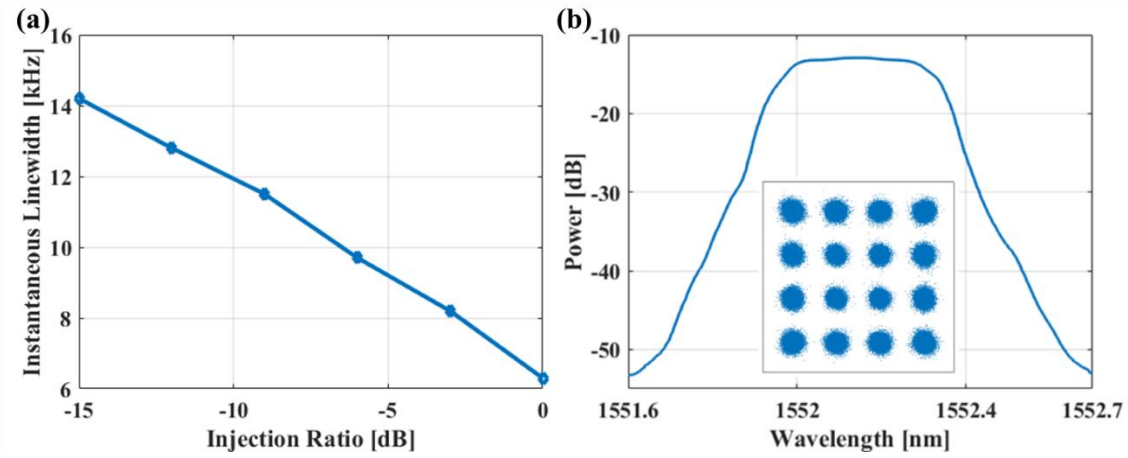

Figure 64. (a) Linewidth vs. Injection Ratio (b) Back-to-back spectrum and constellation

The Q-factors measured at the transmission distance of 2125 km are shown in Figure 65 (a). For electronic dispersion compensation, the performance peaked at a Q-factor of 6.1 dB, which fell below the required Soft Decision (SD)-FEC threshold of 6.25 dB. In contrast, DBP yielded an increase in the optimum launch power of 1 dB and an

improvement in Q-factor of 1.3 dB, easily exceeding the required threshold. The constellations for EDC and DBP are shown in Figure 65 (b) and (c), demonstrating the improvement yielded by the DBP.

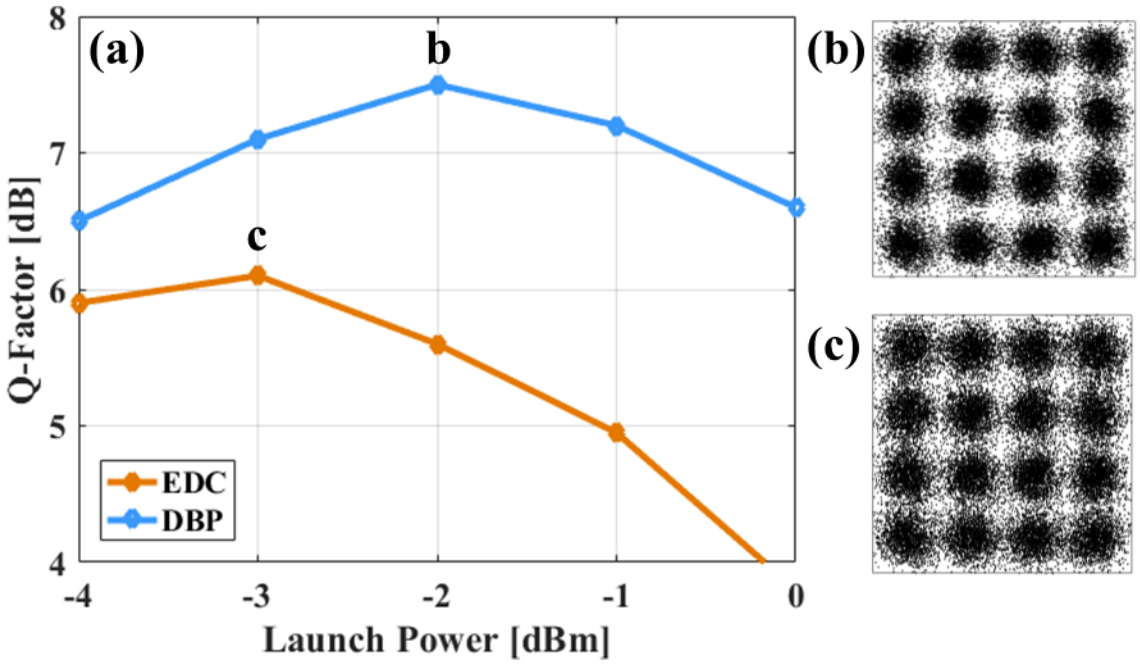

Figure 65. (a) System performance (b) Constellation after NLC (c) Constellation before NLC

4.4 Summary

In this chapter, we have proposed and experimentally demonstrated two alternative architectures to generate frequency-referenced carriers. By injection locking Distributed Feedback and Fabry Perot lasers to an optical frequency comb with lower intrinsic OSNR than the parametric comb used in Chapter 3, we demonstrate the possibility of relaxing the system cost and component specifications of the source of frequency reference.

In the first experimental demonstration, the frequency referenced carriers were generated by injection locking DFB lasers to a reference optical frequency comb generated by amplitude and phase modulation of a CW laser. For a system that comprised of four 16

GBaud 16-QAM channels, nonlinearity cancellation enabled a two-fold enhancement of the system reach, which was extended from 1530 km to 3060 km. Once again, demonstrating the importance of the frequency reference, we observed that the doubling of the system reach was only possible when the transmitter carriers were referenced to the comb.

Additionally, with this transmitter architecture, we have investigated the effect of utilizing an inaccurate back propagation model, firstly by limiting the number of steps-per-span in the DBP computation and secondly by introducing a mismatch between the dispersion parameter in the DBP engine and the real (exact) dispersion parameter. Our findings indicate that in a four-channel system, a departure of the dispersion parameter of only up to 0.5% is allowed at the considered propagation distance, whereas at least 20 steps-per-span in the back-propagation symmetric split step- based computation are needed to achieve sufficient nonlinear impairment reversal to enable the system reach doubling.

In the second experimental demonstration, a frequency referenced carrier was generated by injection lacking a low-cost non-temperature controlled Fabry-Perot laser to an isolated comb line of the same low-cost optical frequency comb. In this experiment, the maximum transmission reach of 2125 km was accomplished by relying on nonlinearity compensation.

Chapter 4, in part is a reprint of the material as it appears in Journal of Lightwave Technology, vol. 34, no. 15, pp. 3544-3549, (2016), titled "Transmitter-Side Digital Back Propagation with Optical Injection-Locked Frequency Referenced Carriers," by Eduardo Temprana, Evgeny Myslivets, Bill P.-P. Kuo, Nikola Alic, and Stojan Radic. In addition, Chapter 4 contains material presented in the Frontiers in Optics Conference, San Jose,

(2015), titled "50 GBaud 16-QAM Transmission Over 2125 km Based on an Injection-Locked Fabry-Perot Laser Carrier," by Eduardo Temprana, Bill P.-P. Kuo, Nikola Alic and Stojan Radic. The dissertation author was the primary investigator, and the primary author of these articles.

Chapter 5. Nonlinearity Compensation in High-Capacity Systems

5.1 Introduction

The experiments shown in previous chapters were achieved with a moderate spectral efficiency; the channel spacing was 25 GHz, whereas the signals were 16 GBd single-polarization 16-QAM, yielding a spectral efficiency of 2.56 bits/Hz. In this chapter, we transmit three 24 GBaud polarization multiplexed (PM) 64-QAM with a 28 GHz channel spacing, yielding a spectral efficiency of 10.3 bit/sec-Hz. More importantly, we demonstrate for the first time a 200% (i.e. a three-fold) reach extension beyond the conventional linear limit in a standard single-mode fiber (SMF)-based link with erbium-doped fiber amplifiers only, reaching a transmission distance of 1275 km.

5.2 Dense Wavelength Division Multiplexing

Keeping up with the capacity demand requires an increase spectral efficiency. The latter, in turn, can only be achieved by transmitting channels that are closely packed together. As explained in section 2.3.2, pulse shaping can significantly constrain the spectrum of modulated signals. However, special considerations must be taken in dense wavelength multiplexing due to the non-ideal output of DACs and driver amplifier (DA), and the nonlinear transfer function of the modulator (i.e. the MZM).

The measured electrical spectrum of the 24 GBd signal generated by the DAC is seen in Figure 66a. The signal spectrum has content up to 12 GHz, however, beyond that there are multiple unwanted tones that appear within the bandwidth of the adjacent channel

and thus will interfere and degrade the system performance. These clock feedthrough tones, occur due to a spurious coupling of the clock to the data signal [56], and are common in Complementary Metal-Oxide Semiconductor (CMOS) based DACs. Additionally, the nonlinearity of the DA will also generate frequency content outside of the signal bandwidth. As seen in Figure 66b, the DA creates "skirts" that can extend the spectral occupancy of the signal well beyond the theoretical expectations.

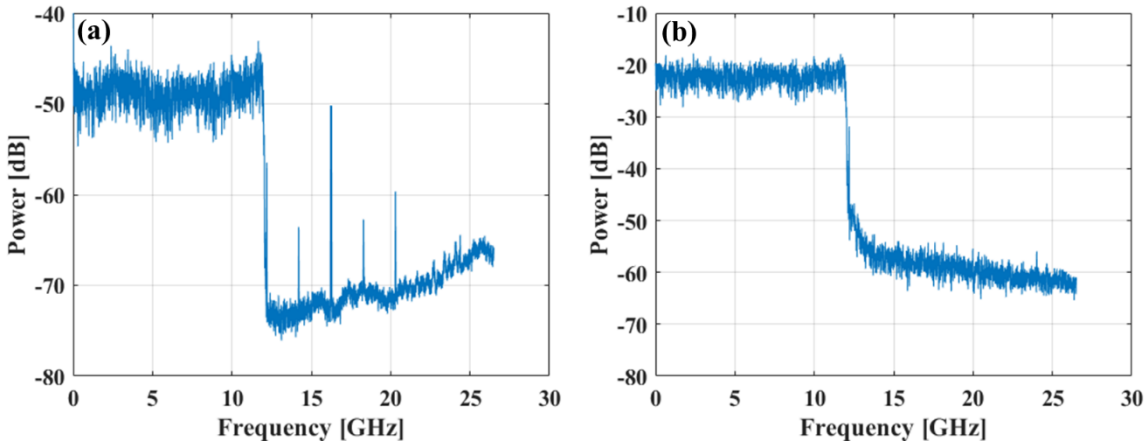

Figure 66. Electrical spectra measured at the output of (a) DAC (b) DA

To eliminate the unwanted electrical spectral content both from the DAC and DA, a 4th order Bessel filter with 12.5 GHz bandwidth was placed after the DA, which achieved the suppression shown in Figure 67 (a). The simulated electrical spectrum overlap for a 28 GHz channel spacing is shown in Figure 67 (b), demonstrating the feasibility of close spectral multiplexing for this baud rate and channel spacing.

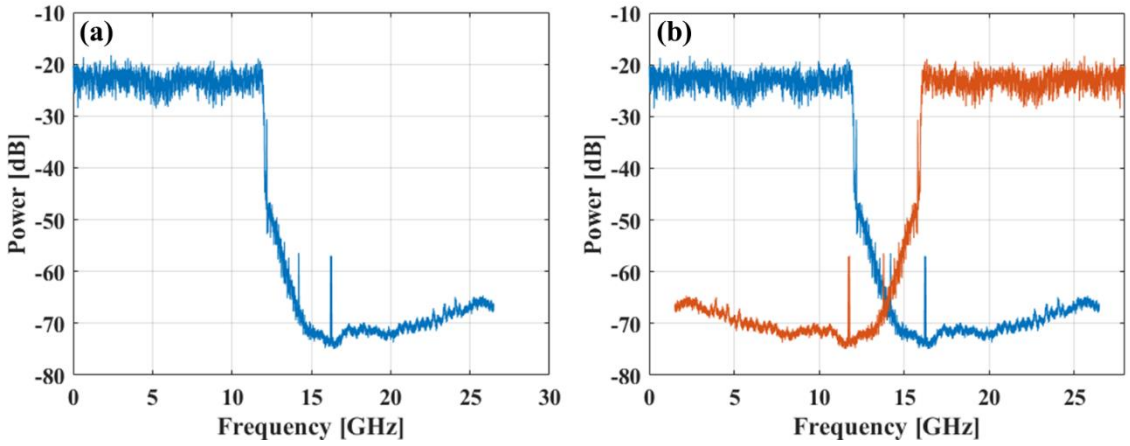

Figure 67. (a) Electrical spectra measured at the output of AD after filtering (b) Simulated electrical spectrum overlap of multiplexed signals

The measured optical spectrum of the filtered signals after being modulated onto an optical carrier with an MZM is shown in Figure 68 (a). When no attenuation was used, the modulator was being driven with a voltage swing equivalent to $2V_{\pi}$, which accentuated the nonlinear transfer function of the MZM and generated significant spectral content outside of the optical signal bandwidth, thus precluding wavelength multiplexing with narrow channel spacing. As the attenuation was increased, the total optical power out of the MZM decreased, and therefore a degradation in the signal OSNR after the EDFA was observed, which can be seen in the increasing level of the noise floor in Figure 68 (a). However, despite the OSNR degradation, the out-of-band spectral content was reduced significantly, thereby improving the overall performance when multiplexing multiple channels with a narrow channel spacing. The measured optical spectrum of the multiplexed signals with a 28 GHz channel spacing can be seen in Figure 68 (b).

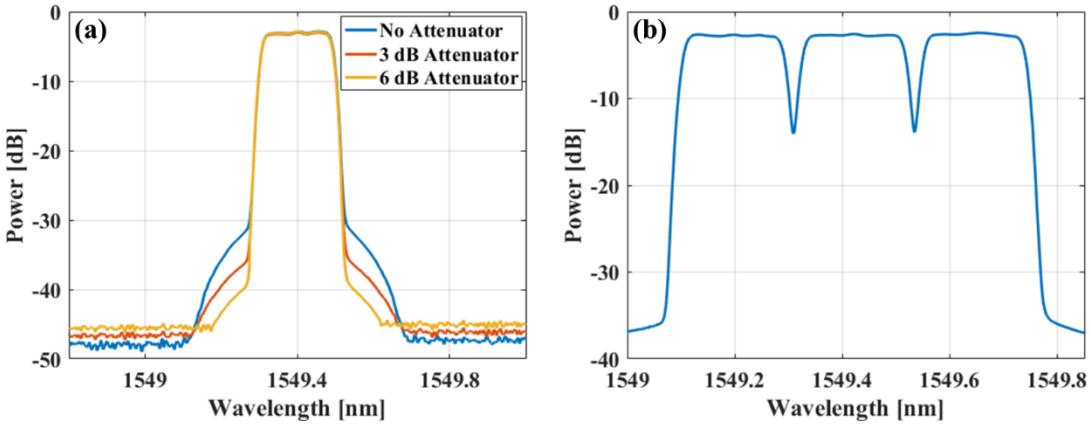

Figure 68. (a) Measured spectra of modulated signals with different attenuation into the MZM (b) Measured optical spectrum of multiplexed signals

5.3 Polarization Multiplexing

Additionally, the spectral efficiency can be further doubled by employing polarization multiplexing, that is, encoding information in the two orthogonal polarization states of the optical field.

In Chapters 2 and 3, we introduced the mathematical formalism for wave propagation in its scalar form, which is suitable to describe pulse propagation effects when the field contains power only in one polarization. When accounting for both polarization tributaries, the electric field equation previously introduced in (2.2.1) takes the vectorial form

$$\boldsymbol{E}(z,t) = \Re\left\{\left[\hat{\boldsymbol{x}}E_x(z,t) + \hat{\boldsymbol{y}}E_y(z,t)\right]e^{-i(\beta_0 z-\omega_0 t)}\right\} \tag{5.3.1}$$

where $\hat{\boldsymbol{x}}$ and $\hat{\boldsymbol{y}}$ are unit vectors that represent the two possible linear states of polarization, and $E_{x,y}$ represent the field amplitudes for their corresponding tributary. Naturally, the Nonlinear Schrodinger Equation also has a vectorial form that accounts for the polarization diversity. However, it is important to realize that the stochastic nature of fiber birefringence generates random scattering events over length scales of ~100 meters, whereas the length

scales of dispersion and the nonlinear effects are in the order of 10 to 100 km, meaning that the state of polarization changes much faster than the envelope of the field. The effect of polarization on the nonlinear interactions can therefore be effectively averaged over the Poincaré sphere, an approximation that transforms the vectorial NLSE into a system of equations called the Manakov equations, which have the form

$$\frac{\partial E_x}{\partial z} = -\frac{\alpha}{2}E_x - i\frac{\beta_2}{2}\frac{\partial^2 E_x}{\partial t^2} + \frac{\beta_3}{6}\frac{\partial^3 E_x}{\partial t^3} + i\gamma\frac{8}{9}\left(|E_x|^2 + \left|E_y\right|^2\right)E_x \qquad (5.3.2)$$

$$\frac{\partial E_y}{\partial z} = -\frac{\alpha}{2}E_y - i\frac{\beta_2}{2}\frac{\partial^2 E_y}{\partial t^2} + \frac{\beta_3}{6}\frac{\partial^3 E_y}{\partial t^3} + i\gamma\frac{8}{9}\left(|E_x|^2 + \left|E_y\right|^2\right)E_y \qquad (5.3.3).$$

To emulate the propagation of dual-polarization signals, the Manakov equations are solved using the Split-Step Fourier Method introduced in Chapter 3.

As in dense WDM, polarization multiplexing introduces practical challenges that must be overcome to achieve its maximum potential. The schematic of a DSP-enabled dual-polarization coherent transmitter is shown in Figure 69. Essentially, the transmitter is comprised of a DSP unit with four digital outputs, four Digital-to-Analog Converters, four electrical Amplifier Drivers with electrical filters and a Dual-Polarization Nested Mach-Zehnder Modulator (DP-NMZM). Per the modulator specifications, in a worst-case scenario, the signals in the two polarizations could suffer a timing skew of up to 15 ps and their power imbalance could reach 1.5 dB. In addition, components such as the DACs, DAs, filters, and coaxial cables will inevitably have different path delays and responses, which will further degrade the polarization skews and power imbalances. Nevertheless, the DSP capability of the transceiver can be used to compensate any front-end based impairments, which is particularly necessary in systems that employ TS-NLC and other complex preprocessing techniques.

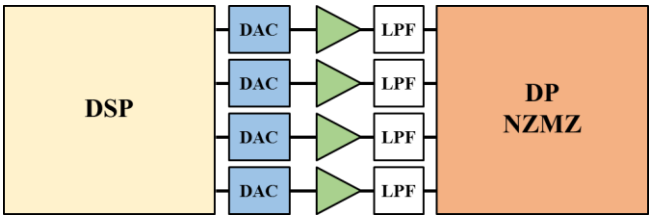

Figure 69. Electro-optic front end of typical coherent transmitters.

To determine the effect of polarization timing skews and polarization power imbalances on the performance of TS- NLC, we transmitted the three dual-polarization channels over 850 km. Three system configurations were investigated: firstly, we measured the performance of TS- NLC with an ideal transmitter, i.e. when the timing skews and power imbalances between the polarizations of all the channels were compensated. Secondly, we artificially introduced a power imbalance by attenuating the Y-Polarization of the center channel, whereas the side channels were kept in their ideal state (i.e. without imbalances nor skews). Lastly, we introduced a time-skew between the polarizations of the center channel by adding a delay in the digital waveform of the Y-Polarization, while again maintaining the side channels in a perfect state.

Table 1. Measured polarization timing skews and power imbalances.

Channel Number	Timing Skew [ps]	Power Imbalance [dB]
1	4.8	-1.2
2	8.2	0.8
3	6.9	1.5

The measured timing skews and power imbalances between the polarizations of the three transmitters in our experiment are shown in Table 1. After compensation, the timing skews were reduced to less than 1 picosecond, and the power imbalance was equalized within 0.1 dB. Figure 70 shows the performance of the center channel when all three transmitters were ideally compensated. As seen, the two polarizations had very similarly

performance for EDC- and DBP-based transmission. Nevertheless, there was a slight advantage from the X-Pol due to the better frequency responses of the front-end components, which, as seen in Figure 71, required less pre-emphasis.

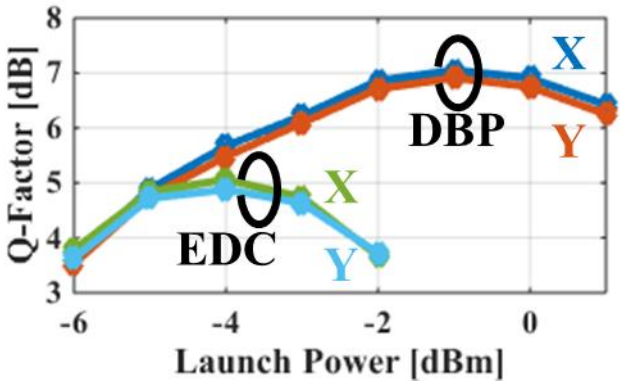

Figure 70. DBP and EDC Center channel performance with ideal transmitter

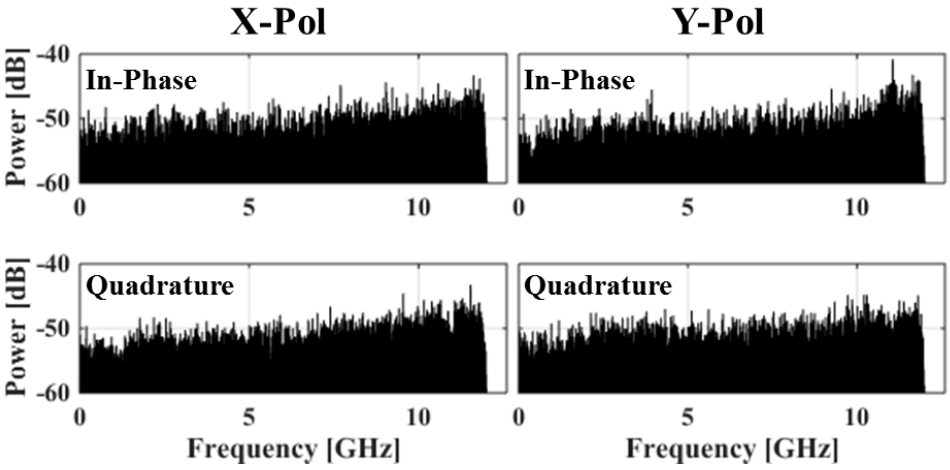

Figure 71. Spectrum of the precompensated digital waveforms with pre-emphasis

When utilizing DBP-based transmission, the effect of an artificially-introduced power imbalance between the two polarizations of center channel is shown in Figure 72. As explained previously, in this instance the imbalance was emulated by attenuating the power of the Y-pol, whereas the power of the X-Pol was not altered. Thus, the performance

of the Y-Pol deteriorated due to the lower received Optical Signal-to-Noise Ratio, whereas in contrast, the performance of the X-Pol was not significantly affected.

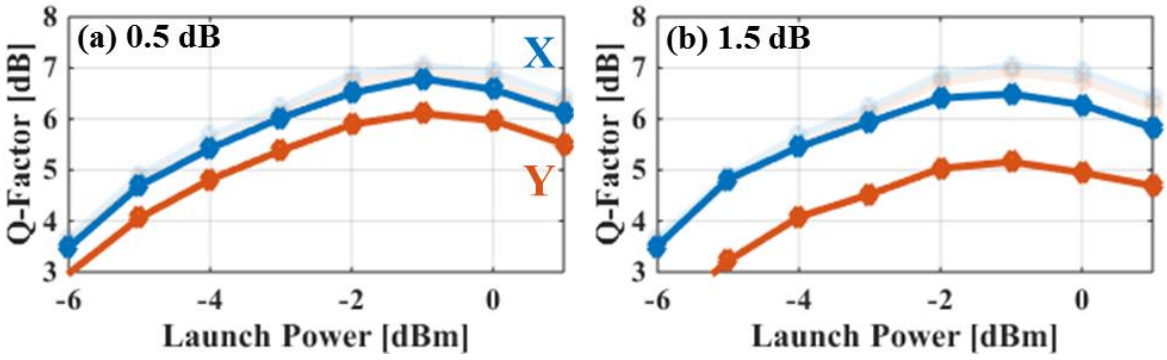

Figure 72. DBP Center channel performance in the presence of a power imbalance of (a) 0.5 dB (b) 1.5 dB. (Transparent lines show ideal case).

Lastly, the effect of a time-skew between the X- and Y-Polarizations of the center channel only is shown in Figure 73. As seen, 5 ps of deskew has a limited effect on the overall performance, given that the delay is only 10% of the symbol period, whereas the nonlinear effects will still evolve close to the prediction of the compensation model. However, as the deskew increases to 15 ps (37% of the symbol period), the penalty on the delayed polarization (Y-Pol) exceeds 1 dB, while a 25 ps deskew (61% of the symbol period) increased the penalty to more than 2 dB. As demonstrated by the results in Figure 73, in contrast to the case with a power imbalance, which mostly affects the polarization with the lower power, a time-skew will affect the performance of both polarizations, whereas the polarization being delayed accrues most of the penalty. The origin of this penalty lays in the substantial time misalignment of the channels, which thereby deviate from the waveform profile assumed in the DBP engine, and directly hinders the nonlinearity compensation process.

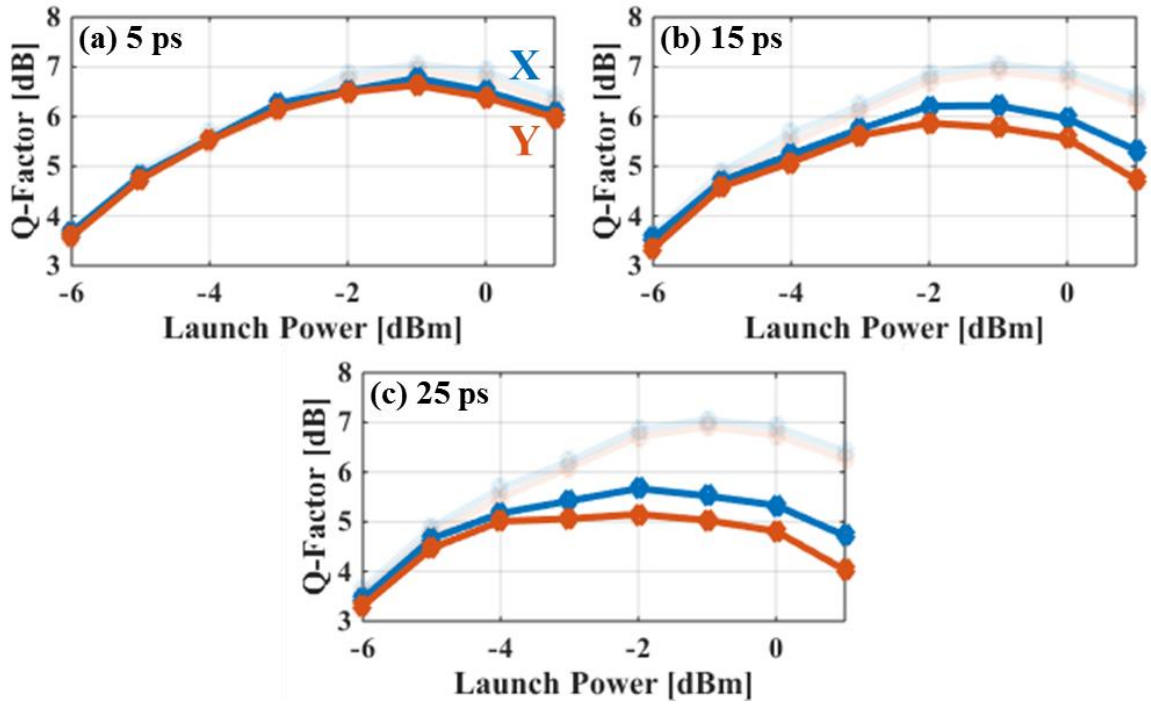

Figure 73. DBP Center channel performance in the presence of a polarization timing skew of (a) 5 ps (b) 15 ps (c) 25 ps (Transparent lines show ideal case).

5.4 Experimental Demonstration 6: The First Demonstration of High-Capacity Transmission Reach Tripling

5.4.1 Experimental Setup

The high-capacity nonlinear crosstalk cancellation test-bed consisted of a frequency-referenced (FR) transmitter array, a transmission link implemented as a recirculating loop and a standard coherent receiver, as shown in Figure 74.

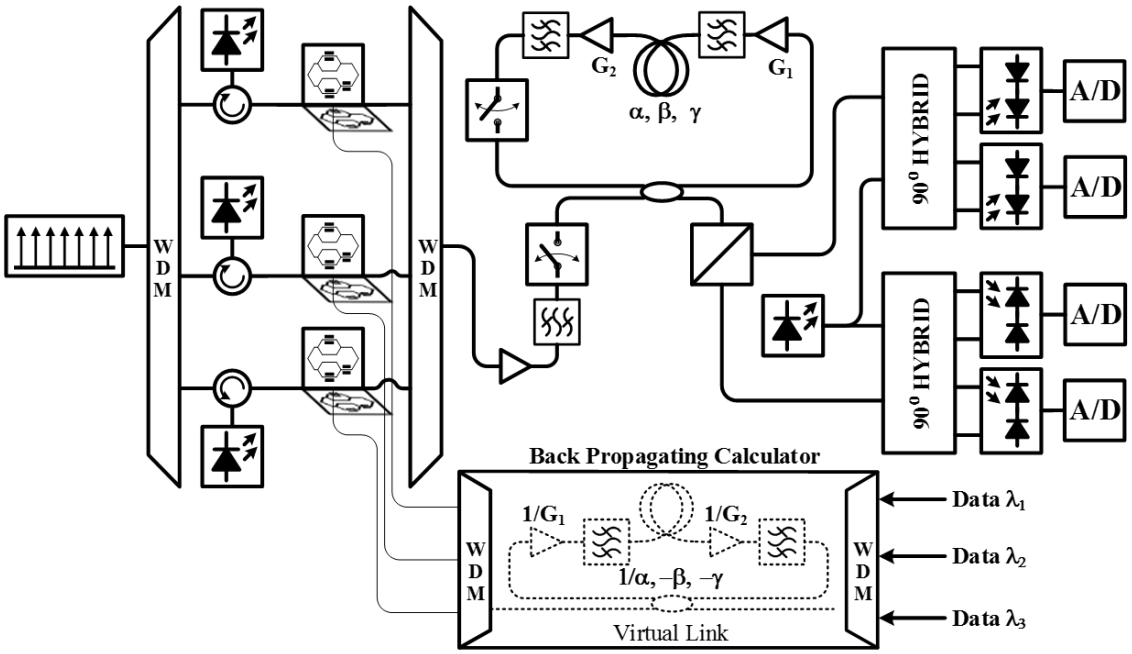

Figure 74. Nonlinear transmission test bed

Similarly to Chapter 4, the setup relies on an indirect frequency reference, which serves to ensure that the mutual walk-off velocities between WDM channels remain fixed with respect to each other, allowing a deterministic evolution, and, consequently, enabling substantial nonlinear interference cancellation.

In the experiment, the 28 GHz-pitched frequency comb shown in Figure 75a served as a frequency reference. To demonstrate the sufficiency of an indirect frequency reference, three distributed feedback (DFB) lasers with native MHz linewidth were injection-locked to selected comb lines, as shown in Figure 75b. The referencing did not incorporate any phase tracking in the WDM channels' paths, but was instrumental in creating mutually coherent optical carriers with OSNRs in excess of 55 dB and sub-5 kHz linewidth.

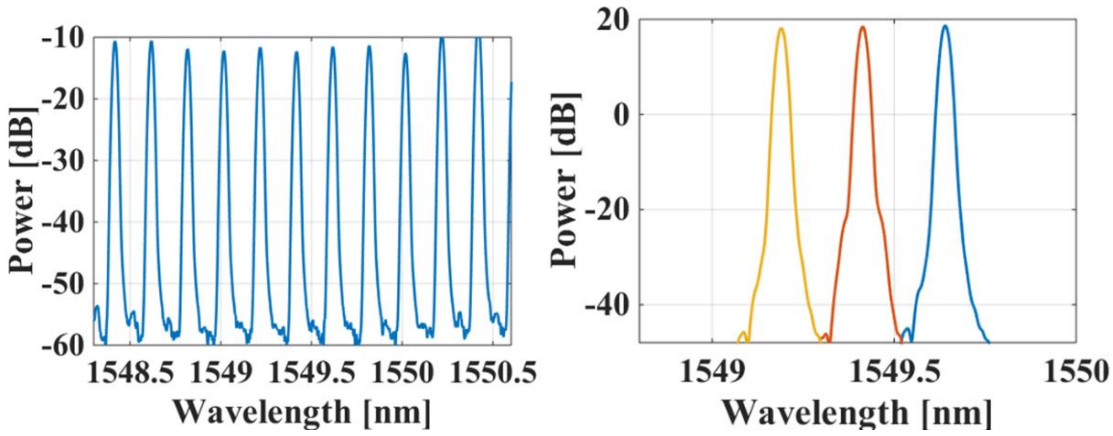

Figure 75. Reference optical frequency comb and injection locked lasers spectra

To achieve the interference cancellation, the transmitted waveforms were pre-distorted using digital back-propagation [57, 58] implemented by a nonlinear Schrodinger (NLS) solver. The transmission performance of nonlinear cancelation (NLC) was compared against the same system with only electronic dispersion compensation (EDC). In both cases (NLC and EDC-only transmission), different shift-register initial conditions were used to generate three pseudo-random bit sequences (PRBS) that were subsequently gray-mapped to 64-QAM symbols. Raised-cosine filtering with 2 samples-per-symbol, 128 filter taps and a roll-off factor of 0.01 was applied prior to the digital back-propagation (DBP) computation to constrain the spectral occupancy. Three sets of four digital-to-analog converters (DAC) [19] were used to generate the electrical pre-distorted signals at the rate of 65 GS/s. The pre-distorted polarization multiplexed 24 GBaud 64-QAM signals were cast onto the optical carriers by means of dual-polarization nested Mach-Zehnder modulators, passively coupled, whereas the channels' polarization alignment was ensured initially by a polarization beam splitter. The precise time alignment of all channels, as in previous experiments, was accomplished by means of optical delay lines and synchronous triggering of the DACs.

The transmission experiment was performed in a recirculating loop shown in Figure 74. A single 85 km span of Standard Single-Mode Fiber (SSMF) with 16 ps/nm/km dispersion, nonlinear coefficient of 1.22 $W^{-1}km^{-1}$ and total attenuation of 15.95 dB was used as a transmission fiber inside the loop. Fiber loss was compensated by an Erbium Doped Fiber Amplifier (EDFA) with 4.5 dB noise figure, while a second EDFA was employed to compensate the loop-associated losses and allow for a wide range of channel launch powers. In addition, a coarse WDM was used to remove out-of-band ASE noise before launching the signals into the fiber.

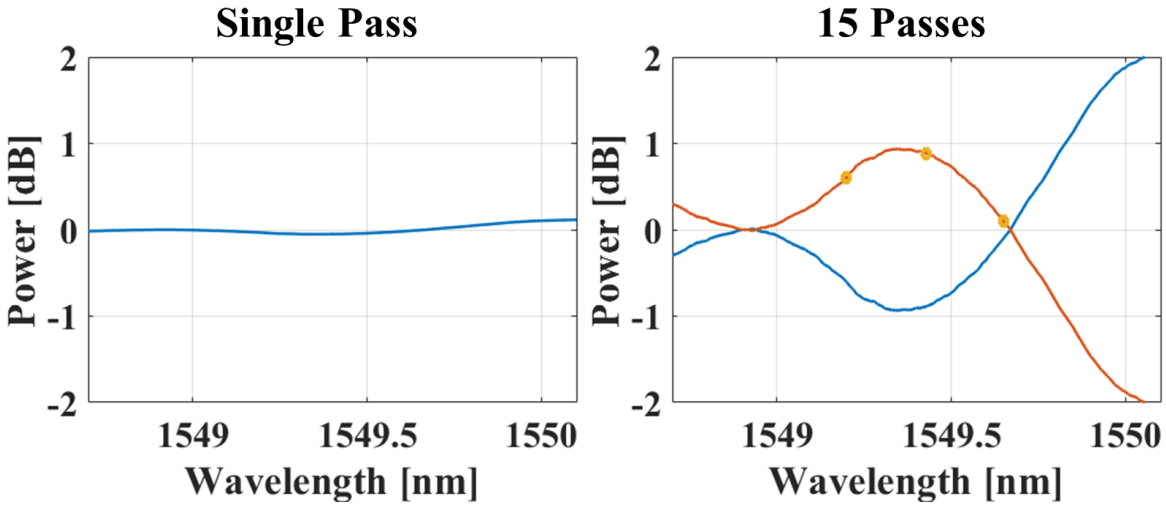

Figure 76. Loop filter power transfer function

As demonstrated in Section 4.2, for NLC to yield the maximum possible improvement, the system model must be accurately replicated in the DBP engine. While Figure 76 and Figure 77(a) suggests that a single pass through the WDM filter had little effect in the spectral shaping and group delay of the signal, it is clear in Figure 76 and Figure 77 (b) that after several passes, the wavelength-dependent loss and group delay

variation was significant. Thus, for this experiment, the shape of the WDM filter was characterized, and the inverse transfer function was used in the backpropagation engine.

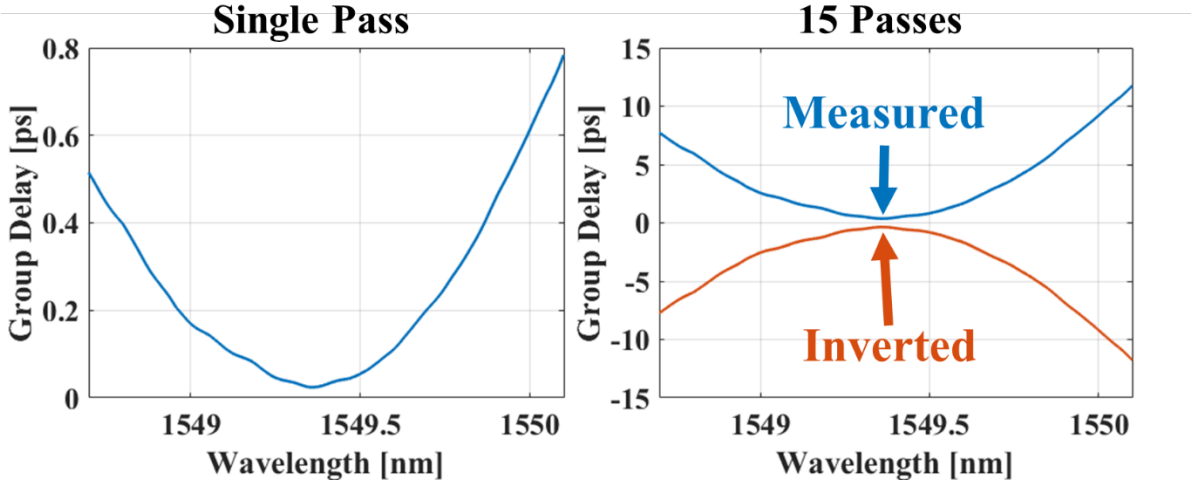

Figure 77. Loop filter group delay transfer function

Additionally, the wavelength-dependent gain and the power evolution for each of the channels was tracked as a function of the span number as shown in Figure 78, and used in the backpropagation engine.

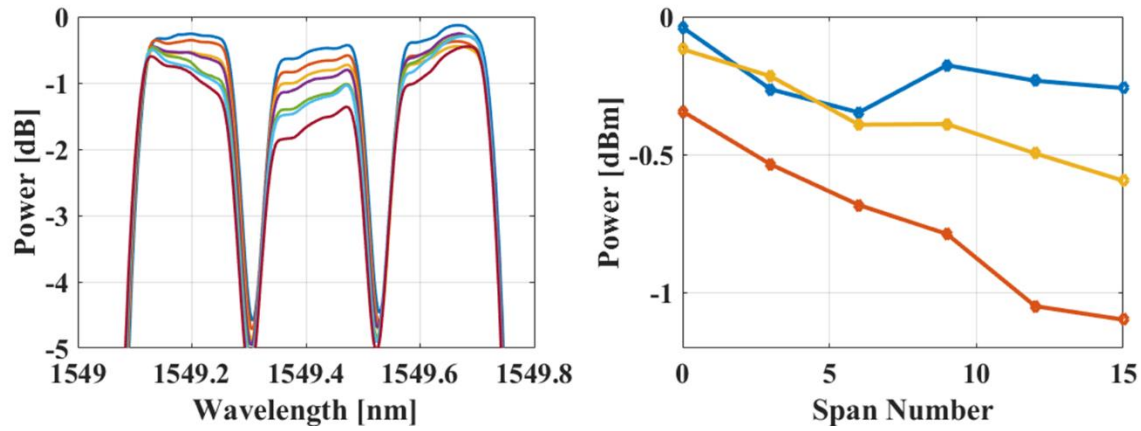

Figure 78. Power evolution of each channel for different transmission lengths

As can be seen in Figure 78, the wavelength-dependent filtering and gain effects in the loop were counteracted with the spectrally shaped signals and adequate power levels

such that after transmission the channels arrived undistorted, i.e. with flat spectrum and equalized power.

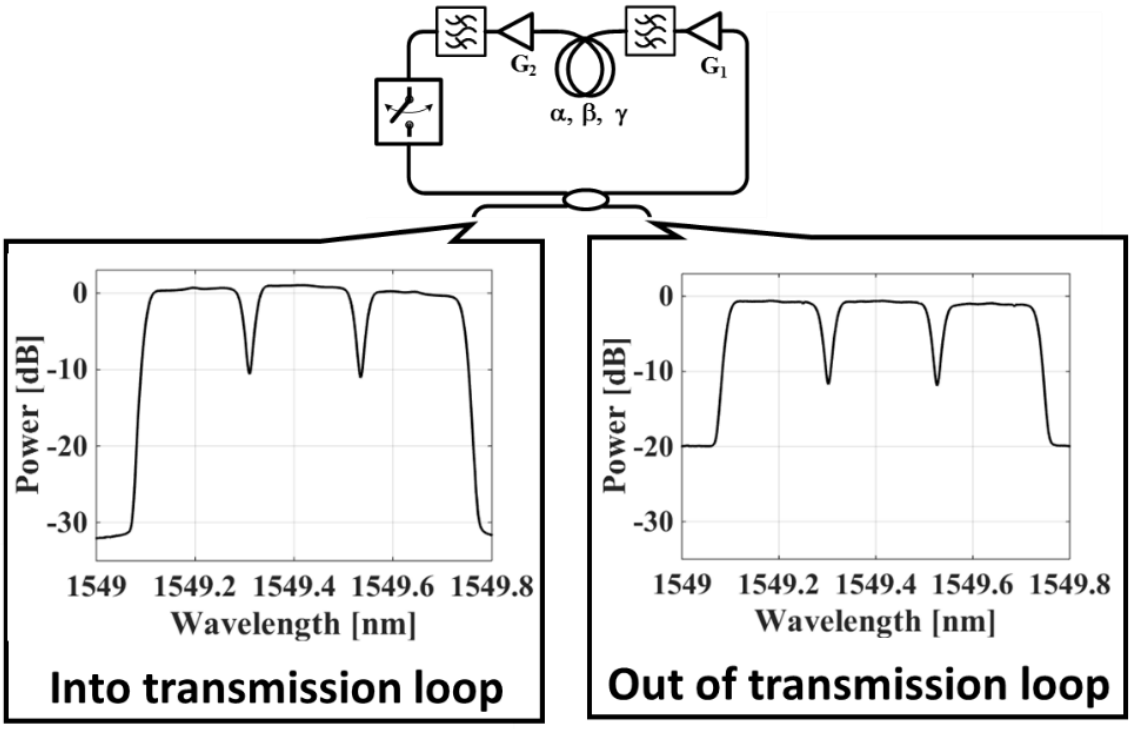

Figure 79. Recirculating loop

After transmission, the signals were independently filtered, and coherently detected using a local oscillator (LO) with sub-100 kHz linewidth. The coherent receiver consisted of a dual-polarization 90-degree hybrid and four pairs of balanced, 40 GHz-bandwidth detectors. The electrical signals were digitized using real-time oscilloscope operating at 50 GS/s sampling rate, and subsequent processing was performed offline relying on the DSP engine introduced previously.

Two distinct transmission conditions were investigated. In the first case, only linear impairment compensation was applied, i.e. without the pre-compensating block, and with only EDC applied at the receiver by means of an ideal frequency domain compensator. In

the second case, both linear and nonlinear impairment compensation was employed at the transmitter side, i.e. the pre-compensation block was enabled, effectively eliminating the need for any further dispersion compensation at the receiver.

5.4.2 Results

The measured improvement in the Q factor strictly defines the reach extension measure, which was the original motivation for this experiment.

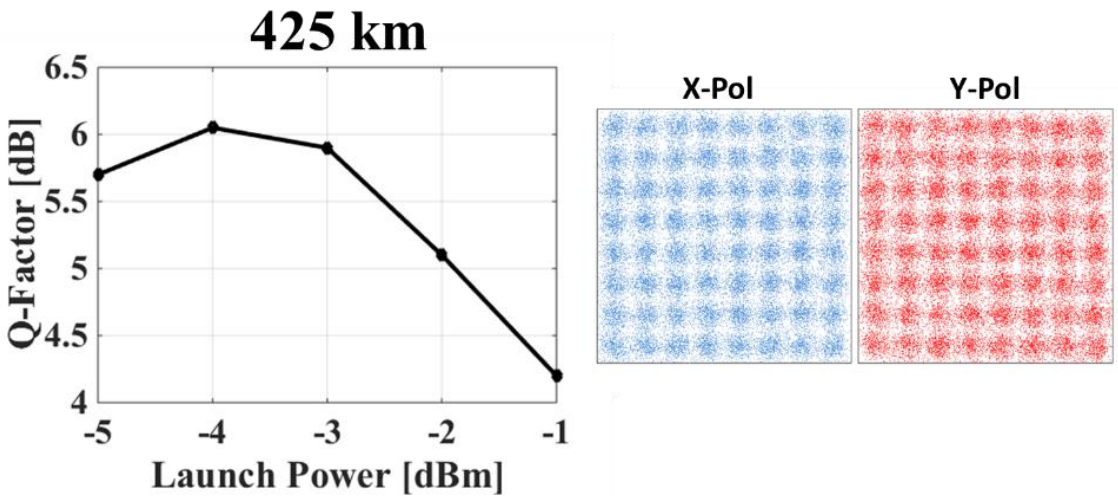

Figure 80. Linear reach performance

The linear reach (i.e. transmission using EDC only) was 425 km for the forward error correction Q^2 threshold of 5.7 dB, as shown in Figure 80. The uncompensated transmission, necessarily operating in the quasi-linear regime, follows a well-known performance trend with clearly distinguishable optimal launch power, as shown in Figure 80, with the cross-talk dominating over the OSNR increase. This ultimately led to a strict reach limitation of 425 km in this case, for the measured Q-factor of 6.03 dB.

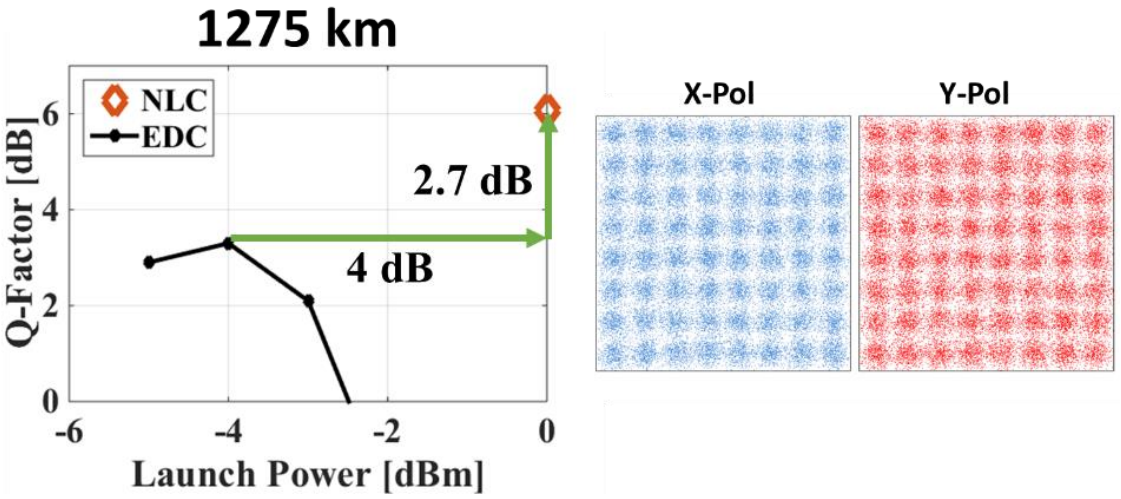

Figure 81. Nonlinear reach performance

In sharp contrast, as shown in Figure 81, the nonlinear crosstalk cancellation allowed the operation in the nonlinear regime that benefited from the elevated OSNR (inherent to the higher launch power condition), enabling the transmission reach extension. As demonstrated by the measurements plotted in Figure 81, in this instance it was possible to increase the average power by 4 dB beyond the optimal quasi-linear level and achieve tripling of the reach, closely approximating the improvement expected from OSNR increase following from the launch power increase. Figure 82 shows the per-channel performance at the nonlinear reach, which was three-times longer than the reach of the EDC-only system.

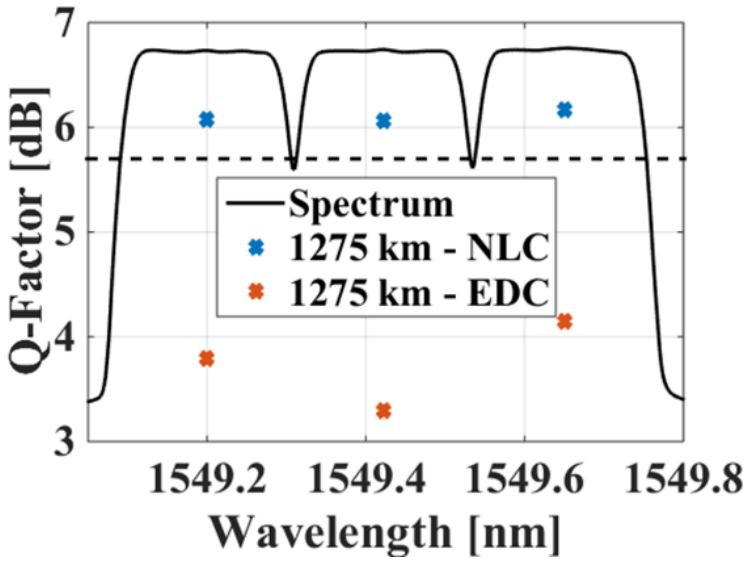

Figure 82. Per-channel performance at three-times the reach of EDC-only system

5.5 Summary

In this chapter, we have developed practical groundwork to apply NLC to a high-capacity system that employs Dense Wavelength Division Multiplexing, high cardinality constellations and polarization multiplexing. We demonstrated, for the first time, the tripling of conventional transmission reach in a coherent WDM link by digital processing, wherein the system reach was extended from 425 km to 1275 km, at a 6 dB Q factor performance level.

To achieve this level of nonlinear crosstalk cancellation, aside from employing frequency-referencing, we relied on the accurate modeling of the link parameters, characterizing every element in the transmission path. The nonlinearity compensation allowed transmission well within the previously prohibited nonlinear regime, and operated at 4 dB higher power with respect to the conventional linear transmission optimum power – a, so far, unmatched experimental achievement.

Furthermore, this demonstration utilized indirect frequency reference provision by injection locking DFB lasers (with native MHz linewidth) to a highly coherent, kHz-linewidth frequency comb, as proposed in Chapter 4.

Chapter 5, in part contains material presented in the European Conference on Optical Communication, (2016), Dusseldorf, titled "Demonstration of Coherent Transmission Reach Tripling by Frequency-Referenced Nonlinearity Pre-compensation in EDFA-only SMF Link," by Eduardo Temprana, Evgeny Myslivets, Vahid Ataie, Bill P.-P. Kuo, Nikola Alic, Vijay Vusirikala, Vinayak Dangui and Stojan Radic. In addition, Chapter 5 in part contains material currently prepared for submission to Photonics Technology Letters, titled “Penalties Associated with Polarization-Power Imbalance and Polarization-Timing Skew in Multichannel Transmitter-Side Digital Back Propagation”, by Eduardo Temprana, Evgeny Myslivets, Bill P.-P. Kuo, Nikola Alic and Stojan Radic. Lastly Chapter 5 in part or in full contains material currently being prepared for submission to Journal of Lightwave Technology, titled “Demonstration of Coherent Transmission Reach Tripling by Frequency-Referenced Nonlinearity Pre-compensation in EDFA-only SMF Link,” by Eduardo Temprana, Evgeny Myslivets, Vahid Ataie, Bill P.-P. Kuo, Nikola Alic, and Stojan Radic. The dissertation author was the primary investigator, and the primary author of these articles.

Chapter 6. Conclusion

6.1 Dissertation Summary

With traffic demands growing at an unprecedented rate, we are rapidly approaching the exhaustion of the available bandwidth of deployed optical networks. It has thus become imperative to develop techniques that will increase the information-carrying capacity of the optical fiber, which is presently only limited by nonlinear crosstalk.

Previous theoretical investigations have predicted that the limit of fiber capacity lies at the onset of the nonlinear crosstalk, wherein the crosstalk was considered an unpredictable phenomenon, much like noise. We must, however, realize that at least in what refers to signal-signal interactions, nonlinear crosstalk is deterministic and must thusly be predictable and lend itself to cancellation. Naturally, nonlinear crosstalk cancellation would increase fiber capacity beyond previously established limits, however, experimental demonstrations that have attempted to compensate nonlinear crosstalk have had limited success. In this dissertation, we have for the first time unequivocally demonstrated the importance of frequency reference in the compensation of nonlinear impairments using DSP-based techniques in high-speed fiber optic transmission systems.

The first step towards demonstrating the feasibility of NLC was to validate its performance in a noise-unimpaired scenario. In the first experimental demonstration featured in this thesis, we force the interaction between a strong pump and a weak probe in a short piece of highly nonlinear fiber. The high nonlinearity of the fiber guaranteed strong interaction while its short length limited the pump and probe attenuation, and thus the accrual and effect of the noise was minimized. The pump, whose power was orders of

magnitude larger than the probe, generated significant crosstalk on the uncompensated probe, and distorted it from its original form. In sharp contrast, when the probe was precompensated for the predicted crosstalk, the probe arrived at the receiver without any distortion, clearly proving that nonlinear crosstalk arising from signal-signal interaction is cancellable in its totality, thus demonstrating that NLC is indeed achievable (at least in a noise free environment).

Second due was to carry out experiments in more realistic conditions, and to verify what system configurations can indeed enable NLC. For this, we carried out a long-haul transmission experiment, wherein three channels were transmitted over 1000 km of SMF, at 2 dBm per channel, a power that was far higher than the optimum level. Such conditions elicited significant nonlinear crosstalk, and severely distorted the constellation of the center channel. In the experiment, the performance of the Nonlinearity Cancellation was investigated with three different configurations with varying degrees of mutual coherence among the propagating carriers. It was observed that when the free-running laser was utilized as the carrier for the center channel, the nonlinearity cancellation was significantly impeded. Similarly, when the two side channels were free-running, the ability to reverse the nonlinear crosstalk dropped even further. Lastly, when all the channels lacked any frequency reference, the cancellation failed altogether. Additionally, the same demonstration was extended to a system that carried 5 channels, where again it was observed that the nonlinearity cancellation was only successful when indeed all channels were frequency-referenced. These experiments effectively prove that NLC is realizable even in practice, and that fiber capacity can be increased over previous estimates.

Nevertheless, fiber capacity cannot be measured in laboratory experiments with limited means, and thus the increase in capacity provided by NLC can only be estimated. Instead, system reach, which is intimately related to fiber capacity, can be measured with and without the aid of NLC. In the third experiment, the linear reach of the same three-channel system, measured at 1530 km, was doubled to 3060 km by compensating the nonlinear crosstalk. Nonlinearity cancellation enabled us to take advantage of the increased signal OSNR provided by a higher launch power without incurring in a penalty due to the crosstalk, increasing the system reach -in this case- by a factor of two.

In this thesis, we have also proposed alternative system implementations with different complexities and component cost. In Chapter 4, we experimentally demonstrated two different architectures which took advantage of frequency-referenced carriers. By injection locking Distributed Feedback and Fabry-Perot lasers to an optical frequency comb with lower intrinsic OSNR than the parametric comb used in Chapter 3, we demonstrate the possibility of relaxing the system cost and component specifications of the source of frequency reference. In addition, injection locked DFB lasers provide high-power frequency referenced carriers that can overcome the large losses of NMZM modulators and other transmitter components, thereby enabling higher launch OSNRs, which prove beneficial in NLC applications.

In the last part of the dissertation, presented in Chapter 6, we developed practical groundwork conducive to a NLC implementation for high-capacity systems that employs Dense Wavelength Division Multiplexing, high cardinality constellations and polarization multiplexing. We demonstrated, for the first time, the tripling of conventional transmission reach in a coherent WDM link by digital processing, wherein the 10.3 bit/sec-Hz system

reach was extended from 425 km to 1275 km. To achieve this level of nonlinear crosstalk cancellation, aside from employing frequency-referencing, we relied on the accurate modeling of the link parameters, characterizing every element in the transmission path. The nonlinearity compensation allowed transmission well within the previously prohibited nonlinear regime, and operated at 4 dB higher power with respect to the conventional linear transmission optimum power.

Thus, in summary, the work covered by this thesis on the one hand firmly proved the necessary condition of frequency reference for successful digital NLC, through a set of rigorous experiments unmatched in complexity and accuracy. Furthermore, we have revealed various obstacles to practical implementation of the NLC – and much to the author's pride, managed to solve those with an outstanding success in this long and arduous journey of discovery. Indeed, while only a couple of years ago NLC seemed only a theoretical possibility, believed to be unrealizable in practice (owing to the repeated failures of many predecessors), it is fair to say that following the contributions of the work presented, this remarkable concept has been brought to the verge of practical reality.

6.2 Future Outlook

While the main challenge in DSP-based NLC methods, namely carrier frequency stability, has been covered and demonstrated, there are several other important factors that remain to be investigated and solved before the NLC is to become widely adopted.

First and foremost is to understand what the limitations of DBP-based NLC are. Figure 83 shows the comparison between the performance at the nonlinear reach of the system presented in Chapter 4, and an equivalent realistic simulation that includes amplifier

noise. It is obvious that the experimental demonstration fails to achieve the performance predicted by the simulation. Research must be dedicated to understand the shortcomings of real-life system implementations, wherein the penalties due to effects such as Polarization-Mode Dispersion, limited resolution in DACs and ADCs, and other practical issues must be quantified and appropriately addressed. Additionally, we must realize that while deployed systems operate in a regime where the signal-noise interactions are weak, at high enough powers, these effects will take over, at which point no further improvement of NLC shall be possible. Thus, the exact onset and the involved tradeoffs of this mode of operation need to be determined.

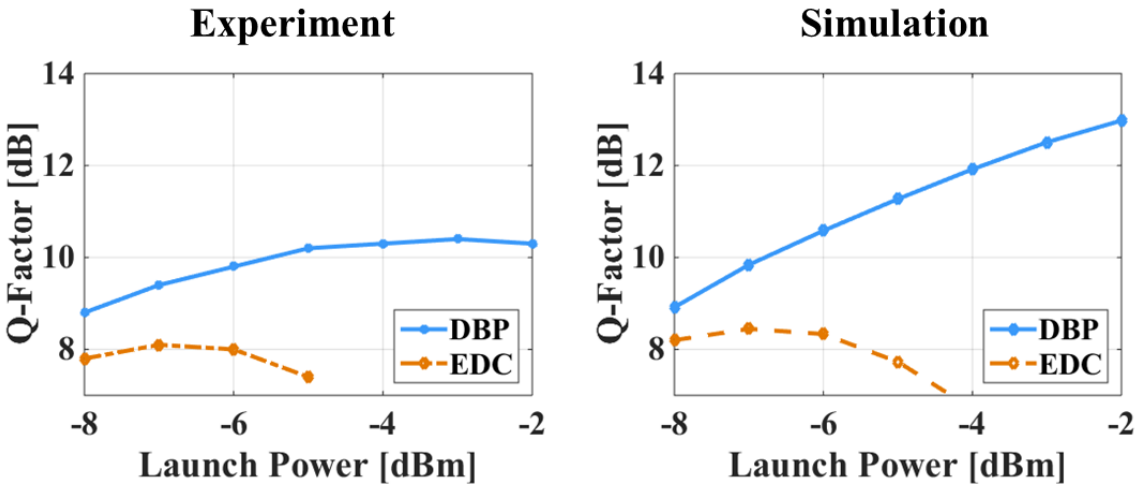

Figure 83. Simulation vs. Experimental performance

Second is the issue of complexity in the NLSE inversion. The Split-Step Fourier Method requires forward and inverse fast Fourier transform operations, whose complexity scales as a $N \log N$, where N is the number of samples and is typically defined by the dispersive length of the system. It is imperative to reduce this complexity for NLC to be applicable in real-time high speed systems. In this regard, there have been reports of implementations that employ a perturbation-based approach to find an analytical

expression for the effect of fiber nonlinearity [59]. Additionally, other approaches have also been developed for nonlinearity compensation, such as Volterra-based [60] or memory polynomial based DBP [61]. For these, a pragmatic investigation must be carried out to weigh the improvement provided of each method versus the required complexity.

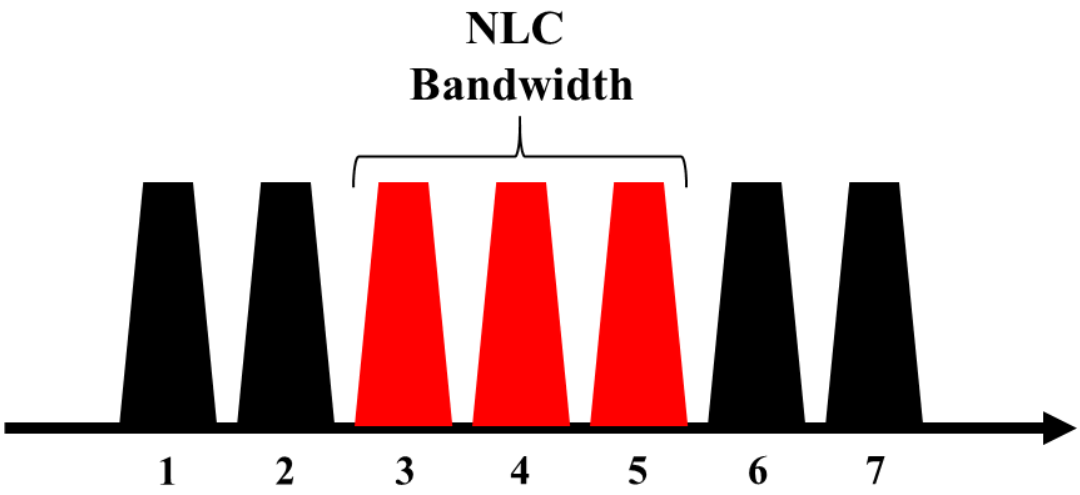

Figure 84. NLC over a subset of channels

Another possible path to reduce the complexity of NLC would be to consider only a subset of channels as shown in Figure 84. It is important to note that the experiments performed in this dissertation were done with at most 5 channels, whereas real systems operate with hundreds of channels. NLC implementations operating over hundreds of channels would be prohibitive in complexity. It would be interesting to investigate the minimum number of channels that need to be considered to achieve sufficient nonlinearity cancellation. Figure 85 shows the results of a simulation of a system that carries 31 channels, whereas NLC is only applied to a subset of channels; the percentage increase in system reach provided by NLC is plotted as a function of the number of channels that are considered.

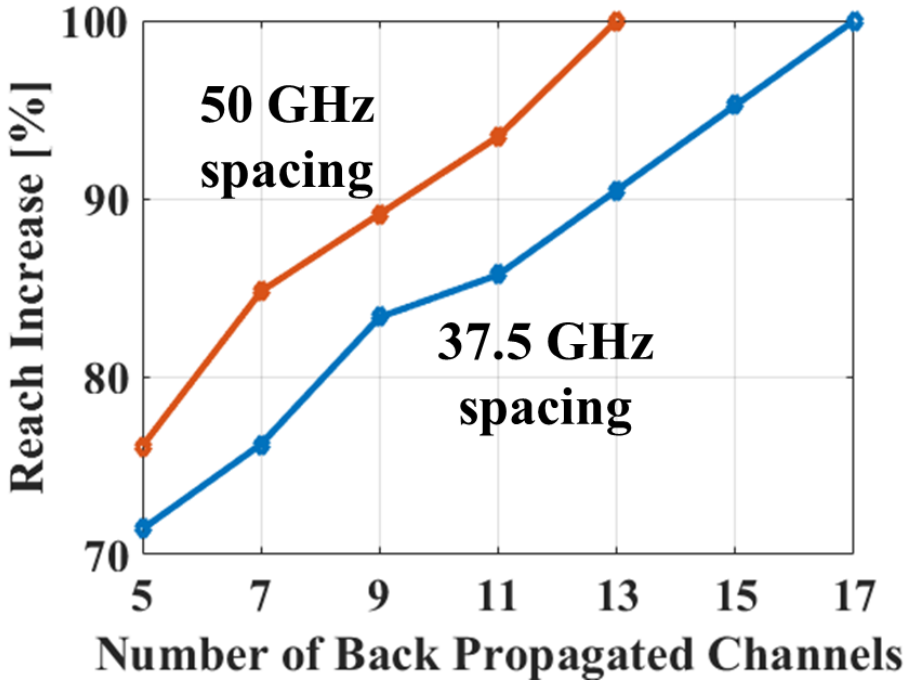

Figure 85. Reach increase vs. Number of channels considered for NLC

As seen, in a system with 50 GHz channel spacing, in order to increase the reach by 100% only 13 of the 31 channels must be considered in the NLC. Similarly, when the channel spacing is 37.5 GHz, the number of channel increases to 17. In both cases, the bandwidth required in the NLC engine is about 650 GHz, implying that the nonlinear effects are confined within a given bandwidth, and are independent of the number of channels and their spacing. Research should be devoted to derive analytical expressions that will predict these optimum bandwidths, and their relation to system parameters such as signal power, channel spacing, fiber nonlinearity, dispersion and attenuation.

As a concluding remark, it is worth noting that the issues posed herein are not fundamental limitations. Hopefully, the results presented in this dissertation will serve to spark inspiration to advance this research field, so that one day digital NLC becomes a practical option that becomes widely adopted in the field.

BIBLIOGRAPHY

[1] Cisco, "The Zettabyte Era: Trends and Analysis," 2015.

[2] D. J. Richardson, "Filling the Light Pipe," *Science,* vol. 15, pp. 327-328, 2010.

[3] K. C. Kao and G. A. Hockham, "Dielectric-fibre surface waveguides for optical frequencies," *IEEE Proceedings Journal of Optoelectronics,* vol. 133, no. 3, 1986.

[4] E. Desurvire, J. R. Simpson and P. C. Becker, "High-gain erbium-doped traveling-wave fiber amplifier," *Optics Letters,* vol. 12, no. 11, pp. 888-890, 1987.

[5] G. C. Papen and R. E. Blahut, Lightwave Communication Systems, San Diego: Draft, 2017.

[6] J. Hecht, "Wavelength Division Multiplexing," MIT Technology Review, 1 March 1999. [Online]. Available: https://www.technologyreview.com/s/400349/wavelength-division-multiplexing/.

[7] K. Kikuchi, "Coherent Optical Communications: Historical Perspectives and Future Directions," in *High Spectral Density Optical Communication Technologies,* Berlin , Springer Berlin Heidelberg, 2010, pp. 11-49.

[8] S. Savory, G. Gavioli, R. I. Killey and P. Bayvel, "Electronic compensation of chromatic dispersion using a digital coherent receiver," *Optics Express,* vol. 15, pp. 2120-2126, 2007.

[9] G. P. Agrawal, Nonlinear Fiber Optics, Academic Press, 2007.

[10] P. P. Mitra and J. B. Stark, "Nonlinear limits to the information capacity of optical fibre communications," *Nature ,* vol. 411, pp. 1027-1030, 2001.

[11] N. Alic, E. Myslivets, E. Temprana, B. P.-P. Kuo and S. Radic, "Nonlinearity Cancellation in Fiber Optic Links Based on Frequency Referenced Carriers," *Journal of Lightwave Technology,* vol. 32, pp. 2690-2698, 2014.

[12] Y. Yamamoto, M. Hirano and T. Sasaki, "Low-Loss and Low-Nonlinearity Pure-Silica-Core Fiber for Large Capacity Transmission," *Sumitomo Electric Industries Technical Review Number,* vol. 76, 2013.

[13] G. P. Agrawal, Fiber-Optic Communication Systems, New York: Wiley, 1997.

[14] J. Kerr, "XL. A new relation between electricity and light: Dielectrified media birefringent," *Philosophical Magazine Series 4,* vol. 50, no. 332, 1875.

[15] J. Yang and K. Akylas, "Continuous Families of Embedded. Solitons in the Third Order Nonlinear Schrodinger Equation," *Studies in Applied Mathematics,* vol. 111, pp. 359-375, 2003.

[16] J. E. Prilepsky, S. A. Derevyanko and S. K. Turitsyn, "Nonlinear spectral management: Linearization of the lossless fiber channel," *Optics Express,* vol. 21, no. 20, pp. 24344-24367, 2013.

[17] T. R. Taha and M. I. Ablowitz, "Analytical and numerical aspects of certain nonlinear evolution equations. II. Numerical, nonlinear schrödinger equation," *Journal of Computational Physics,* vol. 55, no. 2, pp. 203-230, 1984.

[18] J. Proakis and M. Salehi, Digital Communications, San Diego: McGraw-Hill Education, 2007.

[19] Fujitsu Semiconductor Europe, "LEIA DAC Factsheet," [Online]. Available: www.fujitsu.com/downloads/MICRO/fme/documentation/c60.pdf.

[20] M. Nakazawa, S. Okamoto, T. Omiya, K. Kasai and M. Yoshida, "256 QAM (64 Gbit/s) coherent optical transmission over 160 km with an optical bandwidth of 5.4 GHz," in *Optical Fiber Communications Conference*, San Diego, 2010.

[21] A. H. Gnauck, P. J. Winzer, A. Konczykowska, F. Jorge, J.-Y. Dupuy, M. Riet, G. Charlet, B. Zhu and D. W. Peckham, "Generation and Transmission of 21.4-Gbaud PDM 64-QAM Using a Novel High-Power DAC Driving a Single I/Q Modulator," *Journal of Lightwave Technology* , vol. 30, no. 4, pp. 532-536, 2012.

[22] R. Noé, M. F. Panhwar, C. Wördehoff and D. Sandel, "Realtime digital signal processing in coherent optical PDM-QPSK and PDM-16-QAM transmission," in *European Signal Processing Conference*, Lisbon, 2014.

[23] M. Faruk, Y. Mori, C. Zhang, K. Igarashi and K. Kikuchi, "Multi-impairment monitoring from adaptive finite-impulse-response filters in a digital coherent receiver," *Optics Express,* vol. 18, no. 26, pp. 26929-26936, 2010.

[24] D. Godard, "Self-Recovering Equalization and Carrier Tracking in Two-Dimensional Data Communication Systems," *IEEE Transactions on Communications,* vol. 28, no. 11, pp. 1867-1875, 1980.

[25] S. U. H. Qureshi, "Adaptive equalization," *Proceedings of the IEEE,* vol. 73, no. 9, pp. 1349-1387, 1985.

[26] S. Savory, "Digital filters for coherent optical receivers," *Optics Express,* vol. 16, no. 2, pp. 804-817, 2008.

[27] T. Hasegawa, Y. Yamamoto, Y. Tamura and T. Hayashi, "Advances in Ultra-low Loss Silica Fibers," in *Optical Fiber Communications Conference,* Anaheim, 2016.

[28] C. Shannon, "A Mathematical Theory of Communication," *The Bell System Technical Journal,* vol. 27, no. 3, pp. 379-423, 623-656, 1948.

[29] R. J. Essiambre, G. Kramer, P. Winzer and G. Foschini, "Capacity Limits of Optical Fiber Networks," *Journal of Lightwave Technology,* vol. 28, no. 4, pp. 662-701, 2010.

[30] R. Dar, M. Shtaif and M. Feder, "New bounds on the capacity of the nonlinear fiber-optic channel," *Optics Letters,* vol. 39, no. 2, pp. 398-401, 2014.

[31] E. Agrell, A. Alvarado, G. Durisi and M. Karlsson, "Capacity of a Nonlinear Optical Channel With Finite Memory," *Journal of Lightwave Technology,* vol. 32, no. 16, pp. 2862-2876, 2014.

[32] P. Poggiolini, "The GN Model of Non-Linear Propagation in Uncompensated Coherent Optical Systems," *Journal of Lightwave Technology,* vol. 30, no. 24, pp. 3857-3879, 2012.

[33] A. D. Ellis, M. E. McCarthy, M. A. Z. Al-Khateeb and S. Sygletos, "Capacity limits of systems employing multiple optical phase conjugators," *Optics Express,* vol. 23, pp. 20381-20393, 2015.

[34] R. Dar and P. J. Winzer, "On the Limits of Digital Back-Propagation in Fully Loaded WDM Systems," *Photonics Technology Letters,* vol. 28, pp. 1253-1256, 2016.

[35] X. Li, X. Chen, G. Goldfarb, E. Mateo, I. Kim, F. Yaman and G. Li, "Electronic post-compensation of WDM transmission impairments using coherent detection and digital signal processing," *Optics Express,* vol. 16, no. 2, pp. 880-888, 2008.

[36] E. Ip and J. Kahn, "Compensation of Dispersion and Nonlinear Impairments Using Digital Backpropagation," *Journal of Lightwave Technology,* vol. 26, no. 20, pp. 3416-3425, 2008.

[37] E. Ip, "Nonlinear Compensation Using Backpropagation for Polarization-Multiplexed Transmission," *Journal of Lightwave Technology,* vol. 28, no. 6, pp. 939-951, 2010.

[38] E. B. Treacy, "Optical pulse compression with diffraction gratings," *Journal of Quantum Electronics,* vol. 5, no. 9, p. 454, 1969.

[39] D. Garthe, R. Epworth, W. Lee, A. Hadjifotiou, C. Chew, T. Bricheno, A. Fielding, H. Rourke, S. Baker, K. Byron, R. Baulcomb, S. Ohja and S. Clements, "Adjustable dispersion equaliser for 10 and 20 Gbit/s over distances up to 160 km," *Electronics Letters,* vol. 30, no. 25, pp. 2159 - 2160, 2002 .

[40] N. Litchinitser, M. Sumetsky and P. Westbrook, "Fiber-based tunable dispersion compensation," *Journal of Optical Communications,* vol. 4, no. 41, 2007.

[41] N. K. Fontaine, X. Liu, S. Chandrasekhar, R. Ryf, S. Randel, P. Winzer, R. Delbue, P. Pupalaikis and A. Sureka, "Fiber Nonlinearity Compensation by Digital Backpropagation of an Entire 1.2-Tb/s Superchannel Using a Full-Field Spectrally-Sliced Receiver," in *European Conference on Optical Communications*, London, 2013.

[42] E. Temprana, V. Ataie, B.-P. Kuo, E. Myslivets, N. Alic and S. Radic, "Low-noise parametric frequency comb for continuous C-plus-L-band 16-QAM channels generation," *Optics Express,* vol. 22, pp. 6822-6828, 2014.

[43] B. P.-P. Kuo, E. Myslivets, V. Ataie, E. Temprana, N. Alic and S. Radic, "Wideband Parametric Frequency Comb as Coherent Optical Carrier," *Journal of Lightwave Technology,* vol. 31, no. 21, pp. 3414 - 3419, 2013.

[44] K. Toyoda, Y. Koizumi, T. Omiya, M. Yoshida, T. Hirooka and M. Nakazawa, "Marked performance improvement of 256 QAM transmission using a digital back-propagation method," *Optics Express,* vol. 20, no. 18, pp. 19815-19821, 2012.

[45] L. Dou, Z. Tao, Y. Akiyama, S. Oda, Y. Fan, T. Oyama, H. Nakashima, T. Hoshida and J. C. Rasmussen, "Real-Time 112Gb/s DWDM Coherent Transmission with 40% Extended Reach by Transmitter-side Low-Complexity Nonlinear Mitigation," in *European Conference on Optical Communications*, Amsterdam, 2012.

[46] E. Myslivets, B. Kuo, N. Alic and S. Radic, "Generation of wideband frequency combs by continuous-wave seeding of multistage mixers with synthesized dispersion," *Optics Express,* vol. 20, pp. 3331-3344, 2013.

[47] N. Bergano and C. Davidson, "Circulating loop transmission experiments for the study of long-haul transmission systems using erbium-doped fiber amplifiers," *Journal of Lightwave Technology,* vol. 13, no. 5, pp. 879 - 888, 1995.

[48] D. Rafique, A. Napoli, S. Calabro and B. Spinnler, "Digital Preemphasis in Optical Communication Systems: On the DAC requirements for Terabit transmission applications," *Journal of Lightwave Technology,* vol. 32, no. 19, pp. 3247-3256, 2014.

[49] S. Berber, "An automated method for BER characteristics measurement," *IEEE Transactions Instrumentation and Measurement,* vol. 53, no. 2, pp. 575-580, 2004.

[50] J. P. Gordon and L. F. Mollenauer, "Phase noise in photonic communications systems using linear amplifiers," *Optics Letters,* vol. 15, no. 23, pp. 1351-1353, 1990.

[51] M. H. Taghavi, G. C. Papen and P. H. Siegel, "On the multiuser capacity of WDM in a nonlinear optical fiber: Coherent communication," *IEEE Transactions on Information Theory,* vol. 52, pp. 5008-5022, 2006.

[52] N. Alic and S. Radic, "Optical Frequency Combs for Telecom and Datacom Applications," in *Optical Fiber Communications Conference,* San Francisco, 2014.

[53] E. Temprana, E. Myslivets, B.-P. Kuo, L. Liu, V. Ataie, N. Alic and S. Radic, "Overcoming Kerr-induced capacity limit in optical fiber transmission," *Science,* vol. 348, no. 6264, pp. 1445-1448, 2015.

[54] E. Temprana, E. Myslivets, L. Liu, V. Ataie, A. Wiberg, B. Kuo, N. Alic and S. Radic, "Two-fold transmission reach enhancement enabled by transmitter-side digital backpropagation and optical frequency comb-derived information carriers," *Optics Express,* vol. 23, pp. 20774-20783, 2015.

[55] R. Wu, V. R. Supradeepa, C. M. Long, D. E. Leaird and A. M. Weiner, "Generation of very flat optical frequency combs from continuous-wave lasers using cascaded intensity and phase modulators driven by tailored radio frequency waveforms," *Optics Letters,* vol. 35, no. 19, pp. 3234-3236, 2010.

[56] W. Xu and E. G. Friedman, "Clock Feedthrough in CMOS Analog Transmission Gate Switches," *Analog Integrated Circuits and Signal Processing,* vol. 44, no. 3, p. 271–281, 2005.

[57] K. Roberts, C. Li, L. Strawczynski, M. O'Sullivan and I. Hardcastle, "Electronic precompensation of optical nonlinearity," *IEEE Photonics Technology Letters*, vol. 18, no. 2, pp. 403 - 405, 2006.

[58] R.-J. Essiambre, P. Winzer, X. Q. Wang, W. Lee, C. White and E. Burrows, "Electronic predistortion and fiber nonlinearity," *IEEE Photonics Technology Letters*, vol. 18, no. 17, pp. 1804 - 1806, 2006 .

[59] Y. Gao, J. C. Cartledge, A. S. Karar, S. S.-H. Yam, M. O'Sullivan, C. Laperle, A. Borowiec and K. Roberts, "Reducing the complexity of perturbation based nonlinearity pre-compensation using symmetric EDC and pulse shaping," *Optics Express*, vol. 22, no. 2, pp. 1209-1219, 2014.

[60] F. P. Guiomar, S. B. Amado, C. S. Martins and A. N. Pinto, "Time-Domain Volterra-Based Digital Backpropagation for Coherent Optical Systems," *Journal of Lightwave Technology*, vol. 33, no. 15, pp. 3170 - 3181, 2015.

[61] J. Gonçalves, C. S. Martins, F. P. Guiomar, T. R. Cunha, J. C. Pedro, A. N. Pinto and P. M. Lavrador, "Nonlinear compensation with DBP aided by a memory polynomial," *Optics Express*, vol. 24, no. 26, pp. 30309-30316, 2016.

[62] K. Kikuchi, "Fundamentals of Coherent Optical Fiber Communications," *Journal of Lightwave Technology*, vol. 34, no. 1, pp. 157-179, 2016.

[63] E. Ip, A. Lau, D. Barros and J. Kahn, "Coherent detection in optical fiber systems," *Optics Express*, vol. 16, no. 2, pp. 753-791, 2008.

[64] R. Killey, P. Watts, V. Mikhailov, M. Glick and P. Bayvel, "Electronic Dispersion Compensation by Signal Predistortion Using a Dual-Drive Mach-Zehnder Modulator," in *Optical Fiber Communication Conference and Exposition and The National Fiber Optic Engineers Conference*, Anaheim, 2005.

[65] C. Shannon, The Mathematical Theory of Communication, Champaign, Illinois: University of Illinois Press, 1949.

[66] F. Yaman and G. Li, "Nonlinear Impairment Compensation for Polarization-Division Multiplexed WDM Transmission Using Digital Backward Propagation," *IEEE Photonics Journal*, vol. 1, no. 2, pp. 144-152, 2009.

[67] C. Antonelli, A. Mecozzi, M. Shtaif and a. P. J. Winzer, "Fundamental limits on the energy consumption in fiber-optic communications," in *CLEO*, 2013.

[68] P. J. Winzer, "High-Spectral-Efficiency Optical Modulation Formats," *Journal of Lightwave Technology,* vol. 30, pp. 3824-3835, 2012.

[69] J. Tang, "The Shannon channel capacity of dispersion-free nonlinear optical fiber transmission," *Journal of Lightwave Technology,* vol. 19, pp. 1104-1109, 2001.

[70] K. Turitsyn, S. Derevyanko, I. Yurkevich and S. Turitsyn, "Information capacity of optical fiber channels with zero average dispersion," *Physics Review Letters,* vol. 91, no. 20, p. 203901, 2003.

[71] I. Djordjevic, B. Vasic, M. Ivkovic and I. Gabitov, "Achievable information rates for high-speed long-haul optical transmission," *Journal of Lightwave Technology,* vol. 23, pp. 3755-3763, 2005.

[72] R.-J. Essiambre, G. J. Foschini, G. Kramer and P. J. Winzer, "Capacity limits of information transport in fiber-optic networks," *Physics Review Letters,* vol. 101, p. 163901, 2008.

[73] A. D. Ellis, J. Zhao and D. Cotter, "Approaching the Non-Linear Shannon Limit," *Journal of Lightwave Technology,* vol. 28, no. 4, pp. 423-433, 2010.

[74] E. Agrell and M. Karlsson, "Satellite constellations: Towards the nonlinear channel capacity," in *IEEE Photonics Conference,* Burlingame, 2013.

[75] S. Radic, R. M. Jopson, C. J. McKinstrie, A. H. Gnauck, S. Chandrasekhar and J. C. Centanni, "Wavelength division multiplexed transmission over standard single mode fiber using polarization insensitive signal conjugation in highly nonlinear optical fiber," in *Optical Fiber Communications Conference,* Atlanta, 2003.

[76] S. L. Jansen, D. v. d. Borne, P. M. Krummrich, S. Spalter, G.-D. Khoe and H. d. Waardt, "Long-haul DWDM transmission systems employing optical phase conjugation," *IEEE Journal on Selected Topics on Quantum Electronics,* vol. 12, pp. 505-520, 2005.

[77] I. D. Phillips, M. Tan, M. F. C. Stephens, M. E. McCarthy, E. Giacoumidis, S. Sygletos, P. Rosa, S. Fabbri, S. T. Le, T. Kanesan, S. K. Turitsyn, N. J. Doran, P. Harper and A. D. Ellis, "Exceeding the Nonlinear-Shannon Limit using Raman Laser Based Amplification and Optical Phase Conjugation," in *Optical Fiber Communications Conference,* San Francisco, 2014.

[78] H. Hu, R. M. Jopson, A. H. Gnauck, M. Dinu, S. Chandrasekhar, X. Liu, C. Xie, M. Montoliu, S. Randel and C. J. McKinstrie, "Fiber Nonlinearity Compensation of an

8-channel WDM PDM-QPSK Signal using Multiple Phase Conjugations," in *Optical Fiber Communications Conference*, San Francisco, 2014.

[79] K. Solis-Trapala, T. Inoue and S. Namiki, "Nearly-Ideal Optical Phase Conjugation based Nonlinear Compensation System," in *Optical Fiber Communications Conference*, San Francisco, 2014.

[80] X. Liu, A. R. Chraplyvy, P. Winzer, R. W. Tkach and S. Chandrasekhar, "Phase-conjugated twin waves for communication beyond the Kerr nonlinearity limit," *Nature Photonics,* vol. 7, pp. 560-568, 2013.

[81] D. Rafique and A. Ellis, "Nonlinearity compensation in multi-rate 28 Gbaud WDM systems employing optical and digital techniques under diverse link configurations," *Optics Express,* vol. 19, pp. 16919-16926, 2011.

[82] W. Yan, Z. Tao, L. Dou, L. Li, S. Oda, T. Tanimura, T. Hoshida and J. C. Rasmussen, "Low Complexity Digital Perturbation Back-propagation," in *European Conference on Optical Communications*, Geneva, 2011.

[83] V. Ataie, E. Temprana, L. Liu, Y. Myslivets, P. P. Kuo, N. Alic and S. Radic, "Flex-grid Compatible Ultra Wide Frequency Comb Source for 31.8 Tb/s Coherent Transmission of 1520 UDWDM Channels," in *Optical Fiber Communications Conference*, San Francisco, 2014.

[84] S. T. Le, M. E. McCarthy, N. M. Suibhne, A. D. Ellis and S. Turitsyn, "Phase-conjugated pilots for fibre nonlinearity compensation in CO-OFDM transmission," in *European Conference on Optical Communications*, Cannes, 2014.

[85] F. Inuzuka, E. Yamazaki, K. Yonenaga and A. Takada, "Performance of nonlinear interchannel crosstalk pre-compensation at zero-dispersion wavelength using carrier phase-locked WDM," *Electronics Letters,* vol. 43, no. 13, pp. 729-730, 2007.

[86] T. Tanimura, T. Kato, R. Okabe, S. Oda, T. Richter, R. Elschner, C. Schmidt-Langhorst, C. Schubert, J. Rasmussen and S. Watanabe, "Coherent reception and 126 GHz bandwidth digital signal processing of CO OFDM superchannel generated by fiber frequency conversion," in *European Conference on Optical Communications*, Cannes, 2014.

[87] R. Maher, D. Lavery, D. Millar, A. Alvarado, K. Parsons, R. Killey and P. Bayvel, "Reach Enhancement of 100% for a DP-64QAM Super-Channel using MC-DBP," in *Optical Fiber Communications Conference,* Los Angeles, 2015.

[88] R. Maher, T. Xu, L. Galdino, M. Sato, A. Alvarado, K. Shi, S. J. Savory, B. C. Thomsen, R. I. Killey and P. Bayvel, "Spectrally Shaped DP-16QAM Super-

Channel Transmission with Multi-Channel Digital Back-Propagation," *Nature Scientific Reports,* vol. 5, p. 8214, 2015.

[89] T. Sakamoto, T. Kawanishi and M. Izutsu, "Widely wavelength-tunable ultra-flat frequency comb generation using conventional dual-drive Mach-Zehnder modulator," *Electronics Letters,* vol. 43, no. 19, pp. 1039-1040, 2007.

[90] X. Yang, D. Richardson and P. Petropoulos, "Nonlinear generation of ultra-flat broadened spectrum based on adaptive pulse shaping," in *European Conference on Optical Communications*, Geneve, 2011.

[91] A. K. Mishra, R. Schmogrow, L. Tomkos, D. Hillerkuss, C. Koos, W. Freude and J. Leuthold, "Flexible RF-Based Comb Generator," *Photonics Technology Letters,* vol. 25, no. 7, pp. 701-704, 2013.

[92] D. Hillerkuss, T. Schellinger, M. Jordan, C. Weimann, F. Parmigiani, B. Resan, K. Weingarten, S. Ben-Ezra, B. Nebendahl, C. Koos, W. Freude and J. Leuthold, "High-Quality Optical Frequency Comb by Spectral Slicing of Spectra Broadened by SPM," *Photonics Journal,* vol. 5, no. 5, pp. 7201011-7201011, 2013.

[93] E. Temprana, V. Ataie, B.-P. Kuo, E. Myslivets, N. Alic and S. Radic, "Dynamic reconfiguration of parametric frequency comb for superchannel and flex-grid transmitters," in *European Conference on Optical Communications,* Cannes, 2014.

[94] X. Liu, S. Chandrasekhar, P. J. Winzer, L. B. Maheux, G. Brochu and F. Trepanier, "Efficient Fiber Nonlinearity Mitigation in 50-GHz-DWDM Transmission of 256-Gb/s PDM-16QAM Signals by Folded Digital-Back-Propagation and Channelized FBG-DCMs," in *Optical Fiber Communications Conference*, San Francisco, 2014.

[95] S. L. Jansen, D. v. d. Borne, P. M. Krummrich, S. Spalter, G.-D. Khoe and H. d. Waardt, "Long-haul DWDM transmission systems employing optical phase conjugation," *IEEE Journal on Selected Topics Quantum Electronics,* vol. 12, pp. 505-520, 2005.

[96] K. Kikuchi, "Electronic Post-compensation for Nonlinear Phase Fluctuations in a 1000-km 20-Gbit/s Optical Quadrature Phase-shift Keying Transmission System Using the Digital Coherent Receiver," *Optics Express,* vol. 16, pp. 889-896, 2008.

[97] S. Oda, T. Tanimura, T. Hoshida, C. Ohshima, H. Nakashima, T. Zhenning and J. Rasmussen, "112 Gb/s DP-QPSK transmission using a novel nonlinear compensator in digital coherent receiver," in *Optical Communications Conference*, San Diego, 2009.

[98] M. I. Yousefi and K. R. Kschischang, "Information Transmission Using the Nonlinear Fourier Transform, Part III: Spectrum Modulation," *IEEE Transactions on Information Theory,* vol. 60, no. 7, pp. 4346-4369, 2014.

[99] M. I. Yousefi and F. R. Kschischang, "Information Transmission Using the Nonlinear Fourier Transform, Part I: Mathematical Tools," *IEEE Transactions on Information Theory,* vol. 60, no. 7, pp. 4312-4328, 2014.

[100] M. I. Yousefi and F. R. Kschischang, "Information Transmission Using the Nonlinear Fourier Transform, Part II: Numerical Methods," *IEEE Transactions on Information Theory,* vol. 60, no. 7, pp. 4329-4345, 2014.

[101] E. G. Turitsyna and S. K. Turitsyn, "Digital signal processing based on inverse scattering transform," *Optics Letters,* vol. 38, pp. 4816-4188, 2013.

[102] H. Bulow, "Experimental Demonstration of Optical Signal Detection Using Nonlinear Fourier Transform," *Journal of Lightwave Technology,* vol. 33, no. 7, pp. 1433-1439, 2015.

[103] E. Mateo, L. Zhu and G. Li, "Impact of XPM and FWM on the digital implementation of impairment compensation for WDM transmission using backward propagation," *Optics Express,* vol. 16, pp. 16124-16137, 2008.

[104] D. Rafique, J. Zhao and A. Ellis, "Digital back-propagation for spectrally efficient WDM 112 Gbit/s PM m-ary QAM transmission," *Optics Express,* vol. 19, pp. 5219-5224, 2011.

[105] C. Xia, X. Liu, S. Chandrasekhar, N. K. Fontaine, L. Zhu and G. Li, "Multi-channel nonlinearity compensation of PDM-QPSK signals in dispersion-managed transmission using dispersion-folded digital backward propagation," *Optics Express,* vol. 22, pp. 5859-5866, 2014.

[106] N. Alic, E. Temprana, E. Myslivets and S. Radic, "Nonlinearity compensation: Is the knowledge of absolute amplitude and phase really necessary?," in *Tyrrhenian International Workshop on Digital Communications*, Florence, 2015.

[107] Cisco, "Cisco First to Deliver 100G at 3,000 km Distances Without Need for Regeneration," 22 February 2012. [Online]. Available: https://newsroom.cisco.com/press-release-content?articleId=677338.

[108] P. J. Winzer, "Scaling Optical Fiber Networks: Challenges and Solutions," *Optics and Photonics News,* vol. 26, no. 3, pp. 28-35, 2015.

[109] N. Alic, "Cancellation of Nonlinear Impairments in Fiber Optic Transmission Systems," in *Optical Fiber Communication Conference*, Anaheim, 2016.

[110] A. Chraplyvy, "Limitations on lightwave communications imposed by optical-fiber nonlinearities," *Journal of Lightwave Technology,* vol. 8, no. 10, pp. 1548 - 1557, 1990.

[111] A. Mecozzi and R.-J. Essiambre, "Nonlinear Shannon Limit in Pseudolinear Coherent Systems," *Journal of Lightwave Technology,* vol. 30, no. 12, pp. 2011-2024, 2012.

[112] R. A. Bergh, B. Culshaw, C. C. Cutler, H. C. Lefevre and H. J. Shaw, "Source statistics and the Kerr effect in fiber-optic gyroscopes," *Optics Letters,* vol. 7, no. 11, pp. 563-565, 1982.

[113] P. A. Andrekson and M. Westlund, "Nonlinear optical fiber based high resolution all-optical waveform sampling," *Laser & Photonics Reviews,* vol. 1, no. 3, p. 231–248, 2007.

[114] K. Goda, K. K. Tsia and B. Jalali, "Serial time-encoded amplified imaging for real-time observation of fast dynamic phenomena," *Nature* , vol. 458, pp. 1145-1149, 2009.

[115] N. S. Bergano, "Undersea amplified lightwave systems design," in *Optical Fiber Telecommunications*, San Diego, Academic Press, 1997.

[116] S. Manakov, "Note on the integration of Euler's equations of the dynamics of an nn-dimensional rigid body," *Functional Analysis and Its Applications,* vol. 10, no. 4, p. 93–94 , 1976.